République Algérienne Démocratique et Populaire
Ministère de L'Enseignement Supérieur et de la Recherche Scientifique
Université Mohamed Boudiaf - M'sila
Faculté de technoloqie
Departement De Génie Electrique

Présentée pour l'obtention du **diplôme** de **DOCTORAT** 3ème cycle

En : Electromécanique

Spécialité : Maintenance industrielle

Par : Mohamed Razi MORAKCHI

Thèse

Perfection des performances de l'accéléromètre capacitif et leur application dans l'internet des objets (IoT)

Soutenue publiquement, le 05/03/2024, devant le jury composé de :

M.	Fouad BERRABAH	Professeur	à l'université de M'sila	Président
M.	Zine GHEMARI	Professeur	à l'université de M'sila	Directeur de thèse
M.	Mabrouk DEFDAF	M.C.A	à l'université de M'sila	Co-directeur de thèse
M.	Abderrahim ZEMMIT	M.C.A	à l'université de M'sila	Examinateur
M.	Yahia LAAMARI	M.C.A	à l'université de Batna 2	Examinateur
M.	Abdelhak ABDOU	M.C.A	à l'université de Batna 2	Examinateur
M.	Salah BELKHIRI	M.C.A	à l'université de M'sila	inviter

People's Democratic Republic of Algeria
Ministry of Higher Education and Scientific Research
University of M'sila
Faculty of technology
Department of electrical engineering

Presented to obtain a 3^{rd} cycle **DOCTORATE degree**

In : Electromecanic

SPECIALITY :Industrial Maintenance

By : Mohamed Razi MORAKCHI

Thesis

Refinement of Capacitive Accelerometer Performance and Its Applications in the Internet of Things (IoT)

Publicly defended, on 05/03/2024, before a jury composed of :

Mr.	Fouad BERRABAH	Professor	at University of M'sila	Chairman
Mr.	Zine GHEMARI	Professor	at University of M'sila	Thesis Supervisor
Mr.	Mabrouk DEFDAF	Associate Professor A	at University of M'sila	Thesis Co-Supervisor
Mr.	Abderrahim ZEMMIT	Associate Professor A	at University of M'sila	Examiner
Mr.	Yahi LAAMARI	Associate Professor A	at University of Batna 2	Examiner
Mr.	Abdelhak ABDOU	Associate Professor A	at University of Batna 2	Examiner
Mr.	Salah BELKHIRI	Associate Professor A	at University of M'sila	Invited Guest

Dedication:

I dedicate this thesis as an expression of my deep respect and profound admiration for my cherished father, Mohamed El Kebir, and my beloved mother, Saighi Bouchra. I want to convey my heartfelt appreciation for their unwavering support, affection, love, guidance, and the countless prayers that have accompanied me throughout my academic journey. I pray that God bestows upon them good health and a long, fulfilling life.

I dedicate this work to my family, the unwavering bedrock of support and encouragement that has sustained me on this academic voyage. To my parents, who instilled in me a passion for learning and a strong work ethic, my gratitude knows no bounds. To my siblings—Mouafeq, Thabet, Heythem, Rachik, and my dear sister Khadidja—whose unwavering belief in my capabilities served as a constant wellspring of inspiration, I owe you a debt of gratitude. This achievement stands as a testament to the love and support you have generously provided. I am profoundly thankful for being the unwavering source of my motivation and a special thanks to the ambitious to My dearest Dr. Ch Assia. ...

Acknowledgements

In the celestial grandeur of gratitude, my first and deepest thanks are to the Almighty God, whose unfailing strength and wisdom have been my guiding stars, leading me through challenges with courage and patience.

This journey of intellectual discovery, culminating in the thesis presented, found its nurturing ground at M'sila University, Department of Electrical Engineering, Faculty of Technology, M'sila. Here, I was fortunate to be under the wing of Professor Zine GHEMARI, whose brilliance and insightful guidance illuminated my path. His relentless support and encouragement have been the wind beneath my wings. To Mabrouk DEFDAF, a beacon of knowledge and my Co-supervisor at the University of M'sila, I extend my sincere thanks for his unwavering guidance and support.

I extend my heartfelt gratitude to the esteemed members of my thesis committee examination, whose dedication, time, and expertise were invaluable in supervising and evaluating my work: Mr. Fouad BERRABAH, Professor at the University of M'sila, serving as Chairman; Mr. Abderrahim ZEMMIT, Associate Professor at the University of M'sila, as an Examiner; Mr. Yahi LAAMARI, Associate Professor at the University of Batna 2, also an Examiner; Mr. Abdelhak ABDOU, Associate Professor at the University of Batna 2, likewise an Examiner; and Mr. Salah BELKHIRI, Associate Professor at the University of M'sila, who graciously served as an Invited Guest.

To my dear brother in spirit and academia, Dr. Selman DJEFFAL, my co-supervisor and co-author, I owe a debt of gratitude. His expertise, especially in simulations and continuum robots, was the cornerstone of our shared success.

My journey at the University of Sherbrooke, under the mentorship of Professor Djemel ZIOU during my internship, was a chapter of immense growth and learning. His wisdom and guidance were pivotal in shaping my research.

A special note of gratitude to Mr. Atef Chibani and Larbi Bendada, educators par excellence at CRTI Setif and Larbi Ben M'hidi University in Oum El Bouaghi. Their guidance was a lighthouse in the sea of knowledge.

My heartfelt appreciation goes out my colleagues, the Phd students Saida , Aboura, , Feriel , Khaled , Lina , Khadidja Larbi Fellah, Nacer , Merwane , Ouassama ,and many others whose support and camaraderie enriched my academic journey.

A special thank you to Professor Sebgag Salih, mother of my colleague PhD student Guezzi Abderrahmane, who generously offered us the Turnitin account, a resource we extensively used in our PhD studies. Special thanks for this invaluable support.

To friends like Hamlaoui Ibrahim and Laribi Houssine, whose companionship was a treasure trove of support and inspiration, I extend my warmest thanks.

Dr. Salah Mezbache, a pillar of wisdom and friendship, deserves a special mention. From the initial steps of my academic journey to the zenith of my Ph.D., his guidance was the compass that led the way.

A token of gratitude to my colleagues at CCTE, Engineer Bilel Boukherissa, Fethi Ziadi, and Redouane Maouche, for their invaluable assistance in the experimental phases of my work.

To Djihad Larbi Bengati, whose generous gift of a Raspberry Pi opened new horizons in my thesis, I express my profound gratitude.

A chapter of this journey is dedicated to Dr. Wafia Benhamlaoui, whose support during my Ph.D. examination was nothing short of remarkable. Her unwavering assistance and faith in my abilities were instrumental in turning my dreams into reality.

Abstract

This thesis presents a comprehensive exploration of capacitive accelerometers and their multifaceted roles in sensor technology. It encompasses various aspects, commencing with the fundamental principles of accelerometer technology and of accelerometers within applications. The research is divided into distinct parts. The initial part delves into the foundational concepts of accelerometer technology and state of art about Internet of Things (IoT).

The second part represents a pivotal contribution to the field, focusing on the mathematical modeling and optimization of capacitive accelerometers. It introduces a mathematical model that significantly enhances measurement precision by addressing key parameters damping rate. The result is a breakthrough formula that minimizes measurement errors, making capacitive accelerometers more reliable and stable.

The third part of the thesis extends the practical utility of accelerometers by applying them within the IoT. The integration of accelerometers, is explored, demonstrating their trans-formative potential including cost-effective and user-friendly setups, are discussed, highlighting their role in enhancing data collection, particularly in scenarios where inertial movements need to be translated into numerical signals.

The final part explores the application of accelerometers in the domain of continuum robots. The research presents an empirical formula for the forward kinematic model of single-section continuum robots, employing particle swarm optimization for the inverse kinematic model. Moreover, it investigates the potential for accelerometers to identify the end effector position, thereby reducing the reliance on expensive tools. This novel approach enhances the data recording capabilities of continuum robots.

In summary, this thesis contributes to the advancement of capacitive accelerometer technology by offering new mathematical models, optimizing their performance, and extending their applications into the industry and robotics domains. It signifies a significant step forward in harnessing these sensors for enhanced precision and functionality, opening doors to innovative applications in robotics, especially in continuum robots, and beyond.

Résumé :

Cette thèse présente une exploration complète des accéléromètres capacitifs ainsi que leurs multiples rôles dans le domaine des technologies de capteurs. Elle couvre un large éventail d'aspects, allant des principes fondamentaux des accéléromètres à leur intégration dans des applications de l'Internet des Objets (IoT). La thèse se divise en plusieurs sections, chacune enrichissant la compréhension et l'utilisation des accéléromètres capacitifs.

La première section explore les principes fondamentaux des accéléromètres, détaillant les mécanismes de base et les composants électroniques associés. Cette exploration sert de fondation pour les analyses ultérieures.

Dans la deuxième section, qui constitue une contribution majeure à ce domaine, l'accent est mis sur la modélisation mathématique et l'optimisation des accéléromètres capacitifs. Un nouveau modèle mathématique est introduit, améliorant significativement la précision des mesures en tenant compte de facteurs clés tels que la variation de la capacité, le taux d'amortissement, et l'espacement des électrodes. Cette avancée aboutit à une formule révolutionnaire minimisant les erreurs de mesure, et rendant les accéléromètres plus fiables et précis que jamais.

La troisième section étend l'utilité pratique des accéléromètres capacitifs en les appliquant à l'IoT. L'intégration de capteurs microélectroniques, notamment les accéléromètres à système micro électromécanique (MEMS), est explorée, révélant leur potentiel transformateur dans divers aspects de la vie quotidienne. Les applications IoT, offrant des solutions à la fois économiques et faciles à utiliser, sont examinées, soulignant leur importance pour améliorer la collecte de données, surtout quand il faut convertir les mouvements inertiels en signaux numériques.

La dernière section explore l'utilisation des accéléromètres dans le domaine des robots continus bioniques. Elle valide expérimentalement le modèle géométrique inverse de robots continus à une seule section via l'optimisation par essaims de particules, et examine le potentiel des accéléromètres pour identifier la position de l'effecteur final, réduisant ainsi la dépendance à l'égard d'outils coûteux. Cette approche novatrice améliore la capacité d'enregistrement de données chez les robots bioniques continus, préfigurant de futures avancées, notamment l'emploi d'accéléromètres pour la validation de modèles cinétique de tels robots.

الملخص:

تقدم هذه الأطروحة استكشافًا شاملاً لمقاييس التسارع السعوية وأدوارها المتعددة في مجال تكنولوجيا الاستشعار. ويغطي جوانب مختلفة، بدءًا من أساسيات تقنية مقياس التسارع وانتهاءً بدمجها في تطبيقات إنترنت الأشياء بحيث ينقسم البحث إلى عدة أجزاء، يساهم كل منها في فهم أعمق وتحسين استخدام مقاييس التسارع ومجالات تطبيقه.

يتعمق الجزء الأول في المفاهيم الأساسية لتقنية لمقياس التسارع، ويوضح الآليات الأساسية والميكانزيم الأساسية لهذه المستشعرات إضافة الى دراسة حالة من الفن.

ويشكل الجزء الثاني مساهمة كبيرة في هذا المجال، مع التركيز على النمذجة الرياضية وتحسين مقاييس التسارع السعوية. إنه يقدم نموذجًا رياضيًا جديدًا يعمل على تحسين دقة القياس بشكل كبير من خلال مراعاة المعلمات الرئيسية مثل تباين السعة ونسبة معامل التخميد والتباعد بين الأقطاب الكهربائية. والنتيجة هي صيغة تقلل من أخطاء القياس، مما يجعل مقياس التسارع السعوي أكثر ثبات ودقة.

يوسع الجزء الثالث من الأطروحة الفائدة العملية لمقاييس التسارع السعوية من خلال تطبيقها على إنترنت الأشياء .يتم استكشاف تكامل أجهزة الاستشعار الإلكترونية الدقيقة، وخاصة مقاييس تسارع النظام الكهروميكانيكي الدقيق(MEMS) ، مما يدل على إمكاناتها التحويلية في مختلف جوانب الحياة اليومية. وتتم مناقشة التطبيقات المتعلقة بإنترنت الأشياء، بما في ذلك الإعدادات الفعالة من حيث التكلفة وسهلة الاستخدام، مع تسليط الضوء على دورها في تحسين جمع البيانات في تطبيق صناعي على مستوى جامع بيانات الضغط، لا سيما في السيناريوهات التي تحتاج فيها إلى ترجمة حركات القصور الذاتي إلى إشارات رقمية.

الجزء الأخير يستكشف تطبيق مقاييس التسارع في مجال الروبوتات المستمرة. يتحقق هذا الجزء تجريبيًا من صحة النموذج الهندسي العكسي للروبوتات المستمرة ذات القسم الواحد باستخدام لوغاريتم مبني على تحسين سرب الجسيمات. بالإضافة إلى ذلك، فهو يدرس إمكانات مقاييس التسارع لتحديد موضع المستجيب النهائي للروبوت، وبالتالي تقليل الاعتماد على الأدوات باهظة الثمن. يعمل هذا النهج الجديد على تحسين قدرات تسجيل البيانات للروبوتات الإلكترونية المستمرة، مما يمهد الطريق للتقدم المستقبلي، بما في ذلك استخدام مقاييس التسارع للتحقق من صحة النماذج الديناميكية للروبوتات الإلكترونية المستمرة بالإضافة الى تقديم نموذج جديد من روبوت مستمر أكثر ثبات وصلابة من النماذج السابقة للروبوت المستمر.

Table of contents

List of figures

List of tables

0.1 List of nomenclature

MEMS (Micro-Electro-Mechanical Systems)
- IoT (Internet of Things)
- Ido (Internet des objets)
- On/Off Sensors (TOR)
- PZT (Piezoelectric lead Zirconate Titanate)
- FPI (Fabry-Perot Interferometer)
- FSBM (Front-Side Bulk Micromachining)
- DPU (Differential Pressure Unit)
- SPI (Serial Peripheral Interface)
- I2C (Inter-Integrated Circuit)
- GA (Genetic Algorithm)
- PSO (Particle Swarm Optimization)
- IKM (Inverse Kinematic Model)
- FKM (Forward Kinetic Model)
- VC (Variable Curvature)
- CC (Constant Curvature)
- CCKA (Constant Curvature Kinematic Analysis)
- CPF (Cubic Polynomial Fit)
- CRs (Continuum Robots)
- MSS (Maxillary Sinus Surgery)
- CDCR (Cable-Driven Continuum Robot)

General introduction

Accelerometers, sensors that measure acceleration, velocity, and displacement [1], have progressed significantly due to advances in microelectronics and micro-fabrication technologies [2, 3]. These technological leaps have paved the way for the creation of small, precise, and reliable accelerometers [4]. The 1980s marked a transformative period as micro-fabrication techniques ushered in micro-fabricated capacitive accelerometers [5]. Initially, these sensors has mechanical part with clunky proof masses suspended between electrodes. However, persistent innovation from pioneers like Honeywell and Analog Devices propelled these devices into the digital era [6]. These sensors have become an integral part of smartphones, gaming devices, and various portable electronic gadgets, revolutionizing human-machine interaction [7–9]. Moreover, sensors play a crucial role in Internet of Things (IoT) applications across various fields such as medicine, maintenance, and sports. In medicine, for instance, sensors can be used for remote patient monitoring, detecting vital signs, and managing chronic conditions[10]. In maintenance, sensors can help in predictive maintenance by monitoring equipment and rotary machine health, detecting failures in rotor vibration [11]. In sports, sensors are used for performance tracking, injury prevention, and enhancing training routines[12]. Due to the huge demand for accelerometers in markets and their wide application, many researchers have been working on enhancing accelerometer performance through design and mathematical modeling of accelerometers [13–15]. Among various types of accelerometers such as capacitive, piezoelectric, and tunneling, the capacitive type stands out as the best in terms of performance and sensitivity [16].

0.2 Thesis structure

The thesis is organized into two main parts with distinct chapters:

- Chapter 1: State-of-the-Art Fundamentals of Accelerometer Technology and Its Application in IoT

- Chapter 2: Capacitive Accelerometer Modeling: Optimization-Based parameter for Refining Its Performance
- Chapter 3: Accelerometer-Based Raspberry Pi for circular chart recorder
- Chapter 4: Kinematic Modeling of Continuum Robots Utilizing Accelerometer Data
- Chapter 5: Optimized Design of Continuum Robots and Dynamics Modeling

This structure guides the reader through the exploration of capacitive accelerometers and their applications in diverse domains.

0.3 Publication list

1. **Article** MORAKCHI, M. R et al. A novel technique based on IoT accelerometer for transmitting circular chart recorders to electrical data. *UPB Sci. Bull. Ser. C*, 84, 274–286 (2022). https://www.scientificbulletin.upb.ro/rev_docs_arhiva/rez769_818860.pdf[17].

2. **Article** Djeffal, S., Ghoul, A., Morakchi, et al. Optimized Computer Torque Control and Dynamic Model of a Spatial Single Section Continuum robot. *Results Control Optim.*, 12, 100264 (2023) DOI:10.1016/j.rico.2023.100264[18].

3. **Conference proceedings** MORAKCHI, M. R et al. The ideal capacitive accelerometer damping rate choice to minimize the measurement error. In *2022 2nd International Conference on Advanced Electrical Engineering (ICAEE)*, 11–15 (IEEE Xplore, 2022). DOI:10.1109/ICAEE53772.2022 [16].

4. **Conference proceedings** MORAKCHI, M. R et al. Prototype of an affordable continuum robot-based IoT accelerometer and its kinematic modeling. In *ICATEEE*, 1–6 (IEEE, 2022). DOI:10.1109/ICATEEE57445.2022.10093759 [19].

5. **Conference proceedings** Ghemari , Z. BELKHIRI, S. and Morakchi, M. R. Improvement of the vibration analysis technique by optimizing the parameters of the piezoelectric accelerometer. In *2022 IEEE 21st International Conference on Sciences and Techniques of Automatic Control and Computer Engineering (STA)*, 183–186 (IEEE, 2022). DOI:10.1109/STA56120.2022.10018991 [20].

6. **Chapter in a book** MORAKCHI, M. R. et al, M. A Model-Free Approach for Solving the Inverse Kinematics of Continuum Robots. In *Advances in Engineering Research Volume 53* (ed. Petrova, Victoria M.) 197–214 (Nova Science Publishers, 2023) [21].

Chapter 1

State-of-the-Art fundamentals of accelerometer technology and its application in IoT

1.1 Introduction

This chapter aims to provide a comprehensive understanding of the principles, development, and applications of accelerometer technology. We begin by exploring the historical evolution of accelerometers, tracing their journey from early mechanical models to the sophisticated microelectromechanical systems (MEMS) used today. This historical context sets the stage for a deeper appreciation of the technological advancements and challenges overcome in this field. Following the historical overview, the chapter focuses on the operational principles of accelerometers, elucidating how these devices capture and convert physical movements into measurable electrical outputs. This section lays the groundwork for understanding the different types of accelerometers and their specific applications. Then categorizes and discusses various accelerometer types, including capacitive, piezoresistive, and piezoelectric models, highlighting their unique functionalities and suitability for different applications. Additionally, the chapter examines the role of accelerometers applications and their integration into emerging technologies, such as the Internet of Things (IoT), emphasizing their growing significance in the digital era. To conclude, we offer insights into the selection and implementation of accelerometers in industrial settings, providing practical guidance for professionals in the field.

1.2 Historical development of accelerometers

The evolution of accelerometer technology showcases a remarkable journey of innovation, reflecting significant advancements in science and engineering. This section presents a unified narrative of their development, from the early mechanical devices to the present-day microelectromechanical systems (MEMS) . The 1960s and 1970s marked a significant period of progress, aligned with breakthroughs in semiconductor technology. This era saw the emergence of MEMS accelerometers, offering substantial improvements in size, accuracy, and application versatility [22]. The 1970s marked the advent of capacitive accelerometers, pioneered by Honeywell's design featuring a spring-suspended proof mass. Subsequent innovations by companies like Analog Devices enhanced these accelerometers' design and sensitivity, broadening their application scope [1]. The 1980s witnessed the introduction of micro-fabricated capacitive accelerometers, with silicon becoming the preferred material for proof masses and electrodes. These advancements led to significant size reduction and improved accuracy, expanding their use in automotive, aerospace, industrial, and consumer electronics [23, 24]. MEMS technology revolutionized accelerometer design in the late 20th century. Employing silicon wafers and advanced etching techniques, these devices were significantly more compact, sensitive, and reliable. This period also introduced diverse accelerometer types, such as capacitive, piezoresistive, and piezoelectric, each tailored for specific applications [25]. Recent advancements in microfabrication have resulted in even smaller and more sensitive capacitive accelerometers (see Fig1.1).

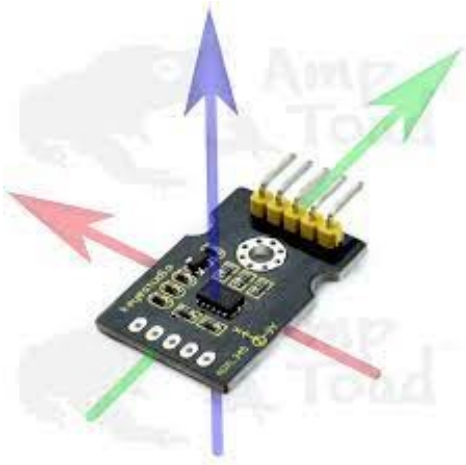

Fig. 1.1: Commercial Micro-Machined Devices Accelerometer [23]

1.3 Fundamentals of accelerometer technology

This section explores the fundamental principles underlying the operation of accelerometers, a type of sensor indispensable in various fields due to its ability to convert mechanical motion into electrical signals. We delve into the core aspects of accelerometer operation, focusing on how these devices measure and represent physical quantities.

In the industrial environment, the term "sensor" is often reserved for compact devices. Larger devices may be referred to as transmitters, and specialized devices used in physicochemical measurements are called industrial analyzers. Sensors are commonly classified into two major families based on the nature of the information they emit [4]:

- On/Off Sensors (TOR): Emit a binary signal, 0 or 1 (true or false), depending on the measured quantity's position relative to a setpoint. Used in sequential automation.

- Analog or Continuous Sensors: Emit an analog or digital signal with a generally linear function relating the signal to the measured quantity.

1.3.1 Vibration measurement chain

The measurement chain consists of elements assembled as shown in Figure 1.2, with each component playing a crucial role [4].

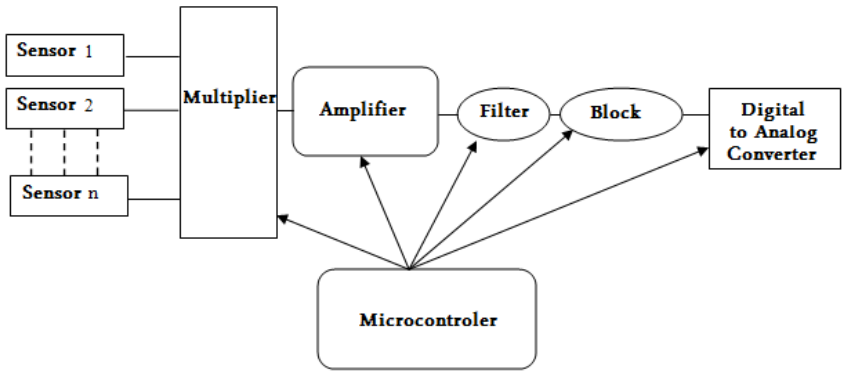

Fig. 1.2: Components of the measurement chain [4]

- Sensors: Provide electrical signals carrying information about the measured quantity at the input of the measurement chain. These signals can be generated directly by active sensors or through passive sensor conditioners.
- Analog Multiplexer: Selects electrical signals when multiple sensors are present.
- Signal Amplifier: Enhances the signal strength.
- Analog Filter: Limits the signal bandwidth to significant frequencies.
- Sample-and-Hold Circuit: Records the analog level for the necessary processing time.
- Analog-to-Digital Converter: Converts analog signals to digital information.
- Microcontroller: Manages measurement chain settings and performs signal processing and data analysis.
- Display/Communication Interface: Presents measurement results on a computer interface.

1.3.2 Importance of measurement accuracy

Accurate measurements are crucial when using sensors. Improving this characteristic involves the following steps [4]:

- Implement algorithms for signal processing and parameter extraction.
- Use a multi-sensor structure for data fusion to compensate for influencing factors.

1.3.3 Emitted signal

Typically, the sensor emits an analog signal in current (4-20mA) or voltage (1-5 volts), powered by electrical energy through a communication line [3].

1.3.4 The Sensor

The measurand (m) is the physical quantity measured, often resulting in an electrical signal (s) representing the quantity and its vibrations [5]. The sensor, a non-electric device, converts the measurand into an electrical characteristic:

$$S = F(m) \tag{II.1}$$

This relationship stems from the physical laws governing the sensor's operation and depends on the sensor's design, materials, and environment. Calibration typically yields a numerical formula, used within a linear range where the sensor's sensitivity S remains constant:

$$\Delta S = S \cdot \Delta m \tag{II.2}$$

Instrumentalists use the sensor's sensitivity S to minimize the effects of non-linearity, bandwidth, aging, and environmental influences on the measurand m [5].

1.3.5 Influencing factors

Several environmental and operational factors can influence accelerometer performance [4]:

- Temperature, ambient pressure, mechanical or acoustic vibrations, shocks, time.
- Sensor position and mounting, humidity, water splashing, immersion.
- Corrosive environments, electromagnetic interference, nuclear radiation.
- Accelerations, gravity, and sensor power supply.

1.3.6 Sensor selection

Choosing the right sensor involves understanding its characteristics, including the nature of the quantity to be measured and its price. The operating constraints of the system where the measurement is made and the metrological characteristics specified in the requirements are also key criteria [4].

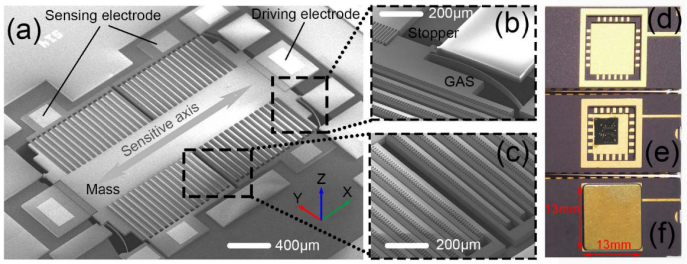

Fig. 1.3: (a) Micrograph of the accelerometer (b) one of the anti-spring curved beams and stoppers. (c) The differential area-variable capacitive comb fingers. (d)–(f) are pictures of the DIP-24 vacuum-packaged accelerometer [26].

1.4 Types of accelerometers and their operating principles

Accelerometers are pivotal in measuring acceleration, vibration, and gravitational forces. Various types of accelerometers, each based on specific operating principles, are employed in diverse applications. This section outlines the main types and discusses their functionalities and applications.

1.4.1 Capacitive detection accelerometer

Currently, capacitive detection accelerometers1.4 are the most widely used. They operate by forming a capacitor between a movable proof mass and a fixed element. Changes in capacitance, due to the movement of the proof mass in response to acceleration, are converted into electrical signals. These accelerometers are known for their high sensitivity and low power consumption, making them ideal for applications in consumer electronics, automotive, and industrial monitoring [20, 27, 28].

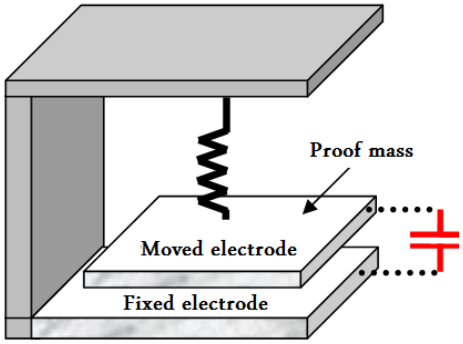

Fig. 1.4: Principle of the capacitive accelerometer [5]

1.4.2 Piezoresistive detection accelerometer

Piezoresistive detection accelerometers1.5 measure structural deformation during acceleration through changes in the resistance of a piezoresistive element. These sensors are typically produced using bulk micromachining processes and are valued for their robustness and precision in high-impact applications [29, 30].

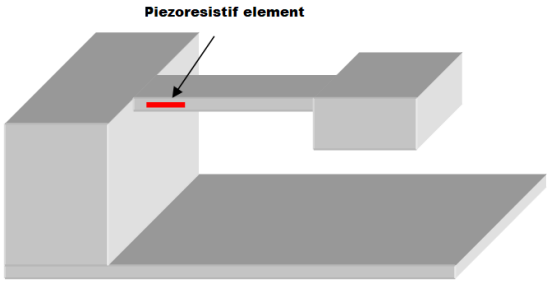

Fig. 1.5: Principle of the piezoresistive detection accelerometer [4]

1.4.3 Transistor-Based piezojunction detection accelerometer

The effects of mechanical stress on transistor behavior have been studied because mechanical stress on electronic circuits can occur during encapsulation. In this type of accelerometer, the piezo-sensitivity of bipolar transistors is used instead of piezoresistive gauges to measure the signal. The required stress causes a repopulation of electrons in the transistor channel, altering the electron movement. In this case, a transistor is used as a sensitive element, greatly reducing the size of the transduction element compared to piezoresistors. This approach has the advantage of significantly reducing power consumption compared to piezoresistive detection, which is beneficial for certain applications [5].

1.4.4 Piezoelectric detection accelerometer

A body that exhibits a potential across its terminals when subjected to a force is called a piezoelectric body. The materials often used are ZnO or PZT (Piezoelectric lead Zirconate Titanate). To provide feedback to the structure, the inverse property of piezoelectricity is used. For this type of accelerometer, a single piezoelectric element can be used (in this case, time is sampled and divided between actuation and measurement) or two piezoelectric elements can be used (here, the two elements form a sandwich, with one serving for actuation and the other for measurement) 1.6. The advantage of this detection method is zero power consumption transduction (stress variations generate potential). Two types of etching are used in piezoelectric detection accelerometers, the first type is bulk micromachining, and the second type is surface micromachining. This detection method is not suitable for full-CMOS fabrication; it requires the deposition of piezoelectric films on the structures. Figure 1.6 illustrates a three-axis piezoelectric detection accelerometer [31, 32].

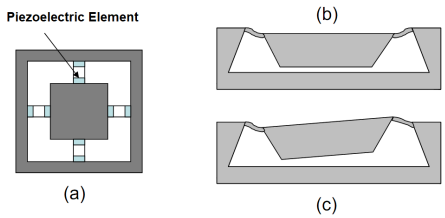

Fig. 1.6: A three-axis piezoelectric accelerometer [5]

1.4.5 Tunnel effect detection accelerometer

This type of accelerometer is developed by researchers at JPL (Jet Propulsion Laboratory, Pasadena), based on the exploitation of tunneling microscope effects. To produce tunneling, electron penetration is required between two metal electrodes, creating a lower insulating barrier between these two electrodes [33, 34]. It requires a current of (1 to 2) between a tip attached to the mobile structure and a fixed electrode, with a separation distance on the order of a few angstroms. Electrostatic force is used to control the position of the tip (see Fig1.7). The necessary voltage is measured during acceleration (to produce electrostatic force) to keep the tunneling tip in the same position, thus maintaining a constant tunnel current. An example of a tunnel effect accelerometer is shown in Figure 1.7. These devices can achieve very high sensitivities (resolution on the order of µg), doubling the tunnel current for each Angstrom of displacement, measurable changes on the milli-Angstrom scale. For a bandwidth of 1.5kHz, resolutions of 0.5µg are obtained.

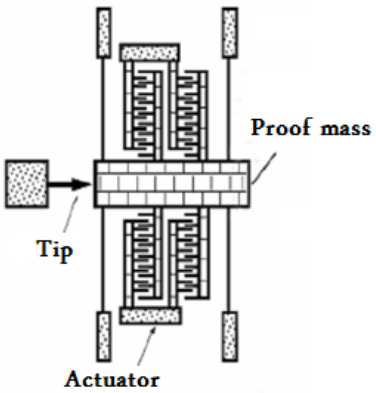

Fig. 1.7: A tunnel effect accelerometer [5]

1.4.6 Resonant structure detection accelerometer

The principle of this accelerometer is to evaluate the change in the resonance frequency of an oscillating structure. This type of detection was used in early accelerometers in 1990, with these devices being micromachined in quartz. Nowadays, these silicon micromachined sensors transfer inertial force from the proof mass to an axial force on the resonant structure, thus changing its resonance frequency [35]. The advantage of resonant structure detection is that it directly provides digital measurements. A digital signal is measured by a counter that shows the output frequency, which can reach very high sensitivities of 700Hz/g. This type of sensor consists of a resonator and a laterally movable seismic mass. The seismic mass compresses or elongates the oscillating structure, thereby changing its resonance frequency during acceleration (Fig. 1.8).

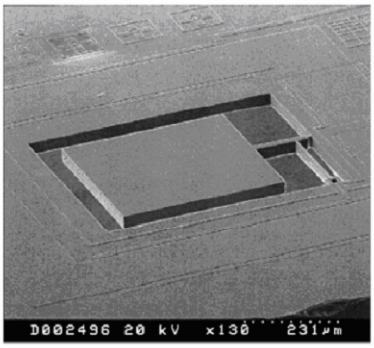

Fig. 1.8: A resonant accelerometer [5]

1.4.7 Optical detection accelerometer

The advantages of both optics and micro-machining are combined in this type of accelerometer, resulting in miniature sensors that are immune to electromagnetic interference noise with a linear response to acceleration. There are two types of detection. The first one measures the intensity of light modulated by acceleration (Fig. 1.9). The second one measures the wavelength of the signal reflected on a seismic mass: one side of the seismic mass acts as a mirror, and the reflected light has a wavelength related to the optical fiber mirror distance (Fabry-Perot interferometer) [4, 36, 22].

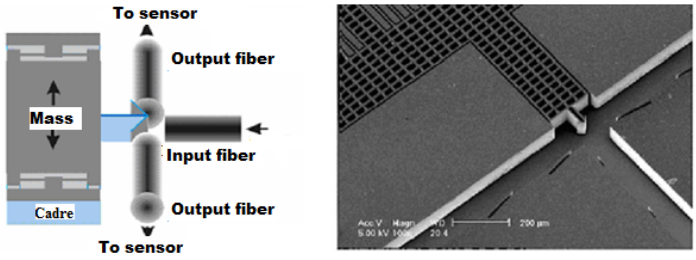

Fig. 1.9: An optical accelerometer [5]

These sensors have drawbacks such as the need for a light source, perfect alignment of optical fibers, and high costs. Today, except for some high-temperature pressure sensors, no MEMS optical fiber sensors are competitive in the market. These sensors are specifically designed for operation in harsh environments (high temperatures, high electromagnetic interference, etc.) [4].

1.4.8 Thermal detection accelerometer

There are two types of thermal detection accelerometers. The first type has a seismic mass suspended above a heat source (a simple heating resistor). The distance between the heat source and the proof body changes due to acceleration, which acts as a "heat sink." A temperature gradient from the heating element to the seismic mass is caused by the temperature difference. If the distance to the mass is small, this gradient becomes more significant. This gradient depends on acceleration, and the temperature near the heating resistor can be measured using thermocouples (polysilicon-aluminum) or thermistors [4, 37].

The second type of thermal detection is a sensor without a proof mass. This type is based on the principle of heat transfer by convection from a heating resistor to thermistors. Figure 1.10 illustrates this type of accelerometer. The heating resistor produces a symmetrical temperature distribution. When acceleration is applied, the distribution becomes asymmetrical, and the lateral sensors measure the temperature difference. The fabrication of thermal accelerometers is straightforward; these accelerometers are exclusively of the FSBM type (front-side bulk micro-machining). The silicon cavity thermally isolates the heating resistor and also reduces energy consumption. Particular attention must be paid to the design of such sensors. When the detectors are close enough to the heating resistor, it is possible to measure the temperature gradient (noting that temperature decreases rapidly as one moves away); however, when the detectors are too close to the central element, sensitivity is reduced. In fact, sensitivity is relative to Δ, with T0 being the temperature of the detectors when there

is no acceleration. Decreased sensitivity results in an increase in ambient temperature (requiring compensation for temperature effects). It is related to the heating power and the square of the air pressure in the cavity, allowing for lower resolutions in the micro-g range [5]. The cutoff frequency of these accelerometers is in the range of a few hundred hertz. Beyond that, the Bode diagram slope becomes second-order, and the signal is no longer usable. To increase bandwidth (which depends on the thermal constant), one must increase pressure, reduce cavity dimensions, and change the gas nature.

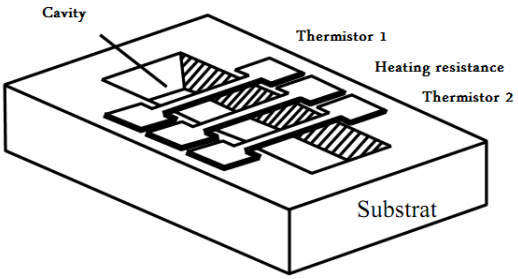

Fig. 1.10: A thermal accelerometer [5]

1.4.9 Accelerometers with unique detections

A magneto-rheological fluid used as a dielectric in a capacitive detection accelerometer has been studied [5]. The solidifying property of the magneto-rheological fluid, when a magnetic field is applied, and returning to a liquid state when the magnetic field is removed is exploited. In the capacitive detection accelerometer, damping calibration and dielectric constant enhancement are achieved using the magneto-rheological fluid. Therefore, the output signal depends on the experienced acceleration and the intensity of the magnetic field. Another innovative accelerometer uses a levitating silicon sphere as a proof mass. Electro-magnetic suspension of the sphere requires a voltage to maintain the sphere in the same position, providing information about the value of acceleration. Figure 1.11 shows a photo of the electromagnetic levitation accelerometer. This accelerometer measures both vertical and lateral acceleration with high resolution. The unconventional manufacturing method of this accelerometer requires a high supply voltage (15-30V). Two inductors are used in this accelerometer, one on the seismic mass and the other, separated by air, on the immobile part. When a current is imposed on the first inductor, a magnetic field is created, resulting in a current proportional to the amplitude of the first current in the second winding, which is in turn proportional to the distance between the two windings [5].

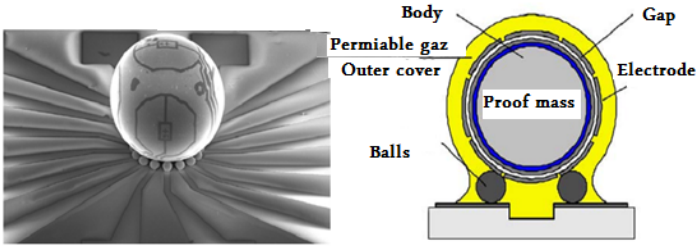

Fig. 1.11: An electromagnetic levitation accelerometer [5]

Each type of accelerometer has distinct advantages and is selected based on the specific requirements of the application, including sensitivity, frequency range, environmental conditions, and power consumption.

1.5 Advantages of choosing capacitive accelerometers

Accelerometers are categorized into various types based on their transduction mechanisms, which convert proof-mass displacement into measurable signals. These categories include piezoresistive, piezoelectric, capacitive, resonant, optical, thermal, and tunneling accelerometers, each with its specific advantages and disadvantages (see Figure 1.12). In this work, we chose the capacitive accelerometer type's due to its remarkable features compared to other types. This section focuses on capacitive accelerometers, a pivotal class of sensors in today's technological ecosystem. They are distinguished by their high precision, measuring acceleration through changes in capacitance caused by the displacement of a proof mass due to external forces. The primary advantage of capacitive accelerometers is their high sensitivity, allowing for the detection of minute changes in acceleration. This feature is crucial for their application in industries such as automotive, aerospace, and consumer electronics, where precise acceleration measurements are vital. Capacitive accelerometers also exhibit superior linearity and low noise levels, further enhancing the accuracy of measurements. Their compact size and light weight make them exceptionally suited for applications with stringent space and weight requirements. Furthermore, these accelerometers are characterized by their robust reliability and long-term stability, ensuring dependable performance over time. They possess a broad dynamic range, enabling accurate measurement of both low and high levels of acceleration. The objective of this section is to provide a comprehensive analysis of capacitive accelerometers, underlining their distinctive advantages, particularly in terms of sensitivity, performance, and reliability [19, 28]. Additionally, we

aim to discuss the modeling and simulation of capacitive accelerometers to enhance their performance and broaden their application spectrum as outlined in Chapter 2. Through detailed examination, we endeavor to unlock the full potential of capacitive accelerometers, highlighting their transformative impact across various technological and scientific fields.

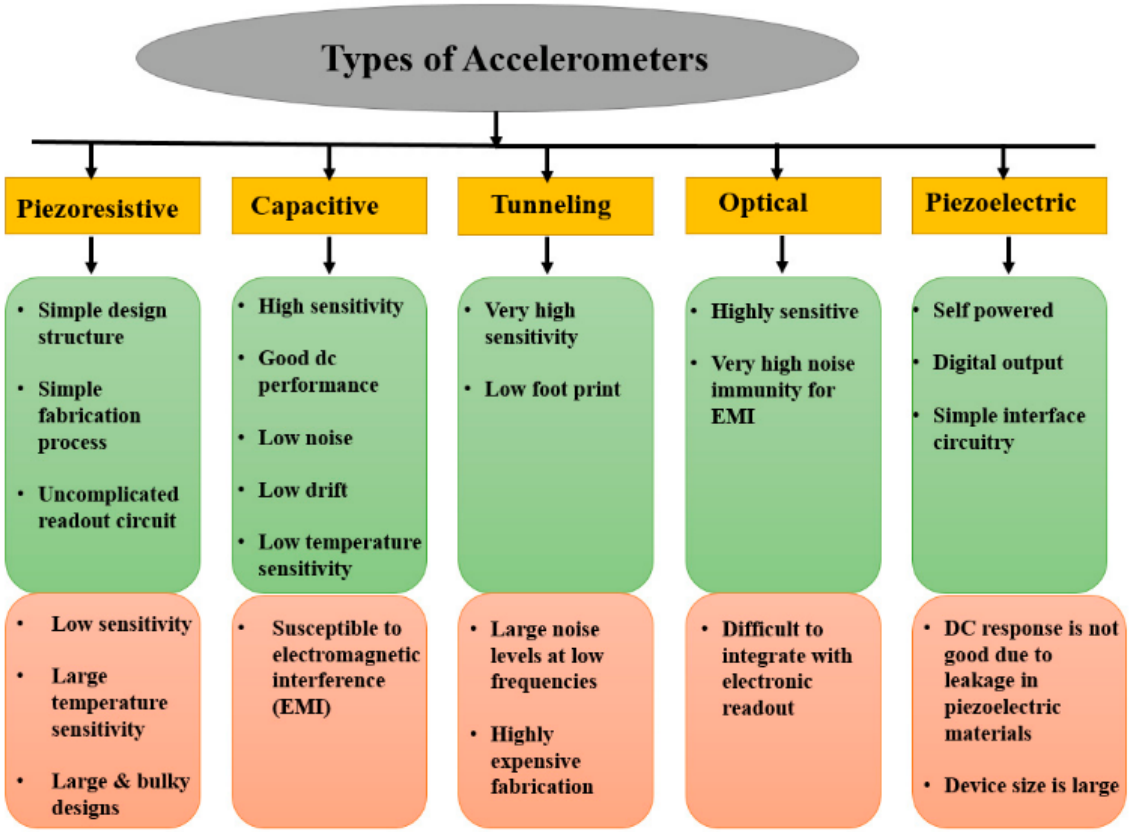

Fig. 1.12: Accelerometer types with its advantages and drawbacks [6]

1.6 Metrological characteristics and influencing factors

1.6.1 Metrological characteristics

Understanding the metrological characteristics of accelerometers is vital for accurate measurements and optimal sensor performance.

1.6.1.1 Sensitivity and frequency response

The sensitivity of an accelerometer is a critical metric, defined as follows:

$$\left|\frac{S}{S_m}\right| = \frac{\frac{1}{\omega_0^2}}{\sqrt{1+\left(\frac{\omega_c}{\omega}\right)^2}\sqrt{\left(1-\frac{\omega^2}{\omega_0^2}\right)^2+\left(2\zeta\frac{\omega}{\omega_0}\right)^2}}$$

Typical values for sensitivity (S_m) range from approximately 10 to 100 pc/g, with the resonant frequency ($f_0 = \frac{\omega_0}{2\pi}$) typically lying between 10 and 50 kHz [4].

1.6.1.2 Measurement range and linearity

The effective measurement range of accelerometers is bounded by:

- Lower limit: Electrical noise from cables and amplifiers, and pyroelectric effects. Sensitivity thresholds can be as low as 0.001g.
- Upper limit: Structural strength of the sensor, typically between 5000 to 10,000g, higher in high-impact applications.

1.6.1.3 Accelerometer response

The response curve of a piezoelectric accelerometer comprises two zones:

- A linear zone where sensor response aligns with the amplitude of the measured signal.
- A resonance zone where measurements are amplified uncontrollably and should be avoided [4].

1.6.2 Sensor mounting

Proper sensor mounting is crucial for accurate measurements. The sensor should be placed as close as possible to the bearings, minimizing the number of intermediary parts. Clean, smooth, flat contact surfaces, aligned with the measurement direction, are essential [4].

1.6.3 Sensor influence factors

Various factors can influence the performance of piezoelectric sensors, affecting the accuracy of measurements:

1.6.3.1 Temperature

Temperature affects both the piezoelectric coefficient and the mechanical-electrical transfer function, impacting the sensor's electrical sensitivity. Understanding the sensitivity variation with temperature is essential for precise measurements [4].

1.6.3.2 Aging

Sensor characteristics may irreversibly change over time due to aging. Regular calibration can help mitigate sensitivity drift due to aging or accidental overload [4].

1.6.3.3 Noise due to cable connection

Cable-induced noise arises from mechanical or thermal changes affecting charge movements. Incorporating a miniaturized signal conditioner within the sensor can eliminate such noise issues [4].

1.6.3.4 Noise due to ambient acoustic pressure

High-intensity acoustic fields can interfere with measurements, especially in cases of direct impact on the piezoelectric element. Decoupling the piezoelectric element from the base-housing assembly is essential in such scenarios [4].

1.6.3.5 Zero offset

Ceramic accelerometers often exhibit an inherent zero offset, which can be minimized temporarily by subjecting the sensor to repeated shocks. However, this offset should not exceed 1 to 2% of the peak amplitude [4].

1.7 Understanding IoT and its applications

1.7.1 Internet of Things (IoT)

The Internet of Things (IoT) refers to a network of interconnected devices that can communicate and share data with each other over the internet without requiring human intervention. This concept represents the convergence of physical devices, digital systems, and the internet, enabling the seamless exchange of information and automation of processes. The origins of the IoT can be traced back to the early 2000s, although the term gained significant popularity around 2010. Its development has been

propelled by advancements in wireless communication, miniaturization of sensors, and the proliferation of internet connectivity [38, 39].

The IoT has the potential to encompass and connect three dimensions: devices such as accelerometers, which are utilized in our study for data collection (see Part **??**), networks, such as the internet or Raspberry Pi, which facilitate communication between IoT devices, and intelligence, including data algorithms or processing methods, which enable meaningful analysis of the collected data (see Fig. 1.13). The proliferation of

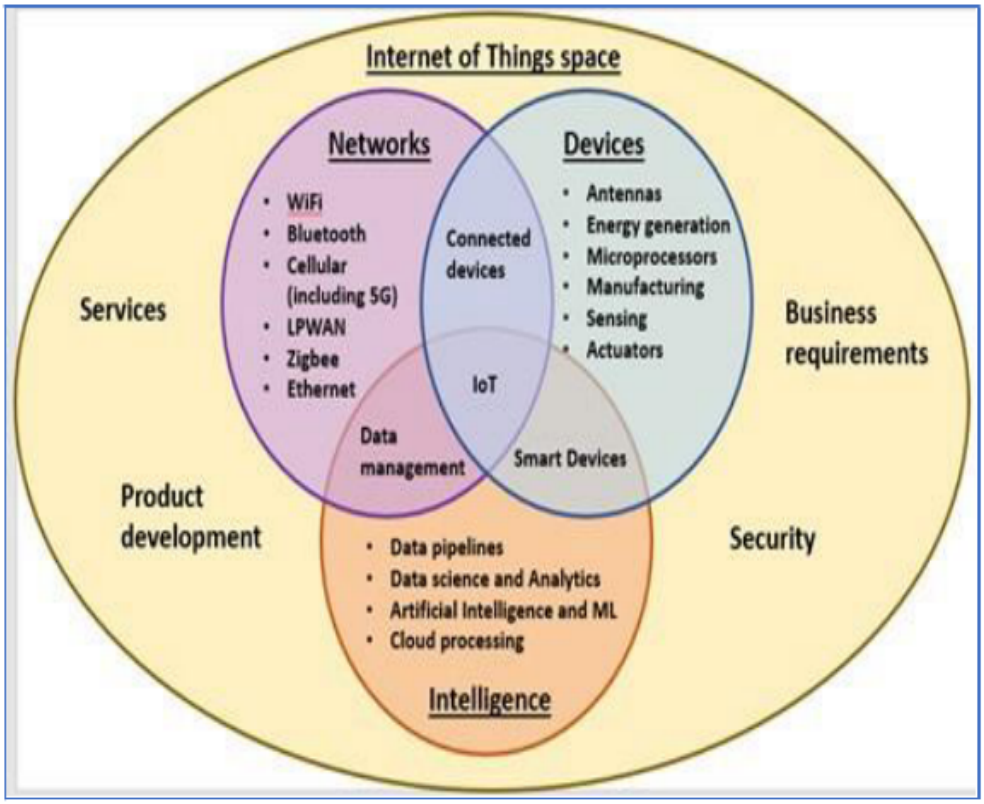

Fig. 1.13: The three Dimensions of IoT [40]

internet connectivity has enabled inanimate objects to understand their environment, have autonomous thoughts, and take action without human intervention. These devices are embedded with sensors, software, and other technologies, enabling them to collect and exchange data, making them "smart" and capable of interacting with their environment [41, 42]. At its core, IoT relies on the seamless integration of hardware, software, and connectivity to enable the exchange of information and automate processes [43]. This interconnected ecosystem of devices opens up a wide range of applications across various industries, transforming how we interact with technology and the world around us.

1.7.2 Key components of IoT

IoT systems typically consist of the following components:

- **Sensors and actuators:** These devices are responsible for collecting data from the environment (sensors) and performing actions based on that data (actuators) [44]. They can measure various parameters such as temperature, humidity, light, motion, and more.
- **Connectivity:** IoT devices rely on internet connectivity to communicate with each other and central servers. This can be achieved through various means such as Wi-Fi, Bluetooth, cellular networks, or specialized IoT protocols like LoRaWAN and Zigbee [45, 46].
- **Data processing:** The data collected by IoT devices needs to be processed to extract meaningful insights. This can involve filtering, aggregation, analysis, and storage of data, often leveraging cloud-based services or edge computing capabilities [46].
- **User interface:** Interfaces such as mobile apps or web dashboards allow users to interact with IoT devices, monitor their status, and control their behavior remotely [45].

1.7.3 Applications of IoT

The versatility of accelerometer-based IoT enables its application across a wide range of domains. Today, accelerometers are pivotal in various sectors, including astronomy, where their role, particularly as gyroscopes in satellites, is invaluable [47]. Accelerometers find versatile applications in various domains, from assessing the longevity of bridges through vibration-based inspection to seismic monitoring [48, 49], and collecting data in hexacopters [50]. Furthermore, commercial accelerometers such as the ADXL345 have been employed in innovative applications such as an IoT-enabled accelerometer-based home security system [51] and smart IoT helmet for motorbike riders [52]. This technology finds application in numerous other fields as well, including but not limited to:

- **Smart homes:** IoT devices enable homeowners to automate and remotely control various aspects of their homes, including lighting, heating, security systems, and appliances[53].

- **Healthcare:** IoT technologies play a crucial role in remote patient monitoring, personalized medicine,sport for predicting injuries, and healthcare management systems, improving the quality of care and patient outcomes[54–61].
- **Industrial IoT (IIoT):** In industries such as manufacturing, transportation, and agriculture, IoT facilitates predictive maintenance, supply chain optimization, asset tracking, and process automation, leading to increased efficiency and productivity[62, 63].
- **Smart cities:** IoT enables cities to optimize resource utilization, enhance public safety, and improve infrastructure management through applications like smart traffic management, waste management, and environmental monitoring[45].

These applications represent just a fraction of the potential of IoT, which continues to evolve and expand into new domains, driving innovation and transforming industries worldwide. The future of accelerometer technology is intrinsically linked to advances in materials science and nanotechnology. In summary, the evolution of accelerometers demonstrates the field's capacity for adaptability lead a stage has expanded the realm of possibilities application in this thesis in industry 3 and robotics 4 .

1.8 Conclusion

As we conclude this chapter on the state-of-the-art fundamentals of accelerometer technology, we reflect on the profound impact and diverse applications of these remarkable devices. From their inception in the early 20th century to the advanced microelectromechanical systems (MEMS) of today, accelerometers have undergone a significant transformation. This journey, marked by continuous innovation and adaptation, has positioned accelerometers as a cornerstone in modern technology, influencing sectors from automotive and aerospace to consumer electronics and healthcare.

The historical development of accelerometers highlights a path of relentless pursuit of precision, miniaturization, and versatility. The transition from mechanical models to MEMS technology underscores the ingenuity and resourcefulness of scientists and engineers in overcoming technical challenges. Today's accelerometers, benefiting from advancements in materials science and microfabrication, offer unprecedented sensitivity and reliability, opening new horizons in various applications.

This chapter has delved into the operational principles of accelerometers, shedding light on the intricate process of converting mechanical motion into electrical signals. Understanding these principles is crucial for professionals and researchers who rely on

accurate and reliable vibration measurements. Moreover, the exploration of different types of accelerometers, including capacitive, piezoresistive, and piezoelectric models, has provided insights into their unique characteristics and suitability for specific applications. The integration of accelerometers in emerging technologies, particularly in the realm of IoT, signifies their growing importance in the digital era. As accelerometers continue to play a pivotal role in shaping future technological advancements.

In summary, this chapter has offered a comprehensive overview of accelerometer technology, emphasizing its historical evolution, operational principles, and diverse applications. As we look forward to future developments in this field, it is evident that accelerometers will continue to be an essential component in the advancement of technology. The journey of accelerometer technology, characterized by innovation and adaptability, stands as a testament to human ingenuity and the endless possibilities of scientific exploration.

Chapter 2

Capacitive accelerometer modeling: optimization-Based parameter for refining Its performance

2.1 Introduction

The evolution of sensor technology has been pivotal in advancing various scientific and technological fields. Among these sensors, capacitive accelerometers have emerged as a cornerstone in applications ranging from navigation systems in aerospace to motion detection in consumer electronics.

This chapter focuses on capacitive accelerometers, which stand out for their precision and lightweight design. Unlike other types of accelerometers, these devices offer distinct advantages in terms of sensitivity and miniaturization, making them ideal for a wide array of applications. In the current technological landscape, where the demand for accurate and compact sensors is ever-growing, understanding and optimizing the performance of capacitive accelerometers is of paramount importance.

The primary aim of this chapter is to present an in-depth exploration of capacitive accelerometer technology. This includes a detailed examination of their working principles, design considerations, and the development of an advanced mathematical model to enhance their performance. By conducting a thorough analysis of these aspects, this study seeks to contribute to the optimization of capacitive accelerometers, thereby broadening their application spectrum and elevating their role in both technological and scientific domains.

In the following sections, we will delve into the principles underpinning capacitive accelerometers, scrutinize key design parameters, and introduce a novel mathematical model that aims to refine accelerometer performance. Through this comprehensive exploration, we aspire to unlock new potentials and applications for capacitive accelerometer technology.

2.2 Principle and design of capacitive accelerometers

2.2.1 Working principle

Capacitive accelerometers are predicated on the principle of capacitive sensing, a method whereby acceleration is discerned through the detection of changes in capacitance. Central to this mechanism is the proof mass, designed to respond to external accelerative forces. This response manifests as a displacement of the proof mass, leading to a variation in the distance between it and a set of strategically placed electrodes, often arranged to form a parallel plate capacitor. Such displacement induces a proportional alteration in the capacitance, a phenomenon that is subsequently transformed into an electrical signal for acceleration quantification. Figure 2.1 illustrates a schematic representation of a single proof mass MEMS-based capacitive accelerometer, highlighting the components and their arrangement within the device. Integral to the

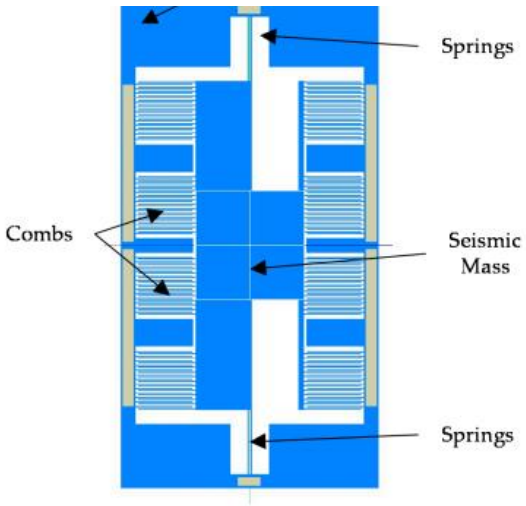

Fig. 2.1: Schematic Representation of a Single Proof Mass MEMS-Based Capacitive Accelerometer[17]

accelerometer structure is the stator, a stationary component that encapsulates the

electrodes. Commonly constructed from materials such as silicon or polymers, the stator plays a pivotal role in ensuring the precision of capacitance measurements. The electrodes are typically configured in a differential layout, a design choice aimed at amplifying sensitivity and mitigating common-mode noise.

2.2.2 Design aspects

The design of capacitive accelerometers involves intricate considerations to optimize their performance and applicability. Key design aspects include:

- **Electrode layout:** The design and arrangement of electrodes are critical for accuracy. Common layouts include parallel plates and interdigitated structures, each offering unique advantages in terms of sensitivity and range.
- **Material choices:** Material selection for both the proof mass and electrodes is pivotal. Silicon, known for its mechanical stability and compatibility with microfabrication, is widely used. Advanced polymers and composites are explored for specific applications, enhancing characteristics like durability and environmental resistance [64, 23].
- **Structural configurations:** The mechanical structure, encompassing the suspension system and proof mass, is tailored to achieve desired performance metrics. This includes the optimization of suspension beam lengths (X2 and X3, typically ranging from 400 µm to 500 µm) and beam width (X4, between 6 µm to 8 µm), impacting the accelerometer's frequency response and sensitivity[65].
- **Comb overlap design:** The overlap length of the comb structure (X1, 150 µm to 250 µm) is fine-tuned to balance sensitivity and stability, directly influencing the device's capacitance and operational range[65].
- **Damping mechanisms:** Careful design of damping systems, integral in controlling the accelerometer's dynamic response, is crucial. These systems mitigate the impact of external vibrations and shocks, ensuring consistent performance.

Figure 2.2 provides a visual representation of a single proof mass, two-degree-of-freedom (2-DoF) MEMS-based capacitive accelerometer. This schematic exemplifies the integration of these design considerations, illustrating how each aspect contributes to the overall functionality and efficiency of the accelerometer.

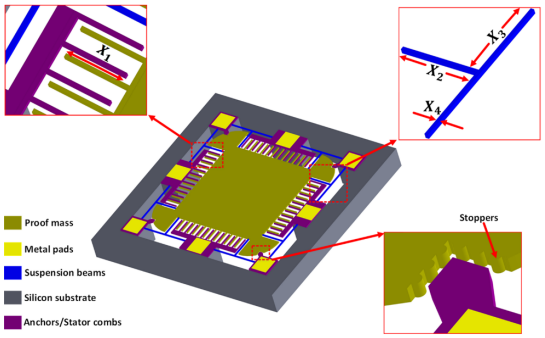

Fig. 2.2: Schematic Representation of a Single Proof Mass, Two-Degree-of-Freedom (2-DoF) MEMS-Based Capacitive Accelerometer[65]

These design aspects are critical in defining the operational efficiency and application scope of capacitive accelerometers. Advances in micro-fabrication technology continue to refine and expand the capabilities of these devices.

2.3 Mathematical modeling of capacitive accelerometers

2.3.1 Modeling of capacitive accelerometer

The mathematical model can be extracted from the accelerometer's mechanical part by using Newton's second law[19].

$$Ma = F_{\text{inertial}} + F_{\text{damping}} + F_{\text{spring}}‘ \tag{2.1}$$

By simplifying equation‘2.1:

$$m\frac{d^2x}{dt^2} + b\frac{dx}{dt} + kx = m\frac{d^2y}{dt^2} \tag{2.2}$$

Where:

- m is the mass
- k is the stiffness constant of the spring
- b is the damping constant of the damper

In order to analyze the dynamic behavior of the system described by equation 2.2 in the frequency domain, we employ the Laplace transformation. This transformation

allows us to express the differential equation in terms of algebraic equations involving the Laplace variable s. Consequently, equation 2.2 transforms into the following form:

$$ms^2 + kX + bsX = -ms^2Y \tag{2.3}$$

The two equations below typically characterize the damping rate and the natural frequency of a capacitive sensor [19]:

Natural frequency:

$$\omega_n = \left(\frac{k}{m}\right)^{1/2} \tag{2.4}$$

Damping rate:

$$\xi = \frac{\text{actual damping}}{\text{critical damping}} = \frac{b}{2m\omega_n} \tag{2.5}$$

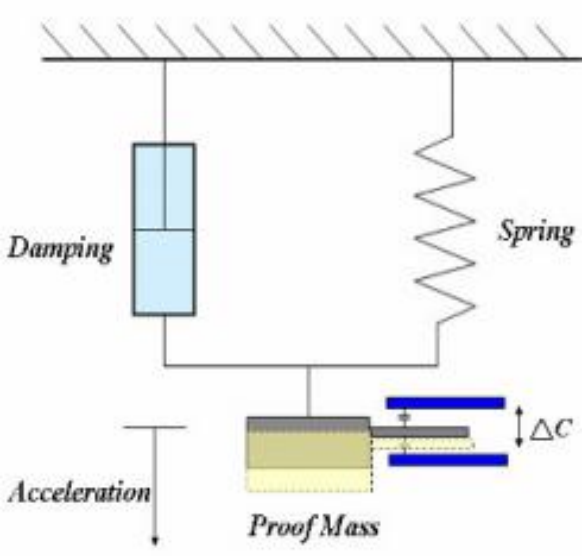

Fig. 2.3: Modeling of capacitive accelerometer [19]

2.4 Simulating measurement errors using damping rate as a parameter

2.4.1 Correlation between error and damping ratio

By replacing equations (2.4,2.5) in equation 2.3 and after simplification, we get:

$$X = \frac{Y\omega^2}{\omega_n^2 \left[\left(1 - \left(\frac{\omega}{\omega_n} \right)^2 \right)^2 + \left(2\zeta \frac{\omega}{\omega_n} \right)^2 \right]^{1/2}} \tag{2.6}$$

The following equation represents the error between relative and absolute acceleration:

$$E = \left[\frac{X}{Y} \right] - 1 \tag{2.7}$$

From equation 2.6 and 2.15, we can express the measurement error as a function of natural and relative frequency:

$$E = \left[\frac{1}{\left[\left(1 - \left(\frac{\omega}{\omega_n} \right)^2 \right)^2 + \left(2\zeta \frac{\omega}{\omega_n} \right)^2 \right]} \right]^{1/2} - 1 \tag{2.8}$$

2.4.2 Simulation correlating error and damping ratio

Table 2.1 provides an overview of the simulation parameters for the proposed mathematical model:

Table 2.1: Parameter's value

Parameter	Value
Spring constant k	$400\,\mathrm{N/m}$
Seismic mass m	$2.51 \times 10^{-5}\,\mathrm{kg}$
Damping constant	$0.2\,\mathrm{kg/s}$
Electrode gap d	$50\,\mu m$
Static capacitance C	$1.25\,\mu F$
Amplitude	2

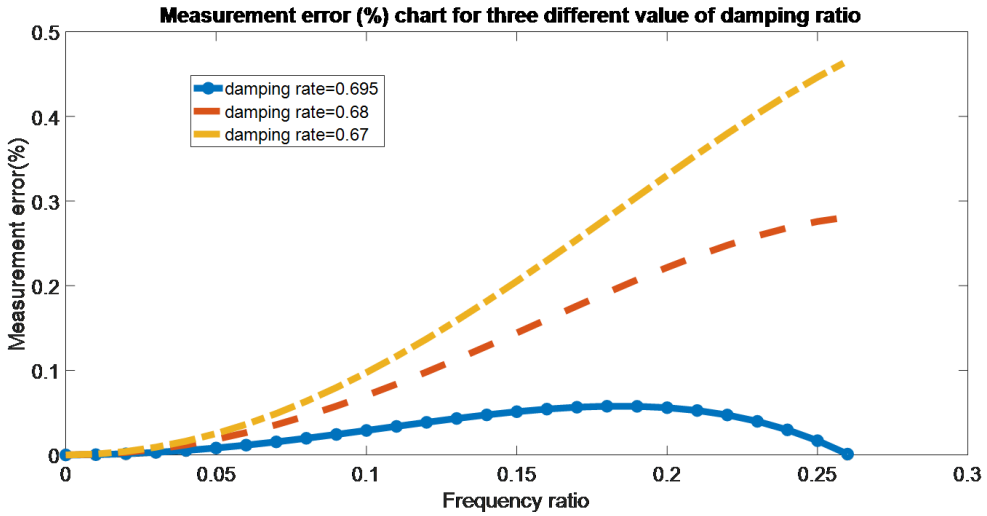

Fig. 2.4: The measurement error as a function of the frequency ratio for three values of the damping rate

Figure 2.4 illustrates the simulation results depicting the relationship between measurement error and frequency ratio for three distinct damping rate values. Notably, the damping rate proposed in this study (0.695) significantly reduces the accelerometer's measurement error, achieving a remarkably low value.

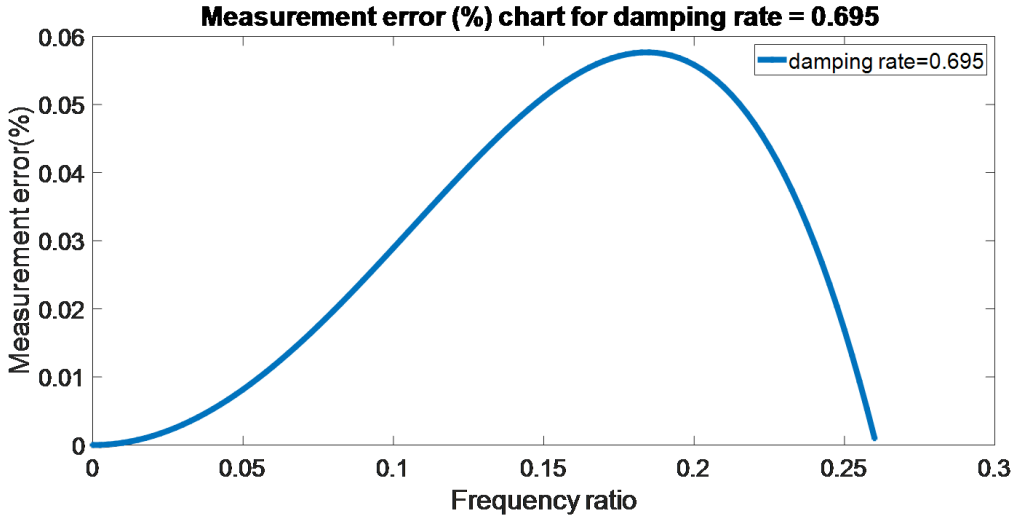

Fig. 2.5: The measurement error as a function of the frequency ratio for damping rate value 0.695

Figure 2.5 presents the simulation results, demonstrating the measurement error's dependency on the frequency ratio, with the frequency ratio varying between 0 and 0.35. These simulations are conducted using the proposed damping rate of 0.695.

The outcomes suggest that for minimal measurement error, the frequency ratio ω/ω_n should not exceed 0.27. Furthermore, the natural frequency-related frequency has been enhanced to 520 Hz.

Table 2.2 provides a comparative analysis between the simulation results of this study and those of previous studies, considering various damping ratio values.

Table 2.2: Comparative results of measurements errors

Model	ξ	$\omega_n\,(Hz)$	Interval of relative frequency $\omega\,(Hz)$	Max error (%)
[31]	0.67	2000	[0.520]	0.47
[27]	0.68	2000	[0.520]	0.28
This work	0.695	2000	[0.520]	0.06

2.4.3 Analysis of settling time

Settling time (t_s) characterizes the duration required for the harmonic response to reach stability following vibration [66–69]. It denotes the time taken for the response to fall within defined threshold values. In this analysis, we consider two threshold levels: $\Delta = 0.02$ and $\Delta = 0.05$. Settling time can be calculated using the following equations:

Threshold $\Delta = 0.05$:

$$t_s = \frac{3.5}{\xi\omega_n} \tag{2.9}$$

Threshold $\Delta = 0.02$:

$$t_s = \frac{4.2}{\xi\omega_n} \tag{2.10}$$

In contrast, the settling time for the model presented in [66] is determined as follows:

$$t_s = \frac{4}{\xi\omega_n} \tag{2.11}$$

The comparative results for settling times of the three models, including the proposed model, across various damping ratio values and both threshold levels $\Delta = 0.02$ and $\Delta = 0.05$ are detailed in Table 2.3:

Table 2.3: Calculate the settling time t_s

Model	ξ	t_s (ms) [66]	t_s (ms) [69] ($\Delta = 0.02$)	t_s (ms) [69] ($\Delta = 0.05$)
[31]	0.67	1.34	1.4	1.17
[27]	0.68	1.36	1.42	1.19
This Study	0.695	1.395	1.45	1.2

The difference in settling time is minimal, indicating that all three models settle or stabilize effectively. However, when $\Delta = 0.02$, the system is more stable.

2.4.4 Simulation of capacitance variation for different damping ratios

Figure2.6 illustrates two parallel beams representing the capacitance of the accelerometer.

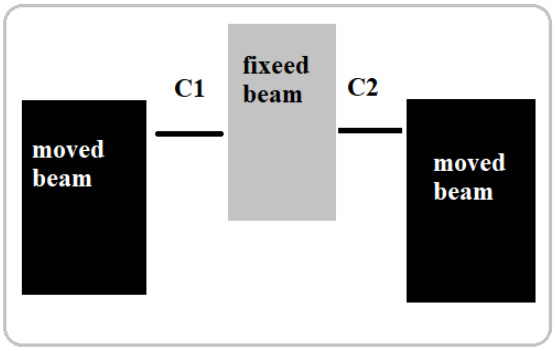

Fig. 2.6: Two parallel beams representing the capacitance of the accelerometer

The relationship of static capacitance is given by [70, 71]:

$$C_0 = \frac{A \times \varepsilon}{d} \tag{2.12}$$

When the moving electrode is displaced, it results in an increase in capacitance due to the change in area A, the distance d between the electrodes, and the permittivity ε of free space.

Assuming a small approximation of displacement ($x << d$), the top and bottom capacitance C_1 and C_2 are changed to:

$$C_1 = \frac{A \times \varepsilon}{d + x} \tag{2.13}$$

$$C_2 = \frac{A \times \varepsilon}{d - x} \tag{2.14}$$

The capacitance variation ΔC due to displacement x is given by:

$$\Delta C = C_1 - C_2 = \frac{2C_0 x}{d} \tag{2.15}$$

By replacing equation2.6 in equation 2.15, we obtain a formula for capacitance variation as a function of displacement:

$$X = \frac{2C_0\omega_n^2 Y}{\omega_n^2 d\left[\left(1-\frac{\omega}{\omega_n}\right)^2 + \left(2\zeta\left(\frac{\omega}{\omega_n}\right)^2\right)\right]^2} \tag{2.16}$$

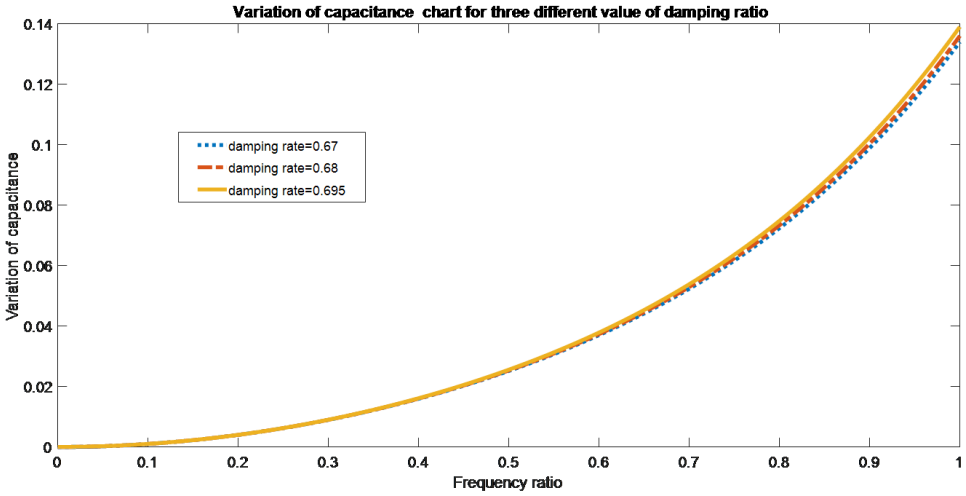

Fig. 2.7: Capacitance variation as a function of frequency ratio for three values of damping ratios

Figure 2.7 presents a graphical representation of how capacitance varies concerning the frequency ratio for three distinct damping ratios (0.67, 0.68, 0.695). Notably, the figure underscores that the proposed model exhibits greater sensitivity compared to the models described in references [31] and [27].

2.5 Conclusion

In this chapter, we have delved into the fascinating realm of capacitive accelerometers and embarked on a journey to unravel their intricate mechanical behavior. Our explorations have culminated in the development of a novel formula that takes into account capacitance variation, damping rate, frequency ratio, electrode gap, and other critical parameters. As we conclude our investigation, we present the following key findings and insights:

1. In the course of this research, we have introduced a novel mathematical model with a damping rate of 0.695, which has proven to be a significant breakthrough

in reducing measurement errors when compared to existing models. The maximum measurement error was substantially mitigated to a mere 0.06%.

2. Remarkably, the settling time of the proposed model is on par with that of existing models, indicating its efficacy in providing a stable and reliable measurement environment.

3. Notably, we have observed that capacitance variation exhibits greater sensitivity in the proposed model as opposed to previous models. This heightened sensitivity can be a valuable asset in applications where precision is paramount.

Through this research, we have added to the body of knowledge surrounding capacitive accelerometers, offering a deeper understanding of their mechanical intricacies. Importantly, our contributions extend to the practical realm, enhancing the accuracy and reliability of these accelerometers in a wide range of applications, spanning aerospace, sports, health monitoring, and beyond. This chapter lays the foundation for further advancements and innovations in the field, ultimately improving the performance and utility of capacitive accelerometers.

Chapter 3

Accelerometer-Based Raspberry Pi for circular chart recorder

3.1 Introduction

This chapter delves into the integration of Raspberry Pi-enabled accelerometers within chart recorders. It capitalizes on advancements in microelectronics, wireless sensor technologies, and cost-effectiveness to usher in a new era of sensor applications across various domains. The chapter's structure unfolds as follows: Section **??** elucidates the components utilized in our experimental setup. Section 3.2 meticulously details the experimental procedures, outcomes, and analyses. In Section 3.4, we underscore the merits of our innovative chart recorder-based accelerometer and draw comparisons with conventional chart recorder systems. Section 3.5 thoughtfully scrutinizes the limitations inherent in our system. Ultimately, the chapter concludes 3.7 by encapsulating pivotal findings and charting a course for prospective research directions. In our experimental setup, accelerometers take center stage, interfacing with a Raspberry Pi, which, in turn, connects to a stylus needle. The ensuing data is transmuted into visual representations on a dedicated monitor. Software configuration involves the deployment of the Raspbian operating system and Thonny Python [72].

3.2 Enhancing data precision with chart recorder-Based accelerometer integration

In this section, we delve into the innovative approach of integrating a novel pressure chart recorder-based accelerometer into our experimental setup. This integration holds

the promise of revolutionizing data acquisition by merging mechanical and electronic charting capabilities. We recognize the indispensable role of pressure circular chart recorders in industrial monitoring processes, and here, we elucidate the rationale behind our decision to embrace this fusion of analog and digital technologies. Pressure circular chart recorders are intrinsic to industrial monitoring, providing reliable data for various applications. They have a proven track record of accuracy and durability, making them an indispensable tool in quality assurance, process control, and system diagnostics. However, in the era of technological advancements, we find ourselves at a crossroads where traditional chart recorders coexist with modern sensor-based solutions. The mains contribution posits that the coexistence of these technologies is not only feasible but also advantageous in many scenarios. By integrating a novel accelerometer into the traditional chart recorder setup, we aim to harness the strengths of both worlds. This symbiotic relationship offers several key advantages:

- Cost-Effective transition: Upgrading or maintaining a hybrid analog-digital pressure data logger alongside existing chart recorders is a cost-effective approach. It requires minimal investment compared to a full-scale digital transformation, making it accessible to a wide range of industries, particularly those engaged in short-term testing.

- Time-Efficiency: The integration process is streamlined, ensuring minimal disruption to ongoing operations. Data can continue to be collected using established chart recorder systems while simultaneously benefiting from the enhanced capabilities of the accelerometer.

- Data accuracy: Accelerometers, though often underestimated, have seen significant improvements in accuracy. Their integration into industrial setups facilitates the acquisition of highly precise data. This newfound accuracy enables companies to make more informed decisions and achieve superior results.

- Versatility: The versatility of the accelerometer cannot be overstated. Its applications span various industries, from monitoring bridges' life expectancy and structural health to innovative uses like fall detection in wearable devices and real-time power grid monitoring.

Our experimental setup involves the strategic deployment of various components, with the accelerometer serving as the cornerstone. The accelerometer is meticulously connected to a Raspberry Pi and affixed to the pen needle for optimal data acquisition. A dedicated monitor visualizes the resultant graphs generated by the accelerometer.

Prior to conducting tests, we ensure the Raspberry Pi is equipped with the Raspbian software system, including Thonny Python, to facilitate seamless data collection and analysis.

In the subsequent sections of this chapter, we will delve into the specifics of the components used in our test bench, the results of our experiments, and a comprehensive comparison between our chart recorder-based accelerometer system and existing chart recorder solutions. Additionally, we will explore the limitations and drawbacks of our proposed system, culminating in a conclusive discussion of our findings and potential avenues for future research and development.

3.3 Description of the used system

The proposed chart recorder-based accelerometer is composed of a Raspberry Pi 3 B+ and an accelerometer, as shown in Fig3.1. For more details about the system used, please refer to the appendix (Appendix A: Raspberry Pi Setup with ADXL345 Accelerometer.

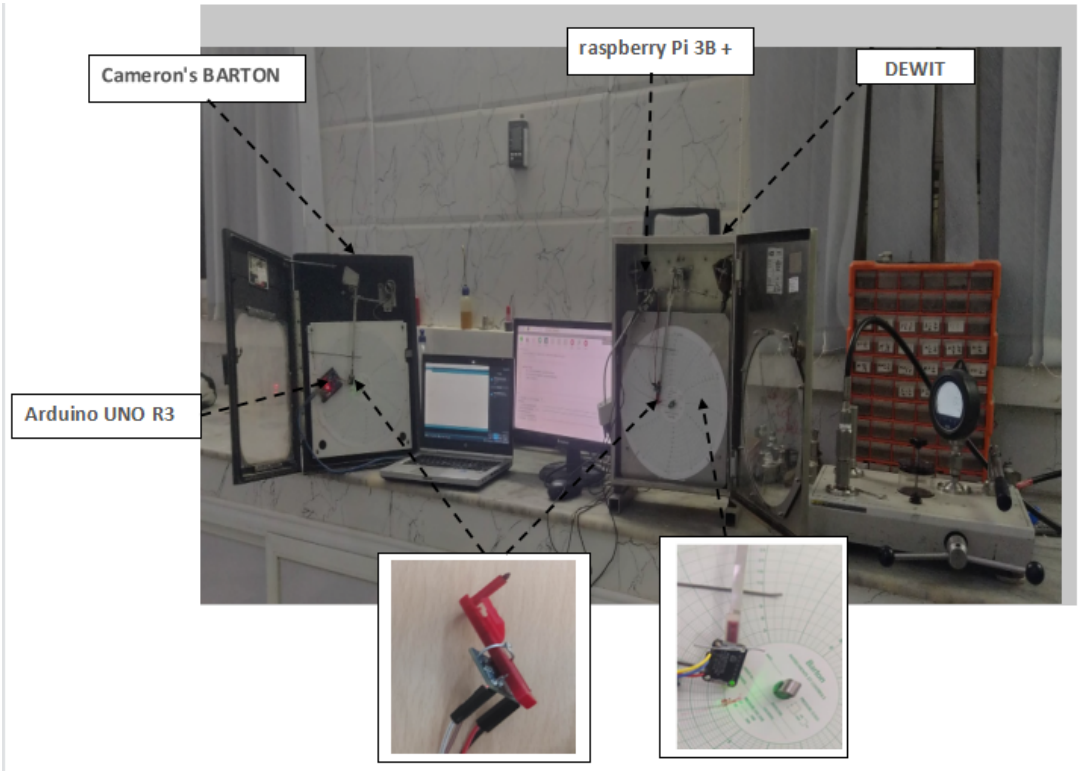

Fig. 3.1: View of the used devices for the considered chart recorder-based accelerometer

3.3.1 Required components

3.3.1.1 Chart recorders

In the context of industrial monitoring and data acquisition, a chart recorder is a substantial and robust instrument employed for tracking and documenting essential system parameters. These parameters encompass variables like gas and liquid flow rates, pressure within vessels, and various other system attributes.

The recording process is facilitated by a slender pen-like device connected to an accelerometer. The primary objective of this arrangement is to meticulously archive operational data over time. In our study, the chart recorder serves the specific purpose of quantifying pressure fluctuations. Within this study, we categorize chart recorders into two distinct types:

- BARTON chart recorders, developed by Cameron, represent the industry's benchmark for precise and accurate pressure measurement and recording. They find extensive applications in controlling pressure variations within pipelines or vessels. These recorders are equipped with a rupture-proof bellows Differential Pressure Unit (DPU), featuring over-range safety measures and pulsing dampening for enhanced performance [73].

- DEWIT chart recorders offer a broad temperature range spanning from -170 to 600 degrees Celsius, a minimum temperature span of 60 degrees Celsius, and a remarkable pressure range of up to 60,000 psi (4000 bar). They feature options for bottom or back connections, mechanical spring-wound clocks, and switchable clockwork, and select models even support dual or triple pens. Additionally, these recorders are designed for convenient panel mounting [74].

3.3.1.2 Accelerometer

The adopted accelerometer types in this paper are:

- The H3LIS331DL tri-axial accelerometer boasts low noise and an impressive high-g range of 200 g per axis [72]. It offers six degrees of freedom and can operate effectively within a wide temperature range, from -50°C to +85°C, making it highly flexible and robust [75].

- The ADXL345 is a compact, slim, and energy-efficient 3-axis accelerometer renowned for its high-resolution measurements (13-bit) of up to ±16 g. Digital

output data is presented in a 16-bit two's complement format and can be accessed via either an SPI (3- or 4-wire) or I2C digital interface.

The ADXL345 finds extensive utility in mobile device applications. It excels at measuring static gravity acceleration for tilt-sensing applications and dynamic acceleration caused by motion or shocks. Its impressively high resolution (4 mg/LSB) empowers the precise detection of inclination changes of less than 1.0 degree [76].

Comprehensive technical specifications of the commercial accelerometers ADXL345 and H3LIS331DL can be found in references [76] and [72], respectively.

3.3.1.3 Raspberry Pi board: 3B+

The Raspberry Pi 3B+ is a third-generation single-board computer with detailed specifications available in the manual [77]. Raspberry Pi serves as a microcomputer in IoT applications, including its use in data collection systems that rely on IoT sensors with onboard processing capabilities for tasks such as cow activity recognition [78].

3.3.1.4 Arduino UNO R3

Arduino is an excellent board for learning both electronics and coding, this multi-functional microcontroller is equipped with the well-known ATmega328P and the AT Mega 16U2 Processor. This board provides a great first experience within the world of Arduino [79]. Basically, the monitor is a multi-sensory smart gadget based on the Internet of Things that monitors cow behavior [80].

Figure 3.1 is a global view of the used components in the carried-out experiments.

Table 3.1: Main Price Components for the Proposed System

Component	Model/Type	Estimated Price Dinar (DZD)
Computing unit	Raspberry Pi 3B+	12 000 DZD
Memory Oracle	Samsung 32G Memory Card	3200 DZD
Sensor	ADXL345 Accelerometer	1 200 DZD
Energy supply	50,000mAh Power Bank	5 000 DZD

In Table 3.1, we present a concise overview of the primary cost components for our proposed system, emphasizing its affordability compared to conventional technologies. The key components, including the Raspberry Pi 3B+ computing unit, Samsung 32G Memory Card, ADXL345 Accelerometer sensor, and the 50,000 mAh Power Bank for energy supply, collectively shape the system's capabilities.

Our analysis indicates that the proposed system stands out as a cost-effective solution when compared to traditional technologies. This affordability not only positions our innovative system as an economically viable choice but also opens avenues for broad accessibility and adoption across various applications within the realm of advanced technologies.

3.4 Discussion and results

Figure 3.2 illustrates the complete experimental setup of the proposed system, detailing its operation. Notably, when the pressure reaches high levels, the needle (represented by element 1 in grey) of the circular chart recorder (depicted as element 2 in green dashed lines) undergoes significant displacement, trailing the pen (element 3 in red) to record pressure values onto the circular chart paper during each displacement. Consequently, the data recorded by this chart recorder can be effortlessly converted into electronic data by affixing an accelerometer (element 4) to the pen's tip.

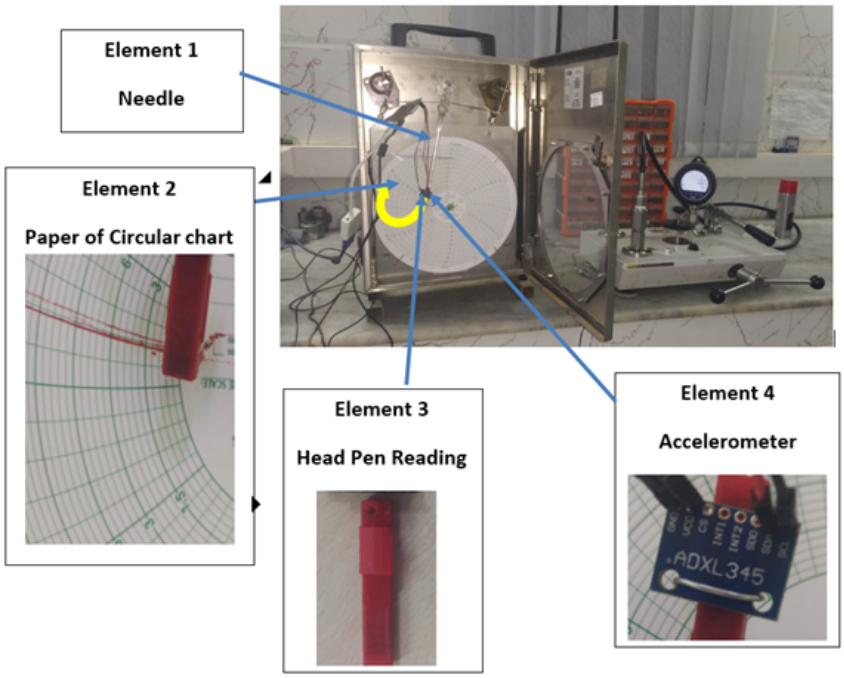

Fig. 3.2: detailed experimental bench

It is worth noting that the pen's tip moves in response to pressure variations; specifically, as pressure increases, the pen's tip moves upward, and vice versa. For

this precise reason, the accelerometer is affixed to the pen's tip, allowing for the convenient acquisition of data for every movement of the tip over extended periods. This approach stands in contrast to the traditional needle-based method, which may encounter issues during data collection due to mechanical failures associated with analog clock mechanisms.

Among the carried out experiments, a select few were chosen to illustrate the significant advantages of employing IoT-based accelerometers for data acquisition from traditional chart recorders. This demonstration underscores the potential for electronic data recording to be expanded and applied to a wide range of tests, particularly when dealing with extensive datasets. To begin, we established the Raspberry Pi-accelerometer system, utilizing the H3LIS331DL accelerometer [81], with the primary aim of visualizing pressure variations on a chart. The resulting graph, generated using the accelerometer (see Figure 3.4), was compared to the output of the conventional circular paper chart recorder, shown on the right side of Figure 3.3.

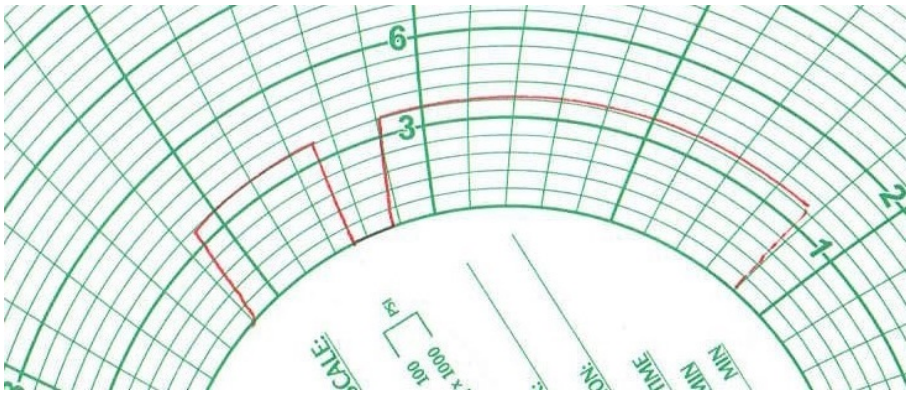

Fig. 3.3: Chart 1 pressure variation

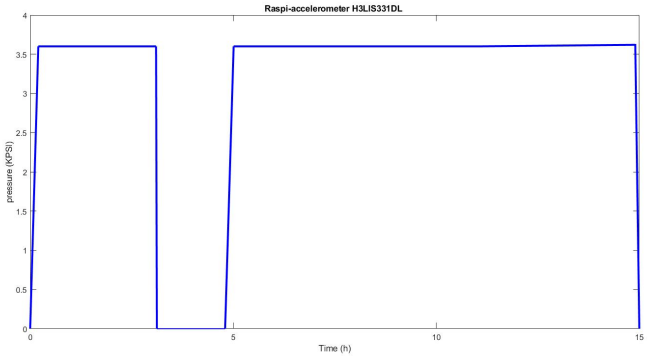

Fig. 3.4: Electronic chart related to chart 1

The initial experiment focused on pressure variation. In this experiment, pressure was intentionally set to both upper and lower limits, as illustrated in Figure 3.5. The objective was to assess the displacement variation of the needle in response to accelerometer data. Conversely, in the latter experiment, pressure variation was systematically increased to evaluate the stability of the needle (refer to Figure 3.6).

It is obviously clear that the resulting graphs of pressure from the proposed accelerometer overlap those obtained from circular paper.

In the second experiment, the system Raspberry pi-accelerometer (ADXL345) is used instead of the previously proposed system.

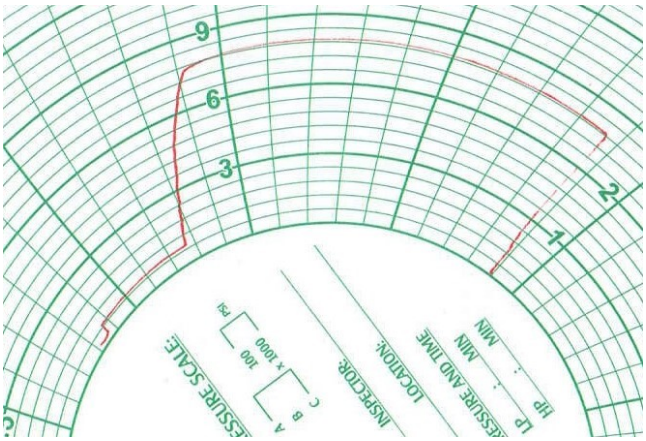

Fig. 3.5: Chart 2 pressure variation

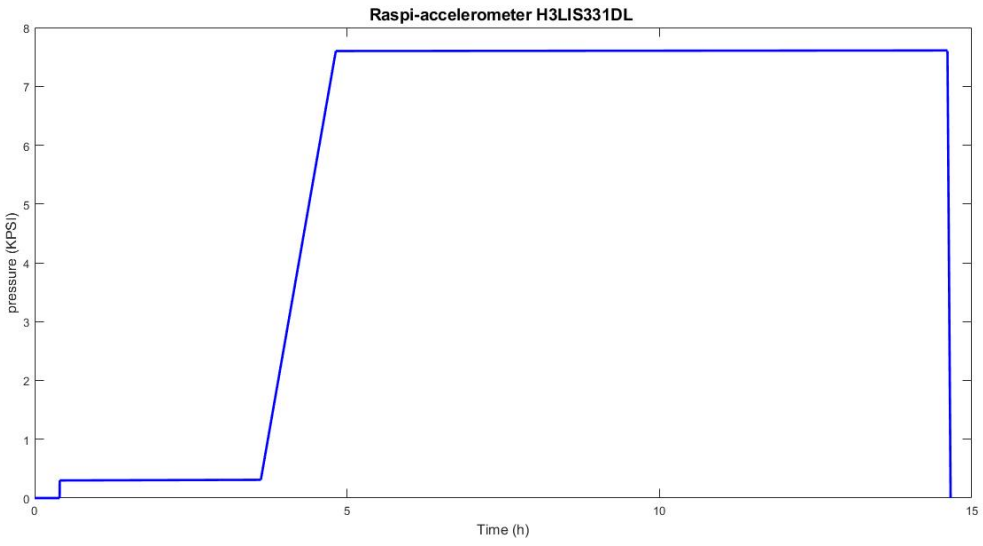

Fig. 3.6: Electronic chart related to chart 2

The accelerometer-based graph (see Figure 3.8) is compared with the circular paper chart as it is shown on the right side of Figure 3.7. Noticeably, ADXL345 fails to record data that represents pressure variation (more than 3900 PSI) when the needle displacement exceeds roughly 125 mm. Remarkably, When the needle of the circular chart recorder displaces progressively within a few seconds, that triggers a sudden failure in recording data which originally bounces back to the massive data being recorded at each caption.

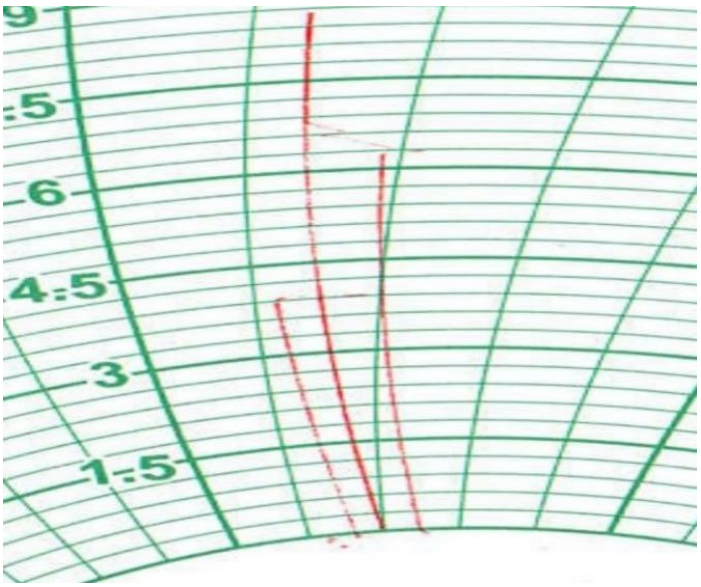

Fig. 3.7: chart related to chart 3

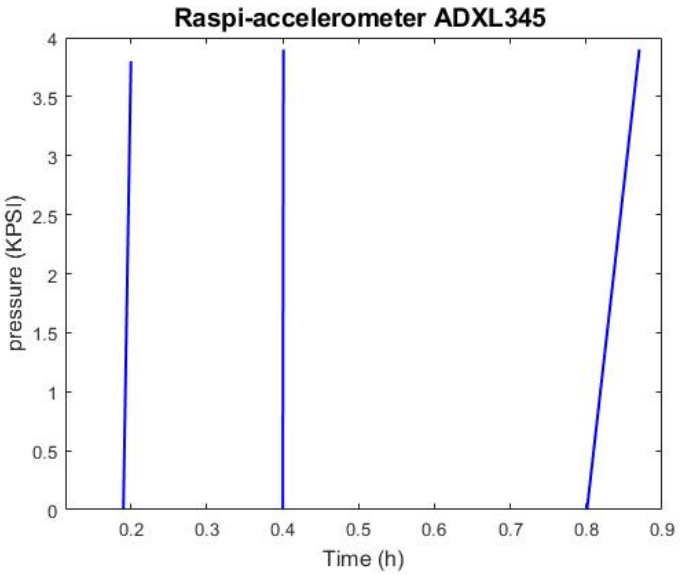

Fig. 3.8: Electronic chart related to chart 3

The accelerometer recorders data which presents the pressure variation. Remarkably, when the needle of the circular chart recorder displaces progressively within a few seconds, that triggers a sudden failure in recording data which originally bounces back to the massive data being recorded at each caption.

We conclude that the accelerometer ADXL345 cannot sense massive variations of the needle of more than 3900 PSI in a few seconds.

3.5 The main feature of the proposed system

The system presented in this paper offers an intriguing blend of advantages. Notably, it provides a cost-effective means of analysis without the need for expensive components. Moreover, it excels at recording instantaneous responses, particularly in capturing data related to pressure variations. This system is intrinsically rooted in the Internet of Things (IoT), rendering it a perfect tool for remote pressure monitoring and functioning as an alert system to detect unwanted pressure fluctuations. Additionally, it significantly enhances the monitoring of oil pipelines, contributing to increased production rates. These inherent features pave the way for the implementation of this IoT system across various industrial applications.

Furthermore, it's worth underscoring the advantages of paperless data recording as an intriguing concept to replace traditional data recording methods. To simplify, the benefits of paperless recording, as highlighted by [82], encompass:

- **Reduced Paperwork**: Users can streamline and reduce their paper-related tasks, eliminating the need to manage, store, or maintain extensive paper records.
- **Electronic Data Formatting and Analysis**: Data can be electronically formatted and analyzed, simplifying the process of data manipulation and interpretation.
- **Cost Efficiency**: Paperless recording eliminates the need for pens, paper charts, or clock charts, making the entire data recording process cost-effective.

3.6 Drawbacks of the proposed system

Despite the numerous advantages of the developed IoT system presented in this paper, it's essential to acknowledge potential drawbacks. These may include the system's energy requirements, especially in tasks that demand extended operational hours.

Furthermore, the IoT system could pose risks of electrical system failures in certain situations, such as potential explosions.

3.7 Conclusion

As we conclude from this chapter, the integration of microelectronic sensors, specifically MEMS-based accelerometers, is profoundly transforming our lives. These sensors make daily tasks more convenient, efficient, and reliable by translating inertial movements into numerical signals.

In addition to our daily lives, there is a growing demand for advanced monitoring in the realm of self-operating machines, surpassing the requirements of conventional machines. IoT-based monitoring, designed for maximum productivity and efficiency with minimal investment, is becoming increasingly crucial.

The Raspberry Pi-based accelerometer system, utilizing the H3LIS331DL, offers a cost-effective, user-friendly setup with versatile data collection capabilities. It not only simplifies data acquisition but also provides precise, high-quality data to the server. Furthermore, the potential for enhancing the IoT-based accelerometer's accuracy and sensitivity lies in optimizing its inherent electrical structure.

A noteworthy application is the use of accelerometers within rotating machines to assess their vibrations during operation without requiring human intervention. This has the potential to enhance maintenance practices and prevent unexpected failures.

Looking ahead, future work could encompass the development of a novel chart recorder based on the Internet of Things, further expanding the horizons of efficient data monitoring. Software monitoring could complement these advancements, paving the way for even more sophisticated and reliable systems.

Chapter 4

Kinematic Modeling of Continuum Robots Utilizing Accelerometer Data

4.1 Introduction

In this chapter, we introduce a novel dimension to the kinematic modeling of continuum robots through the integration of accelerometer data. Our research centers on equipping a data logger to the end-effector of a prototype continuum robot, allowing us to record its positions while simultaneously measuring bending angles using an angle meter. Subsequently, the positions derived from the accelerometer's data serve as inputs for a particle swarm optimization (PSO) algorithm. We meticulously compare the resulting bending angles obtained from both PSO and the angle meter to validate our simulated model.

The main contributions of this chapter include:

- An overview of the current state of the art in continuum robot research.
- The introduction of a pioneering prototype for a constant curvature continuum robot.
- The presentation of an affordable and efficient technique for measuring the robot's end-tip positions using an accelerometer.

4.2 Overview

The field of robotics took its first steps with the creation of the first industrial robot by Griffith P. Taylor in 1937 [83]. In recent years, there has been a remarkable shift towards designing robots that draw inspiration from biology, giving rise to the exciting field of bio-inspired robotics. Natural selection has yielded practical solutions within the realm of nature to this end researchers have looked to nature for inspiration, studying the tentacles of elephants, the movements of worms,snake-like robots , bird-neck manipulators and the elegant necks of ostriches and giraffes [19, 84–87]. These biological systems have provided valuable insights for developing robots with enhanced capabilities and adaptability.

Continuum robots come in single and multi-section variations, but there has been limited research on models for the forward kinematics of conical-shaped continuum robots with variable curvature. Existing forward kinematic models are tailored to specific robot types [88–91]. In terms of analytical complexity, solving the inverse kinematic model (IKM) is no easy feat. To tackle this challenge, researchers have explored meta-heuristic approaches [92–99], neural networks [100], and other innovative techniques. For instance, in [98], the authors addressed the IKM using particle swarm optimization (PSO), achieving highly accurate results with an error less than 0.0008 radians during trajectory tracking. Their approach is rooted in developing an objective function linking the robot's end-effector with a prescribed trajectory. Similarly, in [101], genetic , building upon the same fundamental idea as [97]. The accelerometer, classified as a microelectromechanical system, possesses the capability to translate dynamic quantities such as displacement, velocity, and acceleration into electrical data [20]. In this paper, we introduce a data logger attached to the end-effector of a prototype continuum robot for recording its positions, while bending angles are simultaneously measured using an angle meter. Subsequently, the robot's end-effector positions obtained from the accelerometer's data serve as inputs to the PSO algorithm. We meticulously compare the resulting bending angles derived from both PSO and the angle meter, providing a robust validation of our simulated model.

To summarize, our contributions in this paper encompass a brief survey of the continuum robot field, the introduction of a novel prototype for constant curvature continuum robots, and the presentation of an affordable technique to measure the robot's end-tip positions using an accelerometer. The remainder of this chapter unfolds as follows:

- Section 4.3 presents an exploration of conical and cylindrical continuum robots.

- Sections 4.4 to 4.5 delve into the development of forward kinematics models based on Constant Curvature Kinematic Analysis (CCKA).
- In Section 4.6, we introduce the particle swarm optimization (PSO) approach to solve the inverse kinematic model for single-section continuum robots, using the robot's positions as input.
- Section 4.8 describes the usage of an accelerometer coupled with an angle meter to obtain the robot's end-effector positions and bending angles.
- We proceed to compare the simulation and experimental results derived from the accelerometer.
- Finally 4.9, the chapter concludes with the most significant findings and outlines potential future research directions in the field of continuum robot modeling.

Table 4.1: Nomenclature

i	: cables $i = 1,2,3$	$(x,y,z)_{j,k}$	: local coordinate frame
j	: units $j = 1,2,...,5$	$(X,Y,Z)_k$	: global coordinate frame
k	: sections $k = 1,2$	$\theta_{j,k}$	: bending angle
$\ell_{i,j}$	: non-conic unit cable length	φ_k	: is the orientation angle
$\hat{\ell}_{i,j}$	: is the conic unit cable length	κ_j	: curvature
$l_{j,k}$	: central axis' length of the unit j	$r_{j,k}$	: Disk diameters

4.3 Description of continuum robots' design

Cable-driven continuum robots are mainly composed of a set of disks that are held by a flexible backbone as it is described in [102, 103] and can also be actuated pneumatically as in[104]. Each disk has three holes through which the cables go through and are used to manipulate the robot's movement. To the best of our knowledge, there are two approaches to modeling cable-driven continuum robots, namely constant and variable. Constant curvature continuum robot (see Fig. 4.1a) is typically known by its cylindrical shape and each of its sections are governed by the same bending angle. Noticeably, the constant curvature (CC) continuum robot's section units have the same bending angle. The kinematics nomenclature of the robot is given in tab 4.1. However, the

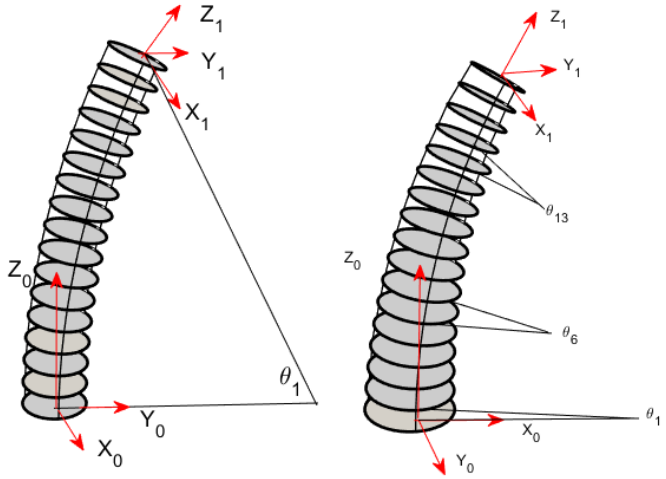

Fig. 4.1: (a) Constant curvature continuum robot; (b) Variable curvature continuum robot (conical shape)[105]

VC continuum robot's (Fig. 4.1b) backbone consists of serially connected units where each unit is governed by its own bending angle. Furthermore, in variable curvature (VC) continuum robot each unit has an upper and lower disk with different diameters forming a conical shape. A detailed description of the robot's unit with CC and VC is illustrated in Fig. 4.2.

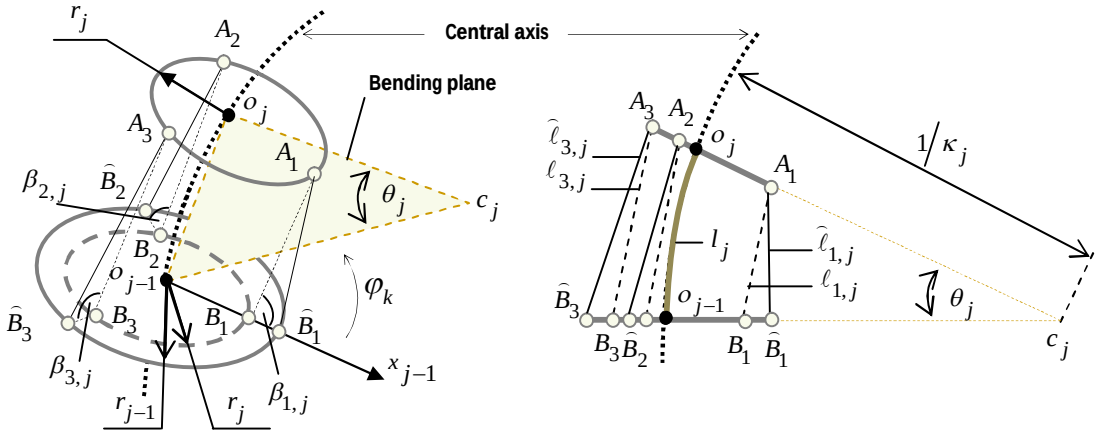

Fig. 4.2: Kinematics nomenclature of a single conically and cylindrically shaped unit[105]

4.4 Forward kinematics modeling of constant curvature continuum robot

The constant curvature kinematic approach (CCKA) is the most commonly used in modeling continuum robots [106] due to its simplicity yet it does not properly describe the geometry of variable curvature continuum robots. In General, this approach can be performed in two steps: a specific transformation between the configuration space followed by an independent transformation between the actuator space and the configuration space. In the following analysis, the orientation angle is considered to be equal to zero (i.e. in planar projection). The specific kinematic mapping gives the arc parameter as a function of the actuator's cable. Therefore, the bending angle be expressed as follows:

$$\theta_j = \frac{2}{3}\frac{\ell_{1,j} - \ell_{2,j}}{r_j} \tag{4.1}$$

While the independent kinematic mapping expresses the relationships between the operational coordinates and arc parameters. More generally, this mapping can be described by the following homogeneous transformation matrix (for more details refer to [107–109]):

$$\mathbf{T}_n^0 = \prod_n^0 \mathbf{T}_{j,k}^{j-1,k} \tag{4.2}$$

in which

$$\mathbf{T}_{j,k}^{j-1,k} = \left(\begin{array}{c|c} \mathbf{R}_{j,k}^{j-1,k} & \mathbf{P}_{j,k}^{j-1,k} \\ \hline \mathbf{0}_{1\times 3} & 1 \end{array}\right) \tag{4.3}$$

where $\mathbf{R}_{j,k}^{j-1,k}$ and $\mathbf{P}_{j,k}^{j-1,k}$ are the rotational matrix and the vector position, respectively. They can be expressed as a function of arc parameters as follows:

$$\mathbf{R}_{j,k}^{j-1,k} = \mathbf{rot}(Z_{j-1,k}, \varphi_k) \cdot \mathbf{rot}(Y_{j-1,k}, \theta_{j,k}) \cdot \mathbf{rot}(Z_{j-1,k}, -\varphi_k) \tag{4.4}$$

and

$$\mathbf{P}_{j,k}^{j-1,k} = \begin{cases} \frac{l_{j,k}}{\theta_{j,k}}(1 - \cos(\theta_{j,k}))\cos(\varphi_k) \\ \frac{l_{j,k}}{\theta_{j,k}}(1 - \cos(\theta_{j,k}))\sin(\varphi_k) \\ \frac{l_{j,k}}{\theta_{j,k}}\sin(\theta_{j,k}) \end{cases} \tag{4.5}$$

4.5 Forward kinematics modeling of variable curvature continuum robot

To derive the Forward Kinematic Model (FKM) of the conical-shaped unit by applying the CCKA [19], Equation (4.1) has to be expressed as a function of the cables length $\widehat{\ell}_{i,j}$ instead of $\ell_{i,j}$ (for more details refer to [110]). The relationship between the cable lengths can be expressed as follows [19]:

$$\widehat{\ell}^{\,2}_{i,j,k} = \ell^2_{i,j,k} + \left(r_{j-1,k} - r_{j,k}\right)^2 - 2\ell_{i,j,k}\left(r_{j-1,k} - r_{j,k}\right)\cos\left(\beta_{i,j,k}\right) \tag{4.6}$$

With:

$$\cos\left(\beta_{i,j,k}\right) = \sin\left(\frac{\kappa_{j,k} l_{j,k}}{2}\right)\cos\left(\frac{2}{3}\pi\left(k-1\right) - \varphi_{j,k}\right)$$

After solving equation (4.6), the cables' lengths $\ell_{i,j,k}$ can be expressed as follows:

$$\begin{aligned}\ell_{i,j,k} = &\sqrt{\widehat{\ell}^{\,2}_{i,j,k} - \left(r_{j-1,k} - r_{j,k}\right)^2 + \left(r_{j-1,k} - r_{j,k}\right)^2\cos^2\left(\beta_{i,j,k}\right)} \\ &+ \left(r_{j-1,k} - r_{j,k}\right)\cos\left(\beta_{i,j,k}\right)\end{aligned} \tag{4.7}$$

According to (4.7), the cables' length $\ell_{i,j,k}$ is in the function of the cables' length $\widehat{\ell}_{i,j,k}$, the variation of the diameters of each unit's disks $(r_{j-1,k} - r_{j,k})$ and angle $\beta_{i,j,k}$. The diameters of the continuum robot's disks can be calculated using the following equation [19]:

$$r_{j,k} = r_{\max,k} - \frac{j}{m_k}\left(r_{\max,k} - r_{\min,k}\right) \tag{4.8}$$

$$\gamma_i = \frac{2\left(i-1\right)\pi}{3}, i = 1,2,3 \tag{4.9}$$

However, due to the coupling of cable length and bending angle, Equation (4.5) does not have an analytical solution. To derive an analytical-approximate solution, the bending angle θ_j is firstly estimated as a function of a given driving cable length $\widehat{\ell}_{i,j}$ using particle swarm optimization where the objective function is to make the root attain specific position using the same cable length for each unit. For this optimization problem, the appropriate cost function to be minimized can be formulated from Equation (4.5), where the unknown variable to be searched is the bending angle θ_j. Secondly, the obtained bending angle θ_j is expressed mathematically as a function of $\widehat{\ell}_{i,j}$ using Cubic Polynomial Fit (CPF). illustrates the geometric parameters of the

considered CDCR. it is noteworthy to say that the developed work in this paper is strongly related to the work done by [19].

Table 4.2: Geometric parameters of the proposed prototype

Description	section length	number of units	r_{min}	r_{max}
value	300 mm	5	20	31

For further use, let's calculate the first bending angle θ_1 of the robot section. For instance, the estimated bending angle θ_1 of the first bending section as a function of a given driving cable length $\widehat{\ell}_{i,j}$ is shown in Fig. 4.3. From this Figure, one can observe that the errors are negligible. By using the Cubic Polynomial Fit (CPF), the obtained bending angle can be approximated as follows:

$$\theta_1 = 1.8912 \cdot 10^{-4} \widehat{\ell}_{1,1}^{3} - 1.068 \cdot 10^{-2} \widehat{\ell}_{1,1}^{2} + 2.4 \widehat{\ell}_{1,1} + 4.9872 \cdot 10^{-4} \tag{4.10}$$

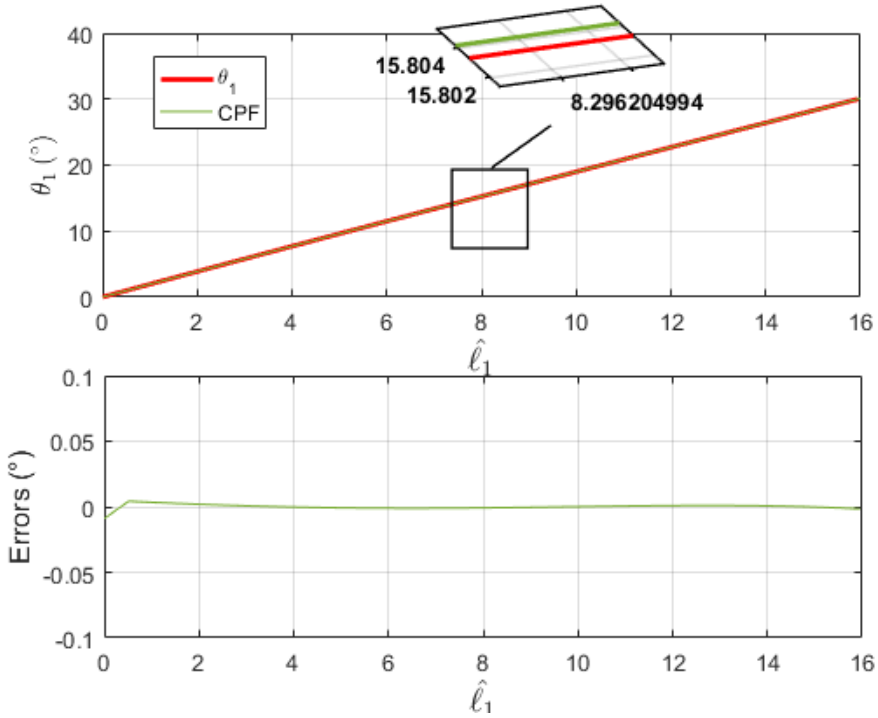

Fig. 4.3: Cables length in function of the first bending angle and their errors

4.5.1 Forward kinematic of a single continuum robot section

As an open kinematic chain of serially connected units, the forward kinematic of a continuum robot section can be obtained according to the homogeneous transformation the matrix as follows:

$$\mathbf{T}_n^0 = \prod_n^0 \mathbf{T}_{j,k}^{j-1,k} \tag{4.11}$$

In which the FKM of each conical-shaped unit can be derived following the same procedures described in the previous subsection. However, in order to reduce the number of variables involved in the model, the rest of the bending angles θ_j with $j = 1, 2, 3$ will be approximated as a function of the first bending angle θ_1 using CPF. The bending angles θ_j of the continuum robot section, composed of five units, can be expressed as follows:

$$\theta_j = c_{1,j}\theta_1^3 + c_{2,j}\theta_1^2 + c_{3,j}\theta_1 + c_{4,j} \tag{4.12}$$

where the coefficients $c_{1,j}$, $c_{2,j}$, $c_{3,j}$, $c_{4,j}$ are given in tab 4.3.

Table 4.3: Coefficients of the cubic polynomial fit

Bending angles	$c_{1,j}$	$c_{2,j}$	$c_{3,j}$	$c_{4,j}$
θ_2	$3.0495 \cdot 10^{-6}$	$-3.608 \cdot 10^{-4}$	1.0898	$1.101 \cdot 10^{-4}$
θ_3	$7.899 \cdot 10^{-6}$	$-9.079 \cdot 10^{-4}$	1.1997	$3.371 \cdot 10^{-4}$
θ_4	$1.584 \cdot 10^{-5}$	$-1.759 \cdot 10^{-3}$	1.3226	$8.109 \cdot 10^{-4}$
θ_5	$2.940 \cdot 10^{-5}$	$-3.099 \cdot 10^{-3}$	1.4984	$1.799 \cdot 10^{-3}$

4.6 Particle Swarm Optimization (PSO)

PSO (Particle Swarm Optimization) was primarily developed by Kennedy and Eberhart in 1995 [111]. This method draws inspiration from the collective movements of flocks of birds[112] and has since found widespread use in solving engineering problems due to its efficiency.

The PSO algorithm begins with the random generation of particles. At each iteration, each particle P is updated based on two best values: (1) the position vector of the best solution achieved by the particle, denoted as $P_{pb(t)}$, and (2) the overall best value achieved by any particle, referred to as $P_{bg}(t)$. In addition, the PSO algorithm randomly adjusts the velocity of each particle towards $P_{pb}(t)$ and $P_{bg}(t)$. The particle then selects the best adjustment based on the task being tackled.

Equations (4.13) and (4.14) represent the updating of velocities $v(t)$ and positions $P(t)$ of each particle, respectively. PSO terminates when it reaches the maximum number of specified iterations.

$$v_p^{t+1} = \omega v_p^t + c_1\rho_1(P_{pb}^t - x_p^t) + c_2\rho_2(P_{bg}^t - x_p^t) \tag{4.13}$$

$$x_p^{t+1} = x_p^t + v_p^{t+1}dt \tag{4.14}$$

where v_p^t is the particle velocity; x_p^t is the particle position; ω is the inertia weight is 0.967 ; c_1 and c_2 are constants [0.4 - 4]; ρ_1, ρ_2 are random numbers uniformly distributed within the interval $[0,1]$; P_{pb}^t represents the local best position; P_{bg}^t represents the global best position.

4.6.1 The objective function and problem formulation

The objective function is defined as the distance between the robot's end effector and the specified position along the prescribed trajectory. The optimal solution minimizes this distance, effectively aligning the robot's end effector with the desired position. In essence, PSO (Particle Swarm Optimization) is employed to determine the bending angles and orientations necessary to achieve the desired position.

The PSO process for solving the inverse kinematic model (IKM) of the robot involves randomly generating bending angles. This random generation results in a variety of robot end effector positions, each corresponding to the desired position. The configuration that achieves the minimum distance between the robot's end effector and the desired position is considered a solution to the inverse kinematic problem.

As the length of the cable is inherently linked to the bending and orientation angles, PSO facilitates the determination of cable lengths required to reach the desired position. This entire process unfolds over a series of iterations, with the calculated angles subsequently input into the Forward Kinematic Model (FKM) for visualization and validation, ensuring accurate tracking at each iteration.

$$F = (P_{x_i} - X_{c_i}) + (P_{y_i} - Y_{c_i}) + (P_{z_i} - Z_{c_i}) \tag{4.15}$$

where X_{c_i},Y_{c_i}, and Z_{c_i} represent the spatial coordinates of a located position on the prescribed trajectory. P_{x_i}, P_{y_i}, and P_{z_i} represent the position of the robot's end tip for each specific position of the prescribed trajectory. The robot's end-tip pose is obtained from the FKM. Explicitly, its position presents the three first components of the fourth column of the matrix which is defined by (4.3), similarly its rotation is also

obtained from (4.3). The obtained positions are used as input to PSO, which generates the needed bending angles according to the given robot's end effector. Accordingly, the generated bending angles from PSO and those obtained from FKM are compared as it is shown in Figure 6 and which can be summarized as follows:

$$\begin{cases} \theta, \phi \xrightarrow{FKM} (X, Y, Z) \\ (X, Y, Z) \xrightarrow[PSO]{IKM} \theta, \phi \end{cases}$$

For more details about the PSO algorithm, please refer to Appendix C.

4.7 Simulation analysis

In this section, simulation analysis is conducted on a single-section continuum robot to validate the mathematical formulas developed in this paper. The initial simulation involves a variable curvature continuum robot consisting of a single section, which is tasked with following an arc-like trajectory. PSO is employed to determine the requisite bending angles of the robot, enabling its end effector to reach each position along the arc-like trajectory.

The objective function utilized in the MATLAB code, as defined by equation (4.15), measures the distance between the robot's end effector and the designated position on the prescribed trajectory. PSO aims to minimize this distance, effectively aligning the robot's end effector with the desired positions.

4.7.1 Verification of the newly proposed formula

In this section, the proposed empirical formula (4.12) is employed to calculate the positions of the robot's end effector during trajectory tracking, as depicted in Fig. 4.4. The obtained positions serve as input for the PSO algorithm (see Appendix C).

Subsequently, the particle swarm optimization generates the necessary bending angles to position the robot's end effector accurately. A comparison is made between the bending angles generated by PSO and those obtained from the FKM, as illustrated in Fig. 4.5.

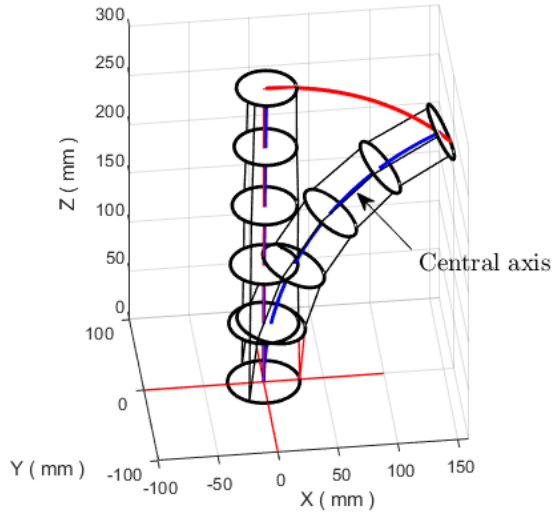

Fig. 4.4: The whole robot follows the arc-like trajectory

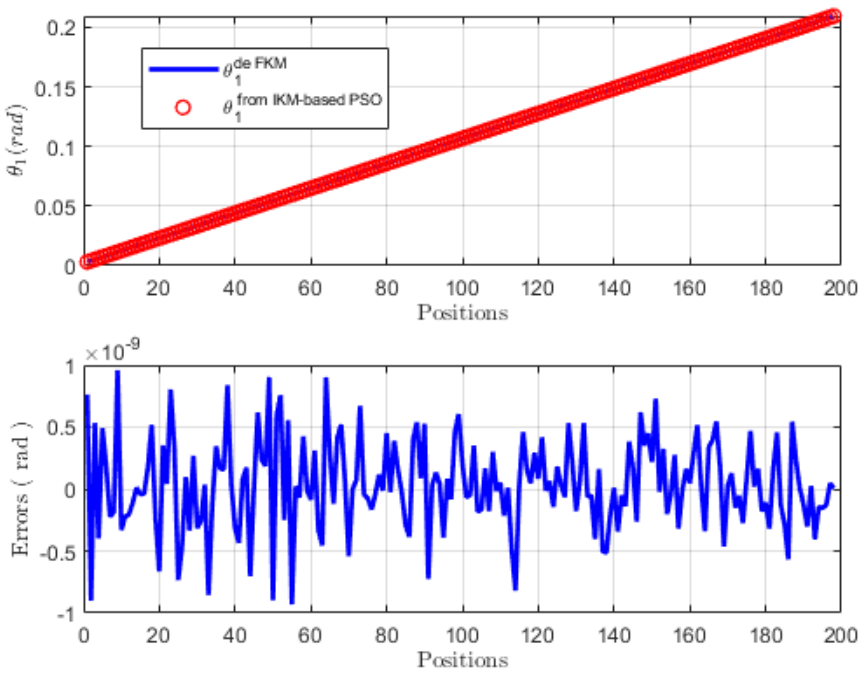

Fig. 4.5: The bending angle for the first five units of the first section and their errors

Remarkably, as evident from Fig. 4.5, the obtained bending angles calculated using the proposed formula align closely with those generated through the PSO method.

This alignment underscores the efficiency of the proposed model and the effectiveness of the PSO algorithm.

It is worth emphasizing that both sets of code are available: the former for generating the positions of the robot's end effector, and the latter for utilizing the Particle Swarm Optimization to solve the inverse kinematic model of the continuum robot's section, as presented in this chapter.

4.8 Experimental verification of PSO through data-based accelerometer

In this section, a prototype for a single-section continuum robot is introduced to validate the accuracy of PSO in solving the IKM. To gather various data about the robot, including the robot's end effector position and the corresponding bending angles, the following equipment was employed:

- Accelerometer ADXL 345: is used to record the robot's end effector along X, Y, Z, which is a tiny, low-power, 3-axis accelerometer [19] with high resolution (13-bit) and measurement at up to 16 g. it also provides digital outputs[113].
- An angle meter is used to measure the robot's bending angle
- Raspberry Pi 3 B+ a single-board computer's final revision with characteristics that can be found in detail in the manual [17] is used to run the accelerometer
- Python is the language used to program the accelerometer and make it record positions[17].

Table 4.4: Comparaison between the obtained angles from PSO and those measured using an accelerometer and an angle meter

Position from accelerometer (mm)	Angles from PSO (degree)	Measured angles (degree)
(1.9014,0,118.6489)	43.89	45.70
(2.9512, 0,116.5491)	40.52	41.57
(3.9996,0,115.4369)	38.61	40.80
(4.0463,0,114.3123)	36.93	34.55
(5.0156,0,113.3123)	34.50	35.60
(6.0463,0,112.3123)	30.68	32.50
(7.0463,0,111.3123)	28.90	31.55

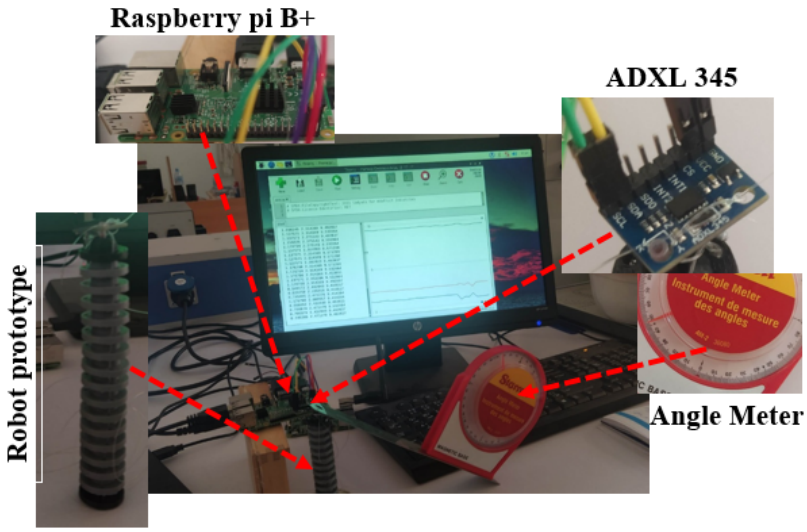

Fig. 4.6: Bench test which depicts the way to track the robot's end effector and the bending angles corresponding to each position

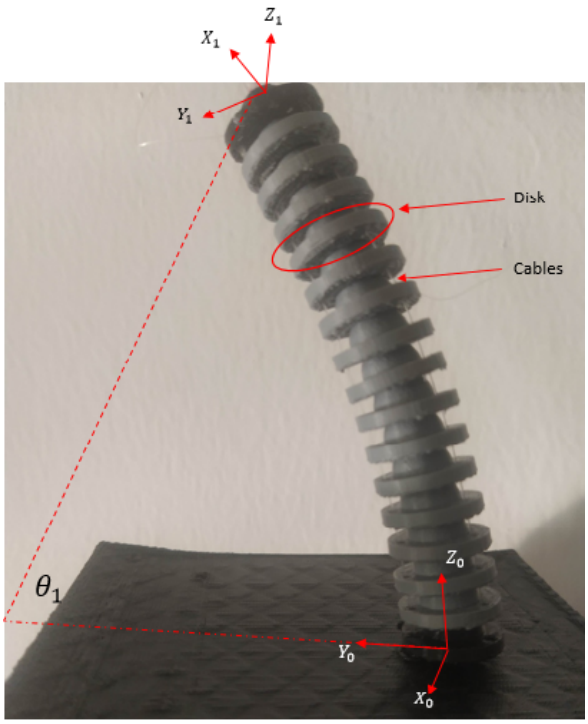

Fig. 4.7: The proposed single-section continuum robot prototype

Due to the limited measurement tools available, we conducted experiments at only eight different positions for the robot's end effector. Interestingly, our primary objective was not just to compare the angles obtained from PSO with those from the

accelerometer but also to showcase the accelerometer's potential as a cost-effective tool for tracking the robot's end effector. With more accurate accelerometer models, we can even approach angles that are theoretically obtained from PSO.

As shown in Table 4.4, there exists a difference between the angles obtained from PSO and those derived from real measurements, with the maximum error being less than 3 degrees.

Essentially, the core concept in this section is to demonstrate the practicality of using an accelerometer to track the robot's end effector without the need for expensive high-tech equipment.

4.9 Conclusion

In this chapter, we have derived and simplified the forward kinematic model of a single-section continuum robot by proposing a new empirical formula. While the non-linearity of the inverse kinematic model presents challenges, we have successfully employed particle swarm optimization to solve it. The IKM problem is formulated as an objective function, which measures the distance between the robot's end effector and a point on the prescribed trajectory. The bending angles generated by the PSO approach closely match those obtained from the forward kinematic model.

For experimental validation, we constructed a single-section continuum robot prototype, recording the bending angles using an angle meter to assess the efficiency and accuracy of particle swarm optimization. Remarkably, we have also explored the use of accelerometers as a cost-effective alternative for identifying the continuum robot's end effector position, reducing the reliance on expensive tools.

As we conclude this chapter, we highlight the potential for further improvements in accelerometer technology to enhance data recording from continuum robots in future research and development.

Chapter 5

Optimized Design of Continuum Robots and its Dynamics Modeling

5.1 Introduction

In this chapter, we will conduct a comprehensive examination of continuum robots, with a specific emphasis on their dynamic modeling. We will intricately investigate the dynamic model of a single-section continuum robot characterized by variable curvature. Furthermore, we will expound upon the description of a prototype continuum robot, accentuating its distinctive disk-based structural design. This will serve as the basis for a comparative analysis within the context of a prototype continuum robot. Ultimately, we will draw this chapter to a close by summarizing our pivotal findings .

5.2 Overview

The field of robotics took its first steps with the creation of the first industrial robot by Griffith P. Taylor in 1937 [83]. In recent years, there has been a remarkable shift towards designing robots that draw inspiration from biology, giving rise to the exciting field of bio-inspired robotics. Natural selection has yielded practical solutions within the realm of nature to this end researchers have looked to nature for inspiration, studying the tentacles of elephants, the movements of worms,snake-like robots , bird-neck manipulators and the elegant necks of ostriches and giraffes [84–87, 103]. These biological systems have provided valuable insights for developing robots with enhanced capabilities and adaptability.

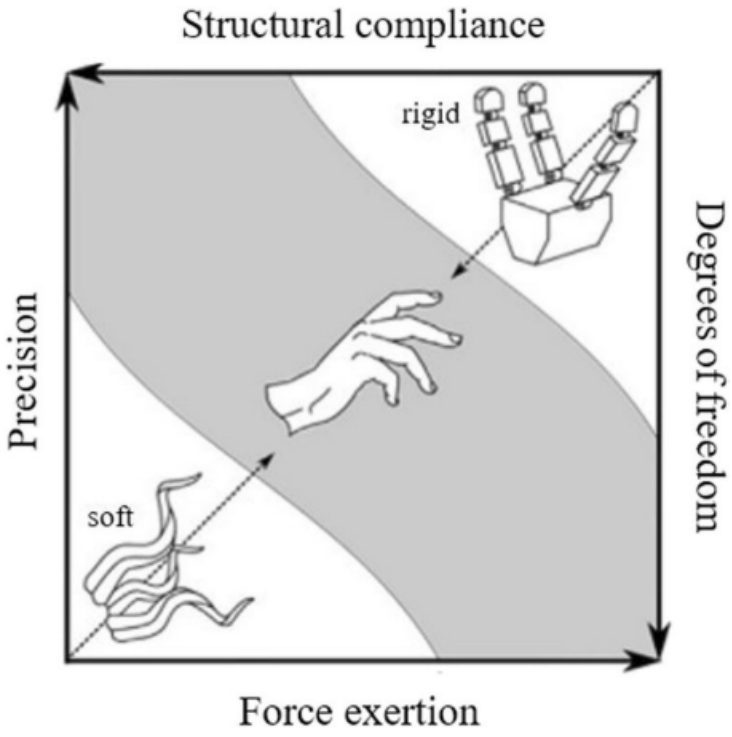

Fig. 5.1: Exploring the Spectrum of Manipulators - A Global View and Comparison between Soft and Rigid Robots[114]

Traditional robots with rigid structures often face limitations due to their restricted degrees of freedom, rendering them less effective in tasks that require flexibility [19]. However, Continuum robots, also known as type of "soft robots," have emerged as a solution to this problem [115]. The compliance of soft manipulators eliminates the need for highly complex calculations, making them well-suited for various applications, including medical minimally invasive surgery [116]-[117] and inspection tasks [118]-[119]. These robots possess a remarkable degree of freedom, enabling them to exhibit dexterity and navigate with precision toward their intended target positions. The gripper is bio-inspired by the human hand's design[120]. In contrast to soft robots, which can have an infinite degree of freedom, a common limitation in the design of exoskeleton robots is that most opt for 4 or 3 degrees of freedom[121]. For its remakable feature Continuum robots (CRs) have been emerged in surgical fields such for maxillary sinus surgery (MSS)[122],microsurgical abdominal surgery [123]. The spectrum of manipulators ranges from soft to rigid robots, each offering unique advantages. Soft material continuum body manipulators, in particular, provide greater degrees of freedom and structural compliance, eliminating the need for complex calculations [124]. However, as the number of degrees of freedom increases, precise movement control becomes more

challenging, and the structural conformity and response to external forces decrease under higher system forces. Soft manipulators leverage their ability to undergo large deformations, granting them increased degrees of freedom and structural compliance see fig 5.1.
Despite the advantages of continuum robots in terms of degrees of freedom, controlling them presents challenges due to the high non-linearity of their equations of motion. In this project, the equations of motion for a variable curvature continuum robot are solved using the fourth-order Runge-Kutta method. To validate the accuracy of the solution, we applied tension to its cable, and measure the robot's vibrations and physical parameters for several type of continuum robot.

5.3 Dynamic modeling of continuum robot

Dynamic modeling is a critical aspect of understanding the behavior of continuum robots. It involves predicting the bending and orientation angles of the robot in response to applied forces on its cables. In this pursuit, multiple methods are employed to solve and simulate dynamic modeling for continuum robots. Notably, two prominent approaches stand out: one based on the Cosserat rod theory, as discussed in [125], and another utilizing the Lagrange-Euler method, as referenced in [126, 127].

The choice of the Lagrange-Euler method in this study is motivated by its efficiency in simulation, making it a preferable option over the Cosserat rod theory. The Lagrange-Euler method streamlines the dynamic modeling process, ensuring rapid and computationally efficient simulations. This method aligns with the project's objectives of achieving practical and efficient dynamic modeling for continuum robots.

In the context of this project, our primary focus is to compare the dynamic modeling of three distinct robot prototypes. We subject these prototypes to various applied forces on their cables to evaluate their stability under different conditions. Through this comparative analysis, we aim to identify the most stable prototype, providing valuable insights into its performance characteristics for the intended application.

5.3.1 Dynamic model of a spatial single-section continuum robot with constant curvature

In this section, we present the forward dynamic model of a CC continuum robot with a single section (k = 1) composed of 5 units using the Lagrange-Euler method. The bending and orientation angles present the generalized coordinates. The equations of

motion of a CC continuum robot can be expressed as follows[128]:

$$\begin{cases} \frac{d}{dt}\left(\frac{dT}{\partial\dot{\theta}_{j,k}}\right) - \frac{dT}{\partial\theta_{j,k}} + \frac{\partial U}{\partial\theta_{j,k}} = Q_1 \\ \frac{d}{dt}\left(\frac{dT}{\partial\dot{\varphi}_k}\right) - \frac{dT}{\partial\varphi_k} + \frac{\partial U}{\partial\varphi_k} = Q_2 \end{cases} \tag{5.1}$$

Where:
Q_1 : The first generalized force
Q_2 : The second generalized force
T : Total kinetic energy of the robot
U : Total potential energy of the robot
$\theta_{j,k}$: The bending angle for each unit
φ_k : The orientation angle for the whole section For a VC continuum robot, each of its units has its own bending angle, thus different generalized coordinates are considered. On the other hand, if we use the previously developed equation as in [126], in which the bending angles of the robot's units can be expressed as a function of the robot's first bending angle (first unit), the generalized coordinates will be reduced to a single generalized coordinate θ_1, k, which can be mathematically expressed as:

$$\theta_{j,k} = \frac{r_{1,k}}{r_{j,k}}\theta_{1,k} \tag{5.2}$$

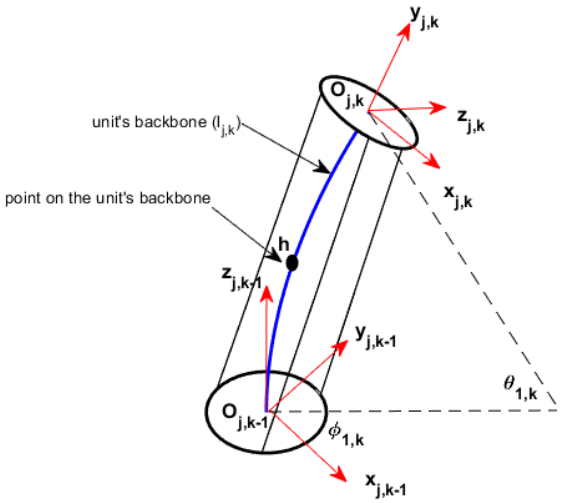

Fig. 5.2: Detailed description of the central axis of the unit[105]

5.3.2 Dynamic model of a spatial single-section continuum robot with variable curvature

The kinetic energy of the robot under consideration resides in the flexible backbone as well as the disks. As mentioned before, the flexible backbone is composed of a concatenation of units, each unit having its own bending angle. Thus, the kinetic energy of the backbone is the sum of the kinetic energy of each unit. Each point on the central axis of the flexible unit (j,k) is specified by the curvilinear abscissa (h), which represents the length from the origin of the reference frame $O_{j,k-1}$ to the specified point (see Fig. 5.4).
To determine the kinetic energy of the backbone, we first calculate the position vector of a point on the central axis using the following equations:

$$U_{j,k} = \begin{cases} x_{U_{j,k}}(h) = \frac{h_{U_{j,k}}}{\theta\left(h_{U_{j,k}}\right)}\left(1-\cos\left(\theta\left(h_{U_{j,k}}\right)\right)\right)\cos(\varphi_k) \\ y_{U_{j,k}}(h) = \frac{h_{U_{j,k}}}{\theta\left(h_{U_{j,k}}\right)}\left(1-\cos\left(\theta\left(h_{U_{j,k}}\right)\right)\right)\sin(\varphi_k) \\ z_{U_{j,k}}(h) = \frac{h_{U_{j,k}}}{\theta\left(h_{U_{j,k}}\right)}\sin\left(\theta\left(h_{U_{j,k}}\right)\right) \end{cases} \tag{5.3}$$

With $\theta\left(h_{U_{j,k}}\right) = \frac{h_{U_{j,k}}\theta_{j,k}}{l_{j,k}}$, $\theta_{j,k} = \frac{r_{1,k}}{r_{U_{j,k}}}\theta_{1,k}$ and $U_{j,k}$ is the position vector of each point located on the central axis of each unit, and $l_{i,k}$ refers to the length of the unit's arc. The linear velocity of any point h distant from the origin can be calculated by differentiation with respect to time:

$$v_{h,j} = \begin{cases} \dot{x}_{U_{j,k}}(h) = \dot{\theta}_{j,k}\left[\frac{h_{U_{j,k}}}{\theta_{j,k}}\sin\left(\frac{h_{U_{j,k}}}{l_{j,k}}\theta_{j,k}\right) - \frac{l_{j,k}}{\theta_{j,k}^2}H\right]\cos(\varphi_k) - \frac{l_{j,k}}{\theta_{j,k}}H\dot{\varphi}_k \\ \dot{y}_{U_{j,k}}(h) = \dot{\theta}_{j,k}\left[\frac{h_{U_{j,k}}}{\theta_{j,k}}\sin\left(\frac{h_{U_{j,k}}}{l_{j,k}}\theta_{j,k}H\right) - \frac{l_{j,k}}{\theta_{j,k}^2}\right]\sin(\varphi_k) - \frac{l_{j,k}}{\theta_{j,k}}H\dot{\varphi}_k \\ \dot{z}_{U_{j,k}}(h) = \dot{\theta}_{j,k}\left[\frac{h_{U_{j,k}}}{\theta_{j,k}}\cos\left(\frac{h_{U_{j,k}}}{l_{j,k}}\theta_{j,k}\right) - \frac{l_{j,k}}{\theta_{j,k}^2}\sin\left(\frac{h_{U_{j,k}}}{l_{j,k}}\theta_{j,k}\right)\right] \end{cases} \tag{5.4}$$

with $H = 1-\cos\left(\frac{h_{U_{j,k}}}{l_{j,k}}\theta_{j,k}\right)$.

- The kinetic energy of the flexible backbone is given by :

$$T_b = \sum_{j=1}^{5} \frac{1}{2} m_b \int_0^{l_{j,k}} \left(\dot{x}_{U_{j,k}}(h)\right)^2 + \left(\dot{y}_{U_{j,k}}(h)\right)^2 + \left(\dot{z}_{U_{j,k}}(h)\right)^2 \tag{5.5}$$

  Where m_b is the mass of the flexible backbone.

- The kinetic energy of the disks: Since each unit has its own bending angle, the potential energy for each unit is considered. Thus, the total kinetic energy of the disks can be expressed as follows:

$$T_d = \frac{1}{2} \sum_{j=1}^{5} v_{h,j}^T m_j v_{h,j} \tag{5.6}$$

  Where m_j is the mass of each disk.

- The total kinetic energy of a single section is given by:

$$T = T_b + T_d \tag{5.7}$$

  Obviously, the VC robot's kinetic energy is in the function of the bending angle of each unit $\theta_j\,(j = 1, 2.....5)$ which is not the case for a CC continuum robot, namely the kinetic energy for CC continuum robot is expressed in function of one bending angle θ_1 .

- Potential energy: the flexible backbone can be virtually divided into a series of flexible backbones (arcs) where each flexible arc has its own bending angle $\theta_j\,(j = 1, 2.....5)$. As long as the disks have a low weight, we can only consider the potential energy of the backbone, which can be considered as follows:

$$E_p = \frac{EI_b}{2L} \sum_{i=1}^{5} \theta_{j,k}^2 (k = 1) \tag{5.8}$$

5.3.3 The generalized forces

The simultaneously applying forces on the robot's cables can give rise to a spatial motion of the robot. So, the relationships between the generalized forces Q_1 and Q_2 in the range as $\varphi \in \left[0 \quad \frac{2\pi}{3}\right]$ can be expressed as a function of tension forces on the cables,

F_1 and F_2, as [129] :

$$\begin{cases} Q_1 = F_1 r\cos(\gamma_1 - \varphi) + F_2 r\cos(\gamma_2 - \varphi) \\ Q_2 = F_1 r\theta\sin(\gamma_1 - \varphi) + F_2 r\theta\sin(\gamma_2 - \varphi) \end{cases} \tag{5.9}$$

where r is the distance from the central axis of the flexible backbone to each actuating cable on the disk. While γ_1 and γ_2 represent, respectively, the angles between the horizontal and the directions of the first and second cables as it is shown in Fig 5.4.

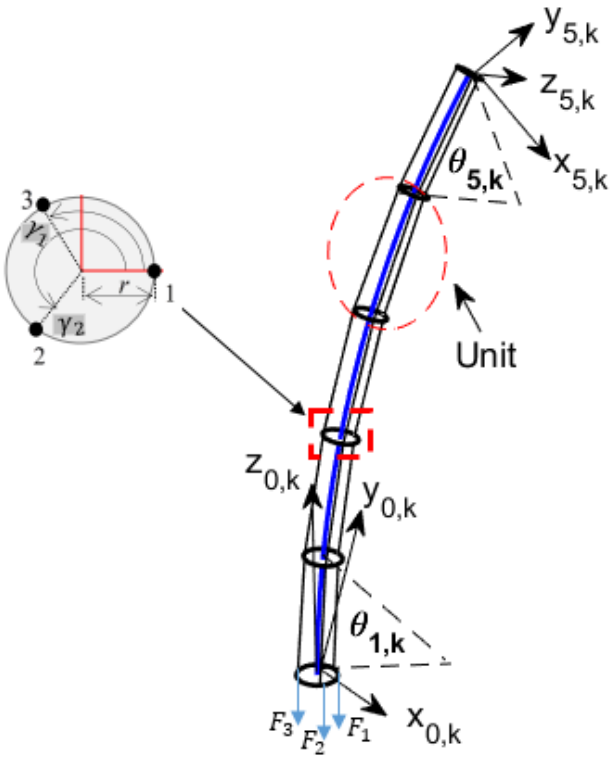

Fig. 5.3: Variable curvature continuum robot with five units [105]

5.3.4 Equations of motion

The development of the equations of motion is done using MATLAB software and which can be written as follows:

$$M_t \begin{bmatrix} \ddot{\theta} \\ \ddot{\varphi} \end{bmatrix} + C_t \begin{bmatrix} \dot{\theta}^2 \\ \dot{\theta}\dot{\varphi} \\ \dot{\varphi}^2 \end{bmatrix} + K_t \begin{bmatrix} \theta \\ \varphi \end{bmatrix} = D_t \begin{bmatrix} F_1 \\ F_2 \end{bmatrix} \tag{5.10}$$

With: The mass (M_t), stiffness (K_t), and damping factors (C_t) are defined from the developed equation and can be obtained using MATLAB software.

5.3.5 Simulation of a spatial single-section continuum robot tilted by an angle of $\frac{\pi}{8}$ from its equilibrium position

In the first simulation, the continuum robot is initially tilted by a bending angle of $\theta = \frac{\pi}{8}$ (see Fig. 5.4) without any tension on its cables (No force). After the robot reaches the given bending angle $\theta = \frac{\pi}{8}$, it is released. Basically, the flexibility of the robot's backbone helps it to bend according to the needed position, and once released, it oscillates as shown in Fig. 5.4.

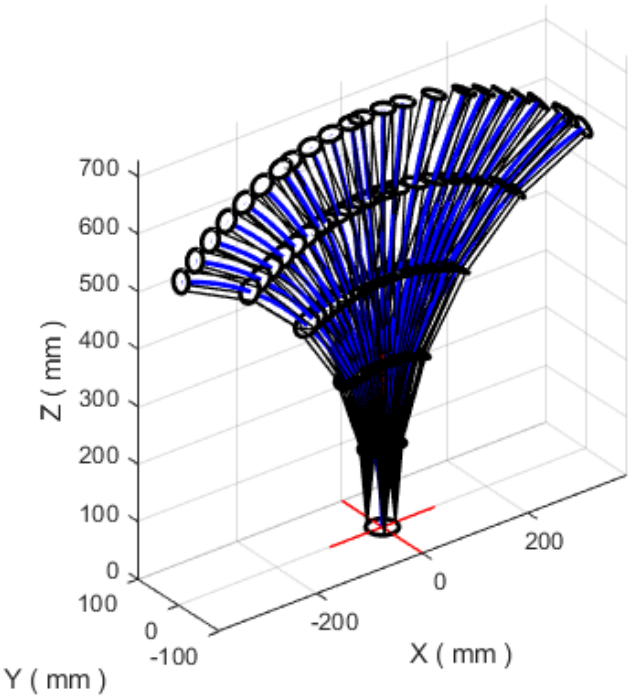

Fig. 5.4: Some robot oscillations occur after releasing it from an initial angle of flexion equal to $\theta = \frac{\pi}{8}$.

5.4 The prototype description of the continuum robot

Regarding rigid link robots, while various types of continuum robots have been extensively explored, including pneumatic, cable-driven, ferromagnetic, eversion, and artificial muscle designs [130–134]. Cable-driven continuum robots primarily consist of a series of disks supported by a flexible backbone, as depicted in Figure 5.5. Each disk features three holes through which cables pass, enabling the manipulation of the robot's motion. In our study, we have chosen a CDCD (Cable-Driven Cable-Driven) continuum robot due to its simplicity and affordability. To construct this robot, we utilized a 3D printer to create both the disks and the backbone(carbon fiber or glass fiber) . An interesting observation was made: when force is applied to a cable, it primarily affects the top disk, while the rest of the disks primarily serve as guides. As a result, we propose an alternative disk design that resembles a ball, as shown in Figure 5.9. This innovative disk serves a dual role as both a disk and a backbone. This design modification offers potential advantages in terms of simplifying the structure and enhancing the robot's performance. During our study, we subjected these prototypes to various applied forces on their cables to evaluate their stability under different conditions. Through this comparative analysis, we found that the proposed design of the continuum robot was more stable compared to previous proposed in[133] . This observation provides valuable insights into its performance characteristics for the intended application.

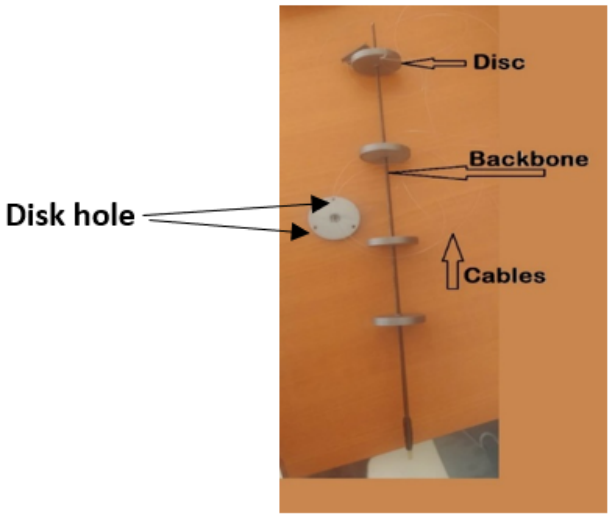

Fig. 5.5: Prototype of a single section of continuum robot type constant curvature

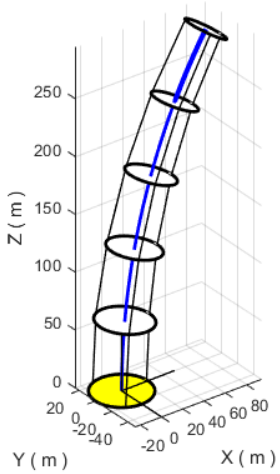

Fig. 5.6: Illustration of the single section of continuum robot

The continuum robot with variable curvature (VC) is modeled as a set of conically shaped units. Each unit is governed by its bending angle differently from the constant curvature (CC) continuum robot (see Fig. 5.7)

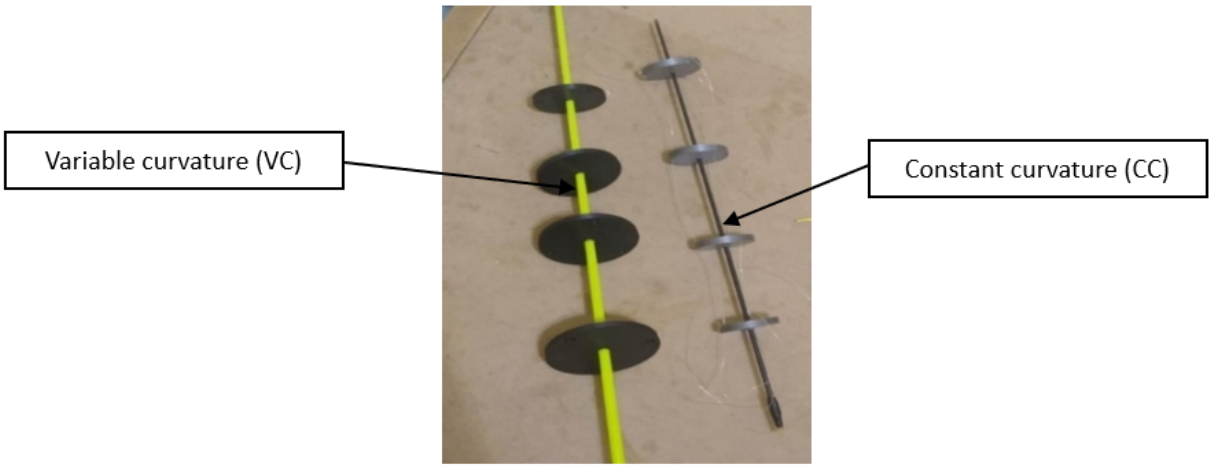

Fig. 5.7: Prototypes of a single section demonstrating two different curvature types in continuum robots: constant curvature and variable curvature

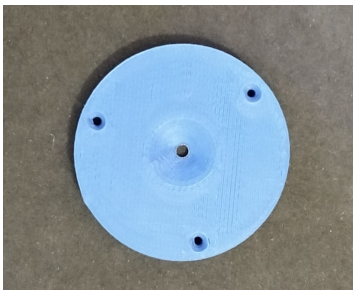

Fig. 5.8: disc

5.5 Proposed Single-Section Continuum Robot Prototype Featuring a Novel Disk Structure

In this work, we introduce an alternative disk design that resembles a ball, as depicted in Figure 5.9. This innovative disk design functions dually as both a disk and a backbone. This modification offers potential advantages, including structural simplification and enhanced performance of the robot.

Fig. 5.9: A section of the continuum robot design with a novel ball disk [19]

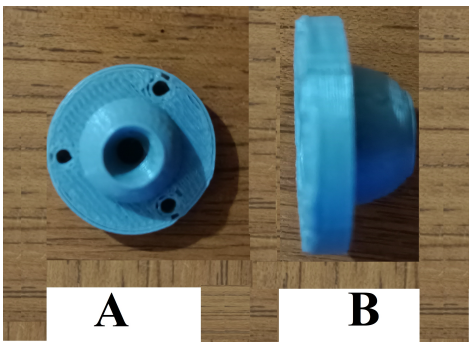

Fig. 5.10: Sole Active Bending Section of the Proposed Continuum Robot Prototype

5.6 Comparative simulation analysis of innovative ball disk and constant curvature continuum robots

In this section, we conduct a comparative simulation study between two types of continuum robots. The first features an innovative ball disk design, illustrated in Figure 5.10. The second is a single-section prototype designed for constant curvature, shown in Figure 5.5.

5.6.1 Examples of prototype oscillation simulations

This subsection focuses on simulating the oscillatory behavior of the prototype continuum robot following an initial bending angle, θ. We investigate the robot's response to three different oscillation scenarios with $\theta = \frac{\pi}{7}$, $\theta = \frac{\pi}{8}$ and $\theta = \frac{\pi}{3}$.

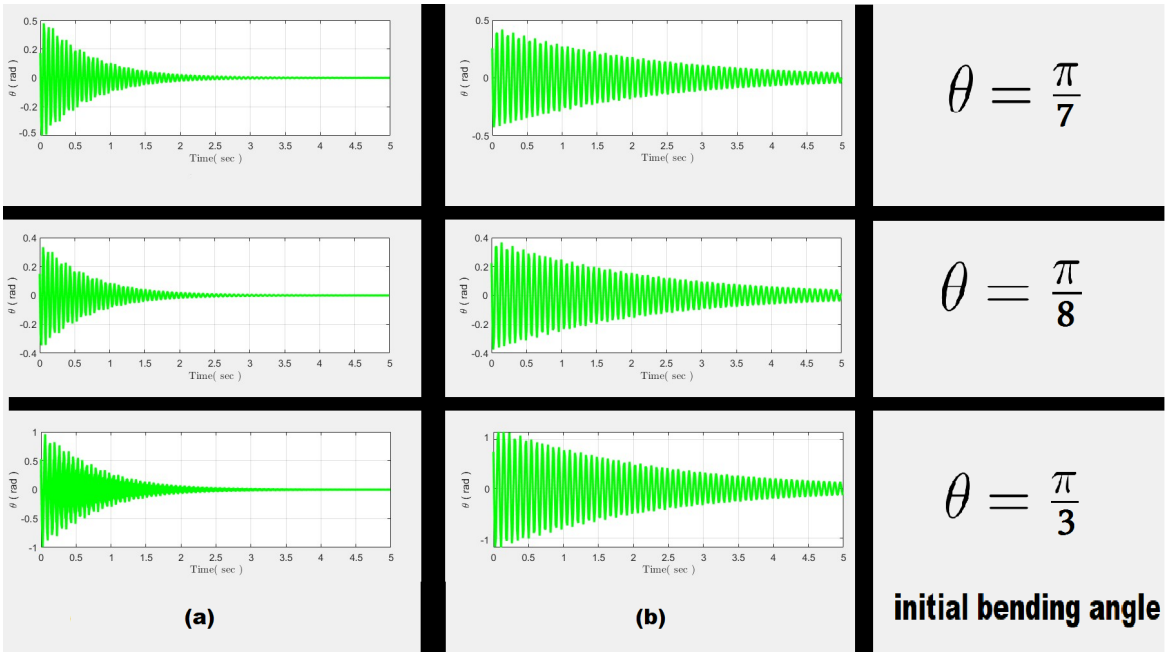

Fig. 5.11: Robot oscillations observed after releasing it from an initial flexion angle θ. (a) Proposed Prototype 5.10, (b) Conventional Prototype 5.5

From Figure 5.11, we conclude that the prototypes were subjected to various applied forces on their cables to evaluate their stability under different conditions. This comparative analysis revealed that the proposed continuum robot design 5.10 exhibited greater stability compared to the design proposed in [133]. These observations provide valuable insights into its performance characteristics, particularly when considering

the use of an accelerometer sensor in an experimental bench to validate the stability of the proposed prototype.

5.7 Conclusion

In this comprehensive chapter, we explored the dynamic modeling and design optimization of continuum robots, a field experiencing rapid advancement and facing unique challenges. Our exploration began with an overview of the evolution of robotics, emphasizing the transition from traditional rigid structures to bio-inspired, flexible continuum robots. This shift has been pivotal in overcoming the limitations of conventional robotics, particularly in applications demanding high adaptability and flexibility.

A key part of our study involved the dynamic modeling of continuum robots, where we employed the Lagrange-Euler method for efficient and accurate simulations. This method facilitated a comparative analysis of three robot prototypes, enabling us to identify the most stable and functional design under varied operational conditions. This analysis highlighted the critical role of dynamic modeling in enhancing our understanding and capabilities of continuum robots.

A major focus was on the novel design of a single-section continuum robot, featuring an innovative disk structure resembling a ball. This design deviated from traditional approaches and demonstrated significant advantages in terms of structural simplification and improved performance. Our simulations compared this novel design with a constant curvature prototype, providing essential insights into their stability and functionality, particularly in oscillatory conditions.

In summary, this chapter has shed light on the complexities and innovations within continuum robotics. Through dynamic modeling, inventive design, and rigorous validation, we have significantly advanced robot designs, making them more adaptable, efficient, and suitable for a variety of applications. The integration of accelerometer data enhanced our understanding of the robots' behavior in real-world scenarios, offering valuable practical insights. As we conclude, we acknowledge the substantial impact of these developments on the future of robotics, particularly in fields that require high flexibility and precision.

General Conclusion and Prospects

In the realm of accelerometer modeling and refinement, we have delved into the fundamental importance of sensors in the industrial landscape. To this end, in Chapter 1, we saw an overview of accelerometer types and the reasons for choosing capacitive accelerometers, along with an overview of IoT. These sensors play a pivotal role in providing reliable kinematic data. As we transition into the next phase of our study, these industrial insights will remain invaluable.

The thesis's scientific core focuses on capacitive accelerometer modeling. In Chapter2 introducing a novel mathematical formulation that optimizes various parameters such as capacitance variation, damping rate, frequency ratio, and electrode gap. Our research has delivered critical findings: the introduction of a groundbreaking mathematical model has revolutionized the field, yielding a damping rate of 0.695. This remarkable achievement significantly reduces measurement errors, minimizing the maximum error to a mere 0.06%. It is noteworthy to mention that the proposed model attests to its stability and reliability in providing precise measurements.

Our work extends beyond scientific discovery into practical applications, with the potential to enhance the integration of accelerometers into existing systems. These applications span a wide range, including aerospace, sports, and health monitoring. As we draw this part of the thesis about the application of an IoT-based accelerometer in Chapter 3, the Accelerometer-based Raspberry system for a circular chart recorder, utilizing the H3LIS331DL, exemplifies the cost-effective, user-friendly setup with versatile data collection capabilities. This system simplifies data acquisition while providing high-quality data to the server. The potential for enhancing accuracy and sensitivity within Accelerometer-based Raspberry remains a fertile ground for future research to connect the proposed system in IoT.

Additionally, in Chapter 4, we introduce a novel dimension to the kinematic modeling of continuum robots through the integration of accelerometer data. Our research centers on equipping a data logger to the end-effector of a prototype continuum robot, allowing us to record its positions while simultaneously measuring bending angles

using an angle meter. Subsequently, the positions derived from the accelerometer's data serve as inputs for a particle swarm optimization (PSO) algorithm. We meticulously compare the resulting bending angles obtained from both PSO and the angle meter to validate our simulated model and find an error in bending angle of less than 1 to 3 degrees.

Our study ventured into the realm of kinematic modeling for continuum robots, particularly the derivation and simplification of forward kinematic models. Overcoming the challenges posed by non-linear inverse kinematic models, we successfully harnessed particle swarm optimization to solve them. These models were posed as objective functions, measuring the distance between a robot's end effector and a point on a prescribed trajectory. The integration of accelerometers as a cost-effective alternative for identifying the continuum robot's end effector position marked a groundbreaking achievement, reducing reliance on expensive tools.

The final chapter 5 of our thesis delved into dynamics modeling, with a focus on the dynamic model of spatial single-section continuum robots featuring variable curvature. Practical examples and a detailed examination of a novel prototype continuum robot with a unique ball disk structure enriched our discussions. This optimization reduced the robot's weight while enhancing its stiffness, preserving overall performance.

As we consider future prospects, an exciting avenue of exploration lies in the extended application of nTop software to optimize prototype and other components within the realm of robotics, including grippers, end-effectors, and even more intricate robotic systems. Such endeavors hold the potential to unlock new capabilities and catalyze groundbreaking advancements across diverse fields.

In closing, our comprehensive exploration into accelerometer modeling, refinement, and application in IoT has laid a sturdy foundation for future scientific inquiries and innovations. This journey is far from over, and we eagerly anticipate the promising explorations and discoveries that lie ahead.

References

[1] Mahmoud Rasras and Ha Duong Ngo. *MEMS Accelerometers*. 2019.

[2] Mourad Benmessaoud and Mekkakia Maaza Nasreddine. interesting Optimization of MEMS capacitive accelerometer. *Microsystem Technologies*, 19(5):713–720, 2013.

[3] Benmesaoud Mourad. *Conception et Modélisation des MEMS : Application aux Accéléromètres*. PhD thesis, Université des Sciences et de la Technologie d'Oran Mohamed Boudiaf Faculté, 2015.

[4] Zine Ghemari. *Modélisation, simulation et analyse expérimentale du capteur de vibration (accéléromètre)*. PhD thesis, University of Badji Mokhtar – ANNABA, 2013.

[5] Aboubacar Chaehoi. *Conception et Modélisation de MEMS monolithique CMOS en technologie FSBM : Application aux accéléromètres*. PhD thesis, UNIVERSITE MONTPELLIER II, 2008.

[6] Zakriya Mohammed, Ibrahim (Abe) M. Elfadel, and Mahmoud Rasras. Monolithic multi degree of freedom (MDoF) capacitive MEMS accelerometers. *Micromachines*, 9(11):1–20, 2018.

[7] Xia Zhang, Hao Wang, Xu Dong Zheng, Shi Chang Hu, and Zhong He Jin. Modeling and noise analysis of a fence structure micromachined capacitive accelerometer system. *Journal of Zhejiang University: Science C*, 11(12):1009–1015, 2010.

[8] Flavio Di Nuzzo, Davide Brunelli, Senior Member, Tommaso Polonelli, Student Member, and Luca Benini. Narrowband IoT and MEMS Sensors. *IEEE Sensors Journal*, 21(14):16371–16380, 2021.

[9] Ashvini Kamble and Sonali Bhutad. IOT based patient health monitoring system with nested cloud security. *2018 4th International Conference on Computing Communication and Automation, ICCCA 2018*, pages 1–5, 2018.

[10] TB. Sivakumar, S. Hasan Hussain, A. Kanmani, and MH. Anand Babu. Surveillance robot for health care applications using IoT and wireless sensor network. *Materials Today: Proceedings*, pages 1–7, 2021.

[11] Ivar Koene, Raine Viitala, and Petri Kuosmanen. Internet of Things Based Monitoring of Large Rotor Vibration with a Microelectromechanical Systems Accelerometer. *IEEE Access*, 7:92210–92219, 2019.

[12] D. King, P. Hume, C. Gissane, M. Brughelli, and T. Clark. The Influence of Head Impact Threshold for Reporting Data in Contact and Collision Sports: Systematic Review and Original Data Analysis. *Sports Medicine*, 46(2):151–169, 2016.

[13] Keya Sanyal and Kalyan Biswas. Design Issues in Beam Structures for Performance Enhancement of MEMS Based Capacitive Accelerometer. *International Journal of High Speed Electronics and Systems*, 26(4):1–11, 2017.

[14] M. Sarvghad Moghadam, H. Arefi, and Kh Mafinezhad. A new design and optimization of capacitive MEMS accelerometer. *International Journal of Simulation: Systems, Science and Technology*, 14(1):23–32, 2013.

[15] S Kavitha, R Joseph Daniel, and K Sumangala. Design and Analysis of MEMS Comb Drive Capacitive Accelerometer for SHM and Seismic Applications. *Measurement*, 93:327–339, 2016.

[16] Morakchi Mohamed Razi, Ghemari Zine, and Djeffal Selman. The ideal capacitive accelerometer damping rate choice to minimize the measurement error. In *2022 2nd International Conference on Advanced Electrical Engineering (ICAEE)*, pages 11–15, Constantine, 2022.

[17] Morakchi Mohamed Razi, Ghemari Zine, Defdaf Mabrouk, Djeffal Selman, and Belhout Nacer. A novel technique based on IoT accelerometer for transmitting circular chart recorders to electrical data. *UPB Scientific Bulletin, Series C*, 84(4):274–286, 2022.

[18] Selman Djeffal. Inverse kinematic model of multi- section continuum robots using particle swarm optimization and comparison to four meta-heuristic approaches. *sage simlation*, 2023.

[19] Mohamed Razi Morakchi, Mabrouk Defdaf, Zine Ghemari, and Selman Djeffal. Prototype of an affordable continuum robot-based IoT accelerometer and its kinematic modeling. In *ICATEEE*, pages 1–6, msila, 2022.

[20] Zine Ghemari, Salah Belkhiri, and Mohamed Razi Morakchi. Improvement of the vibration analysis technique by optimizing the parameters of the piezoelectric accelerometer. In *2022 IEEE 21st international Conference on Sciences and Techniques of Automatic Control and Computer Engineering (STA)*, number December, pages 183–186, Sousse, Tunisia, 2022.

[21] Mohamed Razi Morakchi, Selman Djeffal, Atef Chibani, Zine Ghemari, and Mabrouk Defdaf. *A Model-Free Approach for Solving the Inverse Kinematics of Continuum Robots*, chapter chapter 8, pages 197–214. nova science publishers, 2023.

[22] Kalyan Dusarlapudi, K Narasimha Raju, M Preeti, and Ascs Sastry. Genesis of MEMS Accelerometers for Select the Optimal Accelerometer for Bio Applications. *Blue Eyes Intelligence Engineering and Sciences Publication*, (2):4962–4970, 2019.

[23] Raju Hajare, Vishnuvardhan Reddy, and R. Srikanth. MEMS based sensors – A comprehensive review of commonly used fabrication techniques. In *Materials Today: Proceedings*, volume 49, pages 720–730. Elsevier Ltd, 2021.

[24] Manish Tiwari, Ravi Kumar Maddila, Amit Kumar Garg, Ashok Kumar, and Preecha Yupapin. Optical and Wireless Technologies Proceedings of OWT 2020. In *Optical and Wireless Technologies*, page 180. Springer, 2020.

[25] Selman Djeffal Mohammed razi, Morakchi, Zine Ghemari, Mabrouk Defdaf. a novel Technique Based on Iot Accelerometer for Transmitting Circular Chart Recorders to Electrical Data. *UPBSci. Bull. Ser. C Elect. Eng*, 84(4):274–286, 2022.

[26] Hongcai Zhang, Xueyong Wei, Yang Gao, and Edmond Cretu. Analytical Study and Thermal Compensation for Capacitive MEMS Accelerometer with Anti-Spring Structure. *Journal of Microelectromechanical Systems*, 29(5):1389–1400, 2020.

[27] Zine Ghemari and Salah Saad. Enhancement of capacitive accelerometer operation by parameters improvement. *International Journal of Numerical Modelling: Electronic Networks, Devices and Fields*, 32(3), 2019.

[28] Zine Ghemari and Salah Saad. The use of mechanical sensitivity model to enhance capacitive sensor characteristics. *Analog Integrated Circuits and Signal Processing*, 99(2):349–357, 2019.

[29] Zine Ghemari and Salah Saad. Piezoresistive Accelerometer Mathematical Model Development with Experimental Validation. *IEEE Sensors Journal*, 18(7):2690–2696, 2018.

[30] Mabrouk Defdaf, Zine Ghemari, Aoel Elias Hadjaj, and Salah Saad. Improvement of Method Queues by Progress of the Piezoresistive Accelerometer Parameters. *Journal of Advanced Manufacturing Systems*, 16(3):227–235, 2017.

[31] Zine Ghemari and Salah Saad. Development of measurement precision of sensor vibration. *JVC/Journal of Vibration and Control*, 19(10):1480–1486, 2013.

[32] Zine Ghemari, Salah Saad, Abdelwaheb Amrouche, and Abdelaziz Lakehal. New model of piezoelectric accelerometer relative movement modulus. *Transactions of the Institute of Measurement and Control*, 37(8):932–941, 2015.

[33] Ahmad Abu Alqumsan, Suiyang Khoo, and Michael Norton. Multi-surface sliding mode control of continuum robots with mismatched uncertainties. *Meccanica*, 54(14):2307–2316, 2019.

[34] Kang Rao, Xiaoli Wei, Shaolin Zhang, Mengqi Zhang, Chenyuan Hu, Huafeng Liu, and Liang Cheng Tu. A MEMS micro-g capacitive accelerometer based on through-silicon-wafer-etching process. *Micromachines*, 10(6), jun 2019.

[35] M Xavier Chiementin, M Jean Paul Dron, and Mme Danielle Nuzillard. *Sanaa KERROUMI*. PhD thesis, 2016.

[36] Yi Jia Du, Ting Ting Yang, Dong Dong Gong, Yi Cheng Wang, Xiang Yu Sun, Feng Qin, and Gang Dai. High dynamic micro vibrator with integrated optical displacement detector for in-situ self-calibration of MEMS inertial sensors. *Sensors (Switzerland)*, 18(7), 2018.

[37] Paolo Di Barba and Slawomir Wiak. *MEMS: Field Models and Optimal Design*, volume 573. Springer, 2020.

[38] Partha Pratim Ray. A review on TinyML: State-of-the-art and prospects. *Journal of King Saud University - Computer and Information Sciences*, 34(4):1595–1623, 2022.

[39] Nabila Sabrin Sworna, A. K.M.Muzahidul Islam, Swakkhar Shatabda, and Salekul Islam. Towards development of IoT-ML driven healthcare systems: A survey. *Journal of Network and Computer Applications*, 196(September):103244, 2021.

[40] P. Prakash, G. Manoj, and Samson Immanuel.j. IoT Based Localization and Tracking by Using MIMO Antenna Technology. *ICSPC 2023 - 4th International Conference on Signal Processing and Communication*, (March):77–86, 2023.

[41] Grover Aruquipa and Fabio Diaz. An IoT architecture based on the control of Bio Inspired manufacturing system for the detection of anomalies with vibration sensors. *Procedia Computer Science*, 200:438–450, 2022.

[42] Rowida Meligy, Hicham Klaina, Imanol Picallo, Peio Lopez-iturri, Mohamed Rady, Jesús Villadangos, and Ana Vazquez Alejos. System for LFR Plants. *IEEE Sensors Journal*, 21(21):24855–24868, 2021.

[43] Karattupalayam Chidambaram Saranya, Arunkumar Thangavelu, Ashwin Chidambaram, Sharan Arumugam, and Sushant Govindraj. *Cyclist Detection Using Tiny YOLO v2*, volume 1057. 2020.

[44] Padmalaya Nayak and Souvik Pal. IoT and Analytics for Sensor Networks. In Polish Academy of Sciences Janusz Kacprzyk, Systems Research Institute and Polan Warsaw, editors, *Proceedings of ICWSNUCA 2021 IoT and Analytics for Sensor Networks*, page 502, Hyderabad, India Nadia, India Taipei City, Taiwan, 2021.

[45] C. Scuro, F. Lamonaca, S. Porzio, G. Milani, and R. S. Olivito. Internet of Things (IoT) for masonry structural health monitoring (SHM): Overview and examples of innovative systems. *Construction and Building Materials*, 290:123092, 2021.

[46] Waheb A. Jabbar, Chong Wen Wei, Nur Atiqah Ainaa M. Azmi, and Nur Aiman Haironnazli. An IoT Raspberry Pi-based parking management system for smart campus[Formula presented]. *Internet of Things (Netherlands)*, 14:100387, 2021.

[47] Zine GHEMARI Mabrouk DEFDAF Abderrahmane Guezi Djeffal Selman Khebal Merwane Morakchi, Mohamed Razi. MEMS accelerometer and gyroscope in navigation technology. In *3rd International Conference on Applied Engineering and Natural Sciences*, pages 95–102, Konya, turkey, 2022.

[48] Ali Hafiz, Thomas Schumacher, and Anis Raad. A self-referencing non-destructive test method to detect damage in reinforced concrete bridge decks using non-linear vibration response characteristics. *Construction and Building Materials*, 318(November 2021):125924, 2022.

[49] A. B. Manukin, O. S. Kazantseva, I. I. Kalinnikov, V. P. Matyunin, N. F. Sayakina, A. K. Ton'shev, and N. A. Chernogorova. A Seismometer for Observations on Mars. *Cosmic Research*, 59(5):366–375, 2021.

[50] Srikanth Gururajan, Kyle Mitchell, and William Ebel. Flights of a multirotor uas with structural faults: Failures on composite propeller(s). *Data*, 4(3):1–12, 2019.

[51] U. Vanmathi, Hindavi Jadhav, A. Nandhini, and M. Rajesh Kumar. *Accelerometer Based Home Automation System Using IoT*, volume 1057. Springer Singapore, 2020.

[52] N. Divyasudha, P. Arulmozhivarman, and E. R. Rajkumar. Analysis of Smart helmets and Designing an IoT based smart helmet: A cost effective solution for Riders. *Proceedings of 1st International Conference on Innovations in Information and Communication Technology, ICIICT 2019*, 2019.

[53] Jacob John, Mariam Sunil Varkey, Riya Sanjay Podder, Nilavrah Sensarma, M. Selvi, S. V.N. Santhosh Kumar, and Arputharaj Kannan. *Smart Prediction and Monitoring of Waste Disposal System Using IoT and Cloud for IoT Based Smart Cities*, volume 122. 2022.

[54] Nonita Sharma, Monika Mangla, Sachi Nandan Mohanty, Deepak Gupta, Prayag Tiwari, Mohammad Shorfuzzaman, and Majdi Rawashdeh. A smart ontology-based IoT framework for remote patient monitoring. *Biomedical Signal Processing and Control*, 68(March):102717, 2021.

[55] Ten Yi et al Ting. Development of Smart Healthcare Tracker through Internet of Things. *1st National Biomedical Engineering Conference, NBEC 2021*, pages 95–99, 2021.

[56] Hernandez Fidelet al. Six Degree-of-Freedom Measurements of Human Mild Traumatic Brain Injury. *Annals of Biomedical Engineering*, 43(8):1918–1934, 2015.

[57] Yao Guo, Xiangyu Liu, Shun Peng, Xinyu Jiang, Ke Xu, Chen Chen, Zeyu Wang, Chenyun Dai, and Wei Chen. A review of wearable and unobtrusive sensing technologies for chronic disease management. *Computers in Biology and Medicine*, 129(November 2020), 2021.

[58] Khadidja FELLAH Arbi, Ofiane Soulimane, and Faycal Saffih. IoT technologies combining glucose control with physiological signal: comparative study. *2020 International Conference on Electrical Engineering, ICEE 2020*, (June), 2020.

[59] Khadidja Fellah Arbi, Sofiane Soulimane, and Faycal Saffih. Non-invasive method for blood glucose monitoring using ECG signal. *Polish Journal of Medical Physics and Engineering*, 29(1):1–9, 2023.

[60] Mohammed Bourega, Ibrahim Kromba, Khadidja Fellah Arbi, and Sofiane Soulimane. Effect of Velocity Ratio, Viscosity Ratio, Contact Angle, and Channel Size Ratio on Droplet Formation. *Fluid Dynamics and Materials Processing*, 19(10):2471–2480, 2023.

[61] Khadidja Fellah Arbi, Sofiane Soulimane, Faycal Saffih, Mohammed Amine Bechar, and Omar Azzoug. Blood glucose estimation based on ECG signal. *Physical and Engineering Sciences in Medicine*, 46(1):255–264, 2023.

[62] Shumaila Javaid, Hamza Fahim, Sherali Zeadally, and Bin He. Self-powered Sensors: Applications, Challenges, and Solutions. *IEEE Sensors Journal*, 23(18):1–28, 2023.

[63] Saida Dahmane, Fouad Berrabah, and Mabrouk Defdaf. An Automatic Diagnosis of Bearing Faults of an Induction Motor Based on FFT-ANN. In *2022 International Conference of Advanced Technology in Electronic and Electrical Engineering (ICATEEE)*, pages 1–5, Msila, 2022.

[64] Matic Arh, Janko Slavič, and Miha Boltežar. Design principles for a single-process 3d-printed accelerometer – theory and experiment. *Mechanical Systems and Signal Processing*, 152, 2021.

[65] Shayaan Saghir, Muhammad Mubasher Saleem, Amir Hamza, Kashif Riaz, Sohail Iqbal, and Rana Iqtidar Shakoor. A systematic design optimization approach for multiphysics mems devices based on combined computer experiments and gaussian process modelling. *Sensors*, 21(21), 2021.

[66] S. Veena, Newton Rai, H. L. Suresh, and Veda Sandeep Nagaraja. Design, modelling, and simulation analysis of a single axis MEMS-based capacitive accelerometer. *International Journal of Engineering Trends and Technology*, 69(10):82–88, oct 2021.

[67] Yagyadatta Goswami, Ujjwal Kalra, Suraj Kaul, K. P.S. Rana, and Vineet Kumar. Performance Enhancement of a MEMS Capacitive Accelerometer Using Fuzzy Logic Controller. *Journal of The Institution of Engineers (India): Series B*, 102(2):295–310, 2021.

[68] R. Mukhiya, M. Garg, P. Gaikwad, S. Sinha, A. K. Singh, and R. Gopal. Electrical equivalent modeling of MEMS differential capacitive accelerometer. *Microelectronics Journal*, 99(March):104770, 2020.

[69] Yuming Mo, Lianming Du, Bing Bing Qu, Bo Peng, and Jie Yang. Squeeze film air damping ratio analysis of a silicon capacitive micromechanical accelerometer. *Microsystem Technologies*, 24(2):1089–1095, 2018.

[70] Mabrouk Defdaf Razi, Morakchi Mohamed ,Zine Ghemari. The optimal accelerometer parameter integrated into the mathematical model for avoiding detection errors. In *1st International Conference on Engineering and Applied Natural Sciences on 10-13 May in 2022 at Konya/Turkey.*, pages 6–12, Konya/Turkey.

[71] Hao Chen, Min Chen, Wenjing Zhao, and Limei Xu. Equivalent electrical modeling and simulation of MEMS comb accelerometer. *2010 International Conference on Measuring Technology and Mechatronics Automation, ICMTMA 2010*, 2:116–119, 2010.

[72] Morakchi Mohamed Razi, Ghemari Zine, Defdaf Mabrouk, Djeffal Selman, and Belhout Nacer. A novel technique based on IoT accelerometer for transmitting circular chart recorders to electrical data. *UPB Scientific Bulletin, Series C*, 84(4):274–286, 2022.

[73] Common Components. BARTON Chart Recorders. Technical report.

[74] IFG DEWIT. Data sheet DEWIT chart recorder.pdf, 2018.

[75] Artur Apostolov. *Development And Testing Of Motion Tracking " Smart Rock " Devices For Geotechnical Applications By Artur Apostolov B . S ., Mykolaiv Building College , 2012 THESIS Submitted to the University of New Hampshire in Partial Fulfillment of the Requirements for*. PhD thesis, University of New Hampshire Graduate School, 2016.

[76] Analog Devices. Datasheet ADXL345 (Rev. 0). Technical report, One Technology Way, P.O. Box 9106, Norwood, MA 02062-9106, U.S.A., 2009.

[77] Raspberrypi.org. Raspberry Pi 3 Model B - Raspberry Pi. Technical report, 2016.

[78] C. Arcidiacono, M. Mancino, S. M.C. Porto, V. Bloch, and M. Pastell. IoT device-based data acquisition system with on-board computation of variables for cow behaviour recognition. *Computers and Electronics in Agriculture*, 191(October):106500, 2021.

[79] Product Reference Manual. Arduino ® UNO R3 Target areas : Arduino ® UNO R3 Features. pages 1–13, 2021.

[80] Duc Nghia Tran, Tu N. Nguyen, Phung Cong Phi Khanh, and Duc Tan Trana. An IoT-based Design Using Accelerometers in Animal Behavior Recognition Systems. *IEEE Sensors Journal*, 18(23):1–14, 2021.

[81] Bryan Siepert Last and P M Edt. datasheet H3LIS331. Technical report, 2020.

[82] Ravi Jethra. Data Acquisition for Controls and Instrumentation in 21 Cfr Part 11 Applications.

[83] Electronincs Engg and S Deepak Kumar. Design and Development of IoT-based Robot. In *2020 International Conference for Emerging Technology (INCET) Jun 5-7, 2020 Design*, pages 2020–2023, Belgaum, India., 2020. IEE Xplore.

[84] Wenhao Yang and Wenzeng Zhang. A worm-inspired robot flexibly steering on horizontal and vertical surfaces. *Applied Sciences (Switzerland)*, 9(10), may 2019.

[85] Kazashi Nakano, Megu Gunji, Masahiro Ikeda, Keung Or, Mitsuhito Ando, Katsuma Inoue, Hiromi Mochiyama, Kohei Nakajima, Ryuma Niiyama, and Yasuo Kuniyoshi. RobOstrich Manipulator: A Novel Mechanical Design and Control Based on the Anatomy and Behavior of an Ostrich Neck. *IEEE Robotics and Automation Letters*, PP:1–8, 2023.

[86] Atsuhiko Niikura, Hiroyuki Nabae, Gen Endo, Megu Gunji, Kent Mori, Ryuma Niiyama, and Koichi Suzumori. Giraffe Neck Robot: First Step Toward a Powerful and Flexible Robot Prototyping Based on Giraffe Anatomy. *IEEE Robotics and Automation Letters*, 7(2):3539–3546, 2022.

[87] Vimalesh Muralidharan, Nicolas Testard, Christine Chevallereau, Anick Abourachid, and Philippe Wenger. Variable Stiffness and Antagonist Actuation for Cable-Driven Manipulators Inspired by the Bird Neck. *Journal of Mechanisms and Robotics*, 15(3), 2023.

[88] Achille Melingui, Rochdi Merzouki, and Jean Bosco Mbede. Forward kinematics modeling of a Compact Bionic Handling Manipulator. In *12th African Conference on Research in Computer Science and Applied Mathematics*, number October, pages 305–316, 2014.

[89] Xiaomei Wang, Yingqi Li, and Ka-Wai Kwok. A survey for machine learning-based control of continuum robots. *Frontiers in Robotics and AI*, page 280, 2021.

[90] Achille Melingui, Rochdi Merzouki, Jean Bosco Mbede, Coralie Escande, and Nabil Benoudjit. Neural networks based approach for inverse kinematic modeling of a compact bionic handling assistant trunk. In *2014 IEEE 23rd International Symposium on Industrial Electronics (ISIE)*, pages 1239–1244. IEEE, 2014.

[91] Costanza Armanini, Frederic Boyer, Anup Teejo Mathew, Christian Duriez, and Federico Renda. Soft Robots Modeling: A Structured Overview. *IEEE Transactions on Robotics*, PP:1–21, 2023.

[92] Selman Djeffal, Chawki Mahfoudi, and Ammar Amouri. A Path Optimization Technique with Obstacle Avoidance for multi- section continuum robot using Teaching Learning Based Optimization International Conference on Mechanical Sciences . In *International Conference on Mechanical Sciences 12-13 Nov. 2021*, number November, University Larbi Ben M'Hidi of Oum El Bouaghi, 2021.

[93] Selman Djeffal, Chawki Mahfoudi, and Ammar Amouri. Comparison of three meta-heuristic algorithms for solving inverse kinematics problems of variable curvature continuum robots. In *2021 10th European Conference on Mobile Robots, ECMR 2021 - Proceedings*, number March 2022. IEEE, 2021.

[94] Selman Djeffal and Abdelhamid Ghoul. Experimental and theoretical verification of TLBO and PSO for solving the inverse kinematic model of continuum robots. *Journal of Engineering Research*, (October), 2023.

[95] Selman Djeffal, Chawki Mahfoudi, and Ammar Amouri. Comparison of Three Meta-heuristic Algorithms for Solving Inverse Kinematics Problems of Variable Curvature Continuum Robots. In *2021 European Conference on Mobile Robots (ECMR)*, pages 1–6. IEEE, 2021.

[96] Selman Djeffal, Chawki Mahfoudi, and Ammar Amouri. A Path Optimization Technique with Obstacle Avoidance for multi-section continuum robot using Teaching Learning Based Optimization. In *International Conference on Mechanical Sciences*, volume 12, pages 1–13, Algeria, 2021.

[97] Selman Djeffal and Chawki Mahfoudi. Inverse kinematic model of multi-section continuum robots using particle swarm optimization and comparison to four meta-heuristic approaches. *SIMULATION*, 2023.

[98] Selman Djeffal, Abdelhamid Ghoul, Mohamed Razi Morakchi, Chawki Mahfoudi, and Meriem Belkedari. Optimized Computer Torque Control and Dynamic Model of a Spatial Single Section Continuum robot. *Results in Control and Optimization*, 12:100264, 2023.

[99] Selman Djeffal, Mohamed Razi Morakchi, Abdelhamid Ghoul, and Turhan Can Kargin. DDPG-based reinforcement learning for controlling a spatial three-section continuum robot. *Franklin Open*, page 100077, 2024.

[100] A Ghoul, K Kara, Selman djeffal, M Benrabah, and M L Hadjili. Inverse Kinematic Model of Continuum Robots Using Artificial Neural Network. In *2022 19th International Multi-Conference on Systems, Signals and Devices (SSD'22)*, pages 1826–1831, 2022.

[101] Selman Djeffal, Ammar Amouri, and Chawki Mahfoudi. Kinematics modeling and simulation analysis of variable curvature kinematics continuum robots. *UPB Scientific Bulletin, Series D: Mechanical Engineering*, 83(1):27–42, 2021.

[102] Han Yuan, Lili Zhou, and Wenfu Xu. A comprehensive static model of cable-driven multi-section continuum robots considering friction effect. *Mechanism and Machine Theory*, 135:130–149, 2019.

[103] Chiwon Lee, Myungjoon Kim, Yoon Jae Kim, Nhayoung Hong, Seungwan Ryu, H. Jin Kim, and Sungwan Kim. Soft robot review. *International Journal of Control, Automation and Systems*, 15(1):3–15, 2017.

[104] Yan Peng, Yonggan Liu, Yang Yang, Na Liu, Yi Sun, Yuanyuan Liu, Huayan Pu, Shaorong Xie, and Jun Luo. Development of continuum manipulator actuated by thin McKibben pneumatic artificial muscle. *Mechatronics*, 60:56–65, 2019.

[105] Selman Djeffal. *Contribution to the geometric , kinematic and dynamic modeling of bionic continuum robots*. PhD thesis, University of Larbi Ben M'hdi Oum El Bouaghi, 2022.

[106] Robert J Webster III and Bryan A Jones. Design and kinematic modeling of constant curvature continuum robots: A review. *The International Journal of Robotics Research*, 29(13):1661–1683, 2010.

[107] Coralie Escande, Pushparaj Mani Pathak, Rochdi Merzouki, and Vincent Coelen. Modelling of multisection bionic manipulator: Application to robotinoxt. In *2011 IEEE International Conference on Robotics and Biomimetics*, pages 92–97. IEEE, 2011.

[108] Coralie Escande. *Towards modeling of a class of bionic manipulator robots*. PhD thesis, Lille 1, 2013.

[109] Coralie Escande, Taha Chettibi, Rochdi Merzouki, Vincent Coelen, and Pushparaj Mani Pathak. Kinematic calibration of a multisection bionic manipulator. *IEEE/ASME transactions on mechatronics*, 20(2):663–674, 2014.

[110] Mohamed Razi Morakchi, Selman Djeffal, Atef Chibani, In Industrial, and Zine Ghemari. *A Model-Free Approach for Solving the Inverse Kinematics of Continuum In :*. Number August. 2023.

[111] Priyanka Singh and Rahul Kottath. An ensemble approach to meta-heuristic algorithms: Comparative analysis and its applications. *Computers and Industrial Engineering*, 162(October):107739, 2021.

[112] Badreddine Bendriss. Optimization of distributed generations within radial distribution systems to enhance system performance. In *2023 International Conference on Electrical Engineering and Advanced Technology (ICEEAT)*, volume 1, pages 1–6. IEEE, 2023.

[113] Neel Kamal and Prasun Ghosal. Three tier architecture for IoT driven health monitoring system using raspberry Pi. *Proceedings - 2018 IEEE 4th International Symposium on Smart Electronic Systems, iSES 2018*, pages 167–170, 2018.

[114] Dhruba Jyoti and Sut Prabhu. Soft Manipulator for Soft Robotic Applications : a Review. *Journal of Intelligent Robotic Systems*, 2023.

[115] Oncay Yasa, Yasunori Toshimitsu, Mike Y. Michelis, Lewis S. Jones, Miriam Filippi, Thomas Buchner, and Robert K. Katzschmann. An Overview of Soft Robotics. *Annual Review of Control, Robotics, and Autonomous Systems*, 6(1):33, 2023.

[116] Ibrahim A. Seleem, Haitham El-Hussieny, Samy F.M. Assal, and Hiroyuki Ishii. Development and Stability Analysis of an Imitation Learning Based Pose Planning Approach for Multi Section Continuum Robot. *IEEE Access*, 8:99366–99379, 2020.

[117] Federico Renda, Matteo Cianchetti, Haider Abidi, Jorge Dias, and Lakmal Seneviratne. Screw based modeling of soft manipulators with tendon and fluidic actuation. *Journal of Mechanisms and Robotics*, 9(4), 2017.

[118] Ian D. Walker and Clemson University. Use of continuum robots for remote inspection operations. *Proceedings of Computing Conference 2017*, 2018-Janua(July):1382–1385, 2018.

[119] Mingfeng Wang, Xin Dong, Weiming Ba, Abdelkhalick Mohammad, Dragos Axinte, and Andy Norton. Design, modelling and validation of a novel extra slender continuum robot for in-situ inspection and repair in aeroengine. *Robotics and Computer-Integrated Manufacturing*, 67:102054, 2021.

[120] Dingmin Xu, Xueyong Li, and Yonghui Wang. Bionic design of universal gripper for nursing robot with hybrid joints and variable Equivalent Link Length. *Journal of the Brazilian Society of Mechanical Sciences and Engineering*, 44(12):1–12, 2022.

[121] Alper Kadir Tanyıldızı. A three-DoF upper limb exoskeleton's design, modeling, and interaction-based control. *Journal of the Brazilian Society of Mechanical Sciences and Engineering*, 45(9):1–17, 2023.

[122] Yongfeng Cao, Zefeng Liu, Zheng Liu, Shuang Wang, and Le Xie. Design and path tracking control of a continuum robot for maxillary sinus surgery. *International Journal of Computer Assisted Radiology and Surgery*, (December), 2022.

[123] Shuang Song, Han Ge, Jiaole Wang, and Max Q.H. Meng. Real-Time Multi-Object Magnetic Tracking for Multi-Arm Continuum Robots. *IEEE Transactions on Instrumentation and Measurement*, 70:4008309–4008309, 2021.

[124] M. T. Chikhaoui and J. Burgner-Kahrs. Control of continuum robots for medical applications: State of the art (invited review). *ACTUATOR 2018 - 16th International Conference and Exhibition on New Actuators and Drive Systems, Conference Proceedings*, (January):154–164, 2018.

[125] Aida Parvaresh and S. Ali A. Moosavian. Dynamics and path tracking of continuum robotic arms using data-driven identification tools. *Robotica*, 40(4):1098–1124, 2022.

[126] Valentin Falkenhahn, Tobias Mahl, Alexander Hildebrandt, Rüdiger Neumann, and Oliver Sawodny. Dynamic modeling of constant curvature continuum robots using the Euler-Lagrange formalism. In *2014 IEEE/RSJ International Conference on Intelligent Robots and Systems*, pages 2428–2433. IEEE, 2014.

[127] Zhongzhen Liu, Xingang Zhang, Zhiqin Cai, Haijun Peng, and Zhigang Wu. Real-Time Dynamics of Cable-Driven Continuum Robots Considering the Cable Constraint and Friction Effect. *IEEE Robotics and Automation Letters*, 6(4):6235–6242, 2021.

[128] Wisama Khalil, Guillaume Gallot, Ouarda Ibrahim, and Frédéric Boyer. Dynamic modeling of a 3-D serial eel-like robot. In *Proceedings of the 2005 IEEE International Conference on Robotics and Automation*, pages 1270–1275. IEEE, 2005.

[129] Bin He, Zhipeng Wang, Qiang Li, Hong Xie, and Runjie Shen. An analytic method for the kinematics and dynamics of a multiple-backbone continuum robot. *International Journal of Advanced Robotic Systems*, 10, 2013.

[130] Maxwell Hammond, Venanzio Cichella, and Caterina Lamuta. Bioinspired Soft Robotics: State of the Art, Challenges, and Future Directions. *Current Robotics Reports*, 2023.

[131] Andrea Bajo and Nabil Simaan. Kinematics-based detection and localization of contacts along multisegment continuum robots. *IEEE Transactions on Robotics*, 28(2):291–302, 2012.

[132] Srikanth Kolachalama and Sridhar Lakshmanan. Continuum robots for manipulation applications: A survey. *Journal of Robotics*, 2020, 2020.

[133] Ammar Amouri, Abdelhakim Cherfia, Ayman Belkhiri, and Halim Merabti. Bio inspired a novel dual cross module sections cable driven continuum robot : design , kinematics modeling and workspace analysis. *Journal of the Brazilian Society of Mechanical Sciences and Engineering*, 45(265):1–17, 2023.

[134] Aida Parvaresh and S. Ali A. Moosavian. Dynamics and path tracking of continuum robotic arms using data-driven identification tools. *Robotica*, 40(4):1098–1124, 2022.

Appendix A

Raspberry Pi Setup with ADXL345 Accelerometer

A.1 Introduction

This appendix provides a detailed guide on setting up a Raspberry Pi with the ADXL345 accelerometer, a key component in the context of this thesis.

A.2 Materials

The following hardware components are required for this setup:

- Raspberry Pi board (Model XYZ, specifications ABC)
- ADXL345 accelerometer
- Jumper wires
- Breadboard (if applicable)
- Power supply

A.3 Software Requirements

Ensure the following software is installed:

- Raspberry Pi OS (Version X.Y)
- Python programming language (Version X.Y)

- Necessary libraries (e.g., Adafruit CircuitPython, SMBus for I2C communication)

A.4 Hardware Connection

Follow these steps to physically connect the ADXL345 to the Raspberry Pi. Refer to Figure A.2 for a visual representation.

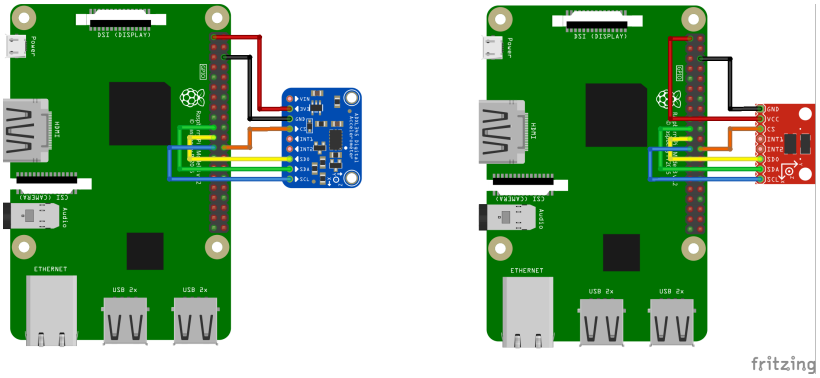

Fig. A.1: Hardware Connection Diagram

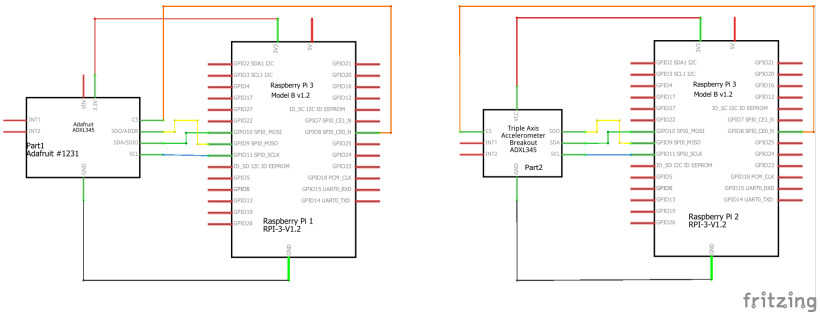

Fig. A.2: Connection Diagram

A.5 Software Setup

Execute the following commands to install the required software on the Raspberry Pi.

```
sudo python ADXL345.py
sudo apt-get update
git clone https://github.com/nagimov/adxl345spi
cd adxl345spi
sudo make
```

```
sudo make install
from ADXL345 import ADXL345
```

A.6 Code Implementation

Use the provided Python code to read data from the ADXL345. Comments in the code explain each segment's purpose.

```
from adxl345 import ADXL345

adxl345 = ADXL345()

axes = adxl345.getAxes(True)
print "ADXL345 on address 0x%x:" % (adxl345.address)
print "   x = %.3fG" % ( axes['x'] )
print "   y = %.3fG" % ( axes['y'] )
print "   z = %.3fG" % ( axes['z'] )
```

A.7 Data Visualization (Optional)

If applicable, use the provided code to visualize data from the ADXL345, for example, using matplotlib.

```
"""
matplotlib-stream.py

Display ADXL345 I2C data to the Raspberry Pi using Python (matplotlib)

Author: Diego Aulet-Leon
"""
import new;print(new.__file__)
import time
from collections import deque
import numpy as np

import matplotlib.pyplot as plt
import matplotlib.animation as animation
```

```
from matplotlib import dates
from matplotlib.font_manager import FontProperties
from matplotlib.ticker import MultipleLocator, FormatStrFormatter
import datetime

import ADXL345

# Variables
MAX_LENGTH = 25
ACC_RANGE = 16

# plot class
class AnalogPlot:
# constr
def __init__(self, Gs, maxLen):

# open i2c port
self.ser = ADXL345.ADXL345(Gs, ADXL345.BW_RATE_1600HZ, ADXL345.MEASURE)

self.ax = deque([0.0]*maxLen)
self.ay = deque([0.0]*maxLen)
self.az = deque([0.0]*maxLen)
self.amag = deque([0.0]*maxLen)
self.maxLen = maxLen

# add to buffer
def addToBuf(self, buf, val):
if len(buf) < self.maxLen:
buf.append(val)
else:
buf.pop()
buf.appendleft(val)

# add data
def add(self, data):
assert(len(data) == 4)
```

```
self.addToBuf(self.ax, data[0])
self.addToBuf(self.ay, data[1])
self.addToBuf(self.az, data[2])
self.addToBuf(self.amag, data[3])

# update plot
def update(self, frameNum, a0, a1, a2, a3):
try:
data = self.ser.read_accel()
mag = round(np.linalg.norm(data),4)
data.append(mag)
#print data
if(len(data) == 4):
self.add(data)
a0.set_data(range(self.maxLen), self.ax)
a1.set_data(range(self.maxLen), self.ay)
a2.set_data(range(self.maxLen), self.az)
a3.set_data(range(self.maxLen), self.amag)
except KeyboardInterrupt:
print('exiting')

return a0,

# main() function
def main():
# plot parameters
analogPlot = AnalogPlot(ACC_RANGE, MAX_LENGTH)

print('plotting data...')

# set up animation
fig = plt.figure()
ax = plt.axes(xlim=(0, MAX_LENGTH), ylim=(-1*ACC_RANGE, ACC_RANGE))
a0, = ax.plot([], [], label="x-axis")
a1, = ax.plot([], [], label="y-axis")
a2, = ax.plot([], [], label="z-axis")
```

```
a3, = ax.plot([], [], label="Magnitude")

ax.xaxis.set_major_locator(MultipleLocator(5))
ax.xaxis.set_major_formatter(FormatStrFormatter('%d'))
ax.xaxis.set_minor_locator(MultipleLocator(1))

ax.yaxis.set_major_locator(MultipleLocator(ACC_RANGE*0.25))
ax.yaxis.set_minor_locator(MultipleLocator(ACC_RANGE))

ax.xaxis.grid(True,'minor')
ax.yaxis.grid(True,'minor')
ax.xaxis.grid(True,'major',linewidth=2)
ax.yaxis.grid(True,'major',linewidth=2)

fontP = FontProperties()
fontP.set_size('small')
plt.legend(prop = fontP)

anim = animation.FuncAnimation(fig, analogPlot.update,
fargs=(a0, a1, a2, a3),
interval=1)

plt.grid()
# show plot
plt.show()

print('exiting.')


# call main
if __name__ == '__main__':
main()
```

A.8 Troubleshooting

Refer to this section for common issues and solutions when setting up the Raspberry Pi with the ADXL345. Tips for debugging and resolving connectivity problems are also provided. During the setup process of the Raspberry Pi with the ADXL345 accelerometer, you may encounter common issues. This section provides guidance on identifying and resolving these issues.

1. **Connection Issues:** Ensure that the wiring between the Raspberry Pi and the ADXL345 is correct. Refer to the hardware connection diagram in Section A for assistance. Check for loose connections or incorrect wiring.

2. **Power Supply:** Verify that the power supply to the Raspberry Pi is stable. Inadequate power can lead to unexpected behavior. Consider using a power supply with sufficient voltage and current for both the Raspberry Pi and the ADXL345.

3. **I2C Configuration:** If you are using the I2C interface, make sure that the I2C interface is enabled on the Raspberry Pi. You can enable it using the Raspberry Pi Configuration tool or by modifying the configuration file. Ensure that the I2C address of the ADXL345 matches the configured address in your code.

4. **Software Dependencies:** Double-check that all required software dependencies and libraries are installed. Ensure that you are using the correct versions of libraries compatible with your Raspberry Pi model and OS version.

5. **Python Code Issues:** Review your Python code for any syntax errors or logical issues. Check if the code is correctly interfacing with the ADXL345 and handling data.

6. **Logging and Debugging:** Implement logging statements in your code to track the flow and identify where errors might be occurring. Use debugging tools available for Python to inspect variables and diagnose issues.

7. **Check Documentation:** Refer to the official documentation of the ADXL345 and the Raspberry Pi for any specific considerations or troubleshooting tips.

8. **Community Support:** If you are still facing issues, consider seeking help from online forums, communities, or the GitHub repository of the library you are using. Others may have encountered similar problems and can provide valuable insights.

By following these troubleshooting steps, you can address common challenges and ensure a successful setup of the Raspberry Pi with the ADXL345 accelerometer.

A.9 Conclusion

Summarize the key steps in setting up the Raspberry Pi with the ADXL345 and emphasize the importance of proper configuration for accurate data acquisition.

A.10 References

List any external sources, tutorials, or documentation referenced during the creation of this guide.

1. Dauletle. (Year). *Raspi-ADXL345*. GitHub. Retrieved from https://github.com/dauletle/Raspi-ADXL345/tree/master (Accessed on Mars 23 , 2022).

2. Nagimov, R. (Year). *ADXL345 SPI for Raspberry Pi*. GitHub. Retrieved from https://github.com/nagimov/adxl345spi (Accessed on Mars 25 , 2022).

3. Nagimov, R. (Year). *ADXL345 SPI for Raspberry Pi*. GitHub. Retrieved from https://github.com/nagimov/adxl345spi (Accessed on Mars 23 , 2022).

Appendix B

Triple Axis Accelerometer Setup with H3LIS331DL

B.1 Appendix B: Triple Axis Accelerometer Breakout - H3LIS331DL

The SparkFun Triple Axis Accelerometer Breakout - H3LIS331DL (SEN-14480) is a versatile device designed for measuring acceleration along three axes. This breakout board utilizes the high-g H3LIS331DL three-axis linear accelerometer and is equipped with a digital I2C/SPI serial interface, making it well-suited for embedded applications. The breakout board exposes all major pins through 0.1" spaced headers and includes four mounting holes for added convenience.

B.2 Repository Contents

- **/Hardware** - Eagle design files (.brd, .sch)
- **/Production** - Production panel files (.brd)

B.3 Documentation

- **Library** - Arduino library for the H3LIS331DL.
- **Hookup Guide** - Basic hookup guide for the H3LIS331DL.

B.4 License Information

This product is released as open source, and its components are governed by the following licenses:

- **Hardware** - Creative Commons ShareAlike 4.0 International.
- **Code** - Beerware; if you find the code helpful, consider buying the SparkFun team a round if you meet them in person.

B.5 Usage Guidelines

Users are encouraged to utilize, reuse, and modify the provided files as needed. However, it is important to maintain attribution to SparkFun Electronics and release any derivative work under the same license.

Disclaimer: The product is distributed as-is, and no warranty is given.

Note: For the latest and most accurate information, please refer to the official SparkFun documentation and resources.

Your exploration and experimentation with the SparkFun Triple Axis Accelerometer Breakout are appreciated.

Appendix C

PSO algorithm

The following is the general form of the PSO algorithm in LaTeX:

Algorithm 1 Particle Swarm Optimization (PSO)

provide the robot with the angles
Initialize the particle positions and velocities:
    $\mathbf{x}i \leftarrow \text{random}(\mathbf{x}min, \mathbf{x}max)$
    $\mathbf{v}i \leftarrow \text{random}(-vmax, vmax)$
Initialize the personal best positions and their corresponding fitness values:
    $\mathbf{p}i \leftarrow \mathbf{x}i$
    $fp,i \leftarrow f(\mathbf{x}i)$
Initialize the global best position and its corresponding fitness value:
    $\mathbf{g} \leftarrow \text{pargmin}i = 1^n f_{p,i}$
    $f_g \leftarrow f_{p,\text{argmin}i=1^n fp,i}$
for $t \leftarrow 1$ to T_{max} **do**
    for $i \leftarrow 1$ to n **do**
        Update the particle velocity:
    $\mathbf{v}_i \leftarrow w\mathbf{v}_i + c_1\text{random}(0,1)(\mathbf{p}_i - \mathbf{x}_i) + c_2\text{random}(0,1)(\mathbf{g} - \mathbf{x}_i)$
        Update the particle position:
    $\mathbf{x}_i \leftarrow \mathbf{x}_i + \mathbf{v}_i$
        Evaluate the fitness of the updated particle position:
    $f_i \leftarrow f(\mathbf{x}i)$
        Update the personal best position and its corresponding fitness value:
        if $f_i < fp,i$ **then**
    $\mathbf{p}_i \leftarrow \mathbf{x}i$
    $fp,i \leftarrow f_i$
        end if
        Update the global best position and its corresponding fitness value:
        if $f_i < f_g$ **then**
    $\mathbf{g} \leftarrow \mathbf{x}_i$
    $f_g \leftarrow f_i$
        end if
    end for
end for
return $\mathbf{g}, f_g$